



THE UNIVERSITY *of* EDINBURGH

Edinburgh Research Explorer

Provenance and magmatic-tectonic setting of Campanian-aged volcanoclastic sandstones of the Kannaviou Formation in western Cyprus: evidence for a Southern Neotethyan continental margin volcanic arc

Citation for published version:

Chen, G & Robertson, A 2019, 'Provenance and magmatic-tectonic setting of Campanian-aged volcanoclastic sandstones of the Kannaviou Formation in western Cyprus: evidence for a Southern Neotethyan continental margin volcanic arc', *Sedimentary Geology*, pp. 114-138.
<https://doi.org/10.1016/j.sedgeo.2019.05.002>

Digital Object Identifier (DOI):

[10.1016/j.sedgeo.2019.05.002](https://doi.org/10.1016/j.sedgeo.2019.05.002)

Link:

[Link to publication record in Edinburgh Research Explorer](#)

Document Version:

Peer reviewed version

Published In:

Sedimentary Geology

General rights

Copyright for the publications made accessible via the Edinburgh Research Explorer is retained by the author(s) and / or other copyright owners and it is a condition of accessing these publications that users recognise and abide by the legal requirements associated with these rights.

Take down policy

The University of Edinburgh has made every reasonable effort to ensure that Edinburgh Research Explorer content complies with UK legislation. If you believe that the public display of this file breaches copyright please contact openaccess@ed.ac.uk providing details, and we will remove access to the work immediately and investigate your claim.



1 **Provenance and magmatic-tectonic setting of Campanian-aged**
2 **volcaniclastic sandstones of the Kannaviou Formation in western Cyprus:**
3 **evidence for a Southern Neotethyan continental margin volcanic arc**

4 Guohui Chen*, Alastair H. F. Robertson

5 School of GeoSciences, University of Edinburgh, West Mains Road, Edinburgh,
6 EH9 3JW, UK

7 * Corresponding author (Guohui.Chen@live.cn)

8

9 Abstract

10 Regionally developed late Cretaceous subduction-related magmatism in the
11 eastern Mediterranean records progressive closure of the Southern Neotethys.
12 In western Cyprus the late Cretaceous (c. 90 Ma) Troodos ophiolite is
13 positionally overlain by volcaniclastic sandstones (up to 750 m thick) that are
14 dominated by redeposited pyroclastic fallout, interbedded with both non-
15 calcareous and calcareous radiolarian-bearing mudstones. The sands were
16 mainly deposited by channelised mass flow processes and to a lesser extent
17 by turbidity currents in a deep-water forearc basin. The succession was folded
18 and locally thrust-deformed related to latest Cretaceous emplacement of
19 adjacent Mesozoic continental margin and oceanic units (Mamonia Complex).
20 SIMS U-Pb analysis of euhedral to subhedral magmatic zircon crystals yielded
21 a weighted mean $^{206}\text{Pb}/^{238}\text{U}$ age of 80.1 ± 1.1 Ma (Campanian). Sandstone
22 petrography including compositional framework ($\text{Q}_{12}\text{F}_{21}\text{L}_{67}$) suggests sediment
23 supply from a volcanic arc. Subordinate continentally derived detritus suggests

24 a continental margin arc setting for the mafic to felsic fallout ash. SIMS analysis
25 of little-altered volcanic glass indicates high Th/Nb and Th/La ratios that
26 suggest the involvement of continental crust and/or subducted terrigenous
27 sediments in magma genesis. Whole-rock chondrite-normalised REE patterns
28 have comparable trends to modern and ancient forearc basin volcanoclastic
29 sands and sandstones (e.g., northwest Pacific region). Trace element
30 chemistry, although scattered towards the continental island arc fields on some
31 geochemical diagrams (e.g., Th-Sc-Zr), mainly suggests an oceanic island arc
32 source for the Kannaviou Formation sandstones, with variable enrichments in
33 V-Cr-Ni-Sc, depletion in Nb-Ta, and relatively low trace element ratios (e.g.,
34 La/Co, Th/Co, La/Sc, Th/Sc). An explanation for this apparent discrepancy is
35 that the volcanoclastic sandstones were derived from a relatively primitive arc
36 constructed on previously depleted, rifted (thinned) Neotethyan continental
37 crust. The inferred continental margin arc developed during early-stage
38 northward subduction of Southern Neotethys beneath a Tauride microcontinent
39 to the north. Large volumes of volcanic ash were derived from continental
40 margin arc volcanism, probably in the vicinity of the Kyrenia Range in northern
41 Cyprus.

42 Keywords: late Cretaceous, volcanoclastic sediments, continental margin arc,
43 provenance analysis, Southern Neotethys, Cyprus

44 1. Introduction

45 Volcanic edifices are commonly localised and may be concealed or eroded,
46 whereas their volcanoclastic products are commonly widely disseminated and
47 easily recognisable in the stratigraphic record (e.g., Fisher and Schmincke,
48 1984; Yamamoto, 2009; Carey and Schneider, 2011). Volcanoclastic sediments
49 (either primary or reworked) preserve petrographic and geochemical evidence
50 that is indicative of magma genesis and tectonic setting of eruption.

51 Here, we present and discuss the results of a comprehensive study on the
52 late Cretaceous volcanoclastic sandstones of the Kannaviou Formation in
53 western Cyprus. We utilise a combination of field-based sedimentology,
54 structural geology, thin-section petrography, and geochemical studies (whole-
55 rock composition, mineral and glass composition) together with U-Pb dating of
56 zircon, in the light of the regional geological setting. The main driver, building
57 on previous studies, is to provide geochemical data for the volcanoclastic
58 sandstones and to date the timing of the related volcanism, both of which are
59 essential to understand the regional tectonic-magmatic setting. For example, it
60 was unknown whether the volcanism relates to either continental or oceanic arc
61 volcanism, and whether or not the source volcanism and the background
62 depositional ages are synchronous. Specifically our objectives are: (1) to
63 understand the deposition of the volcanoclastic sediments, taking account of the
64 stratigraphy, structure and field sedimentary features; (2) to determine the
65 magmatic setting of the source rocks using a combination of petrographic,
66 mineralogical and geochemical studies; (3) to determine the absolute age of
67 the related arc volcanism using U-Pb zircon dating; (4) to compare the
68 Kannaviou Formation with modern and ancient counterparts; and (5) to propose

69 a new magmatic-tectonic model for the late Cretaceous magmatism in the
70 context of the Southern Neotethys in the eastern Mediterranean region. Taken
71 together, the results allow a significant advance in understanding in the
72 tectonic-magmatic development of the Southern Neotethys in the eastern
73 Mediterranean, with implications for comparable volcanoclastic sediments and
74 tectonic settings elsewhere.

75 The most noteworthy feature of the Southern Neotethys in the eastern
76 Mediterranean region is the late Cretaceous Troodos ophiolite (92-90 Ma)
77 (Mukasa and Ludden, 1987). This is generally accepted to have formed during
78 initial stages of northward subduction of the Southern Neotethys (Gass, 1968;
79 Moores and Vine, 1971; Robinson and Malpas, 1990; Robertson, 1990, 2002;
80 Robertson and Xenophontos, 1993; Pearce and Robinson, 2010). The
81 volcanoclastic sedimentary rocks of the Kannaviou Formation depositionally
82 overlie the Troodos ophiolite in the west of the island (Lapierre, 1968, 1975;
83 Robertson, 1977a) and are therefore critical to interpretation of the regional
84 tectonic setting (Fig. 1). Previous studies of the Kannaviou Formation provided
85 field observations, whole-rock analysis, some mineral chemical analysis
86 (Lapierre, 1975; Robertson, 1977a; Gilbert and Robertson, 2013) and
87 paleontological dating (Urquhart and Banner, 1994; Lord et al., 2000). However,
88 this is the first study to include evidence of geochemistry and volcanic source
89 age. The source area of the Kannaviou Formation was previously suggested to
90 be in the Kyrenia Range of northern Cyprus (Robertson, 1977a; Gilbert and
91 Robertson, 2013) (Fig. 1a), a hypothesis that is tested here using new U-Pb
92 dating of detrital zircons.

93

94 2. Geological setting

95 Below, we outline key features of the geology of Cyprus that are specifically
96 relevant to an understanding of the late Cretaceous volcanoclastic sediments.

97 2.1. Setting of the Kannaviou Formation relative to the Troodos ophiolite

98 The Troodos Massif in central and southern Cyprus comprises the late
99 Cretaceous Troodos ophiolite and its *in situ* sedimentary cover including the
100 Kannaviou Formation. Based on paleomagnetic evidence, the Troodos
101 ophiolite and its sedimentary cover underwent anticlockwise rotation of up to c.
102 90°, between the late Campanian and early Eocene (Clube et al., 1985; Clube
103 and Robertson, 1986; Morris, 1996; Inwood et al., 2009). The Kannaviou
104 Formation has to be rotated by 90° clockwise when interpreting its regional
105 tectonic-magmatic formation.

106 The ophiolite is overlain, first by Fe-Mn-rich metalliferous sediments
107 (umbers) of the Campanian Perapedhi Formation (up to c. 10 m thick)
108 (Robertson and Hudson, 1974; Robertson, 1975). In western Cyprus, the
109 Perapedhi Formation begins with localised umbers, as elsewhere in Cyprus
110 (Robertson, 1977a), and passes upwards first into radiolarian mudstones, and
111 then into volcanoclastic sandstones that represent the base of the Kannaviou
112 Formation (Robertson, 1977a; Urquhart and Banner, 1994; Gilbert and
113 Robertson, 2013).

114 The Kannaviou Formation mainly crops out around the western periphery
115 of the Troodos Massif, from near Kannaviou village, the type area, northwards
116 to around Istinjo and Kinousa (Lapierre, 1968) (Fig. 1b). The formation
117 comprises alternating bentonitic claystone, radiolarian mudstone and

118 volcaniclastic sandstone, up to 750 m thick (Robertson, 1977a; Gilbert and
119 Robertson, 2013) (Fig. 2). A Campanian-early Maastrichtian age has been
120 determined mainly using radiolarians (Urquhart and Banner, 1994; Bragina and
121 Bragin, 1995; Lord et al., 2000). In its type area, the Kannaviou Formation
122 passes upwards into submarine debris-flow deposits, known as the Kathikas
123 Formation (Swarbrick and Naylor, 1980) (Fig. 2). Local interbeds of pelagic
124 chalk are dated as late Maastrichtian (Swarbrick and Naylor, 1980; Urquhart
125 and Banner, 1994; Lord et al., 2000). The Kannaviou Formation and/or the
126 Kathikas Formation in different local areas are conformably overlain by deep-
127 sea pelagic carbonates of the Lefkara Formation, ranging in age from
128 Maastrichtian to Oligocene (Robertson, 1976; Lord et al., 2000) (Fig. 2). Lateral
129 facies equivalents of the Kannaviou Formation along the southern margin of the
130 Troodos Massif are restricted to bentonitic clays and radiolarian siltstone, c. 160
131 m thick (Moni Member) (Robertson, 1977b; Swarbrick and Robertson, 1980).
132 In contrast, the formation is entirely absent along the northern and eastern
133 margins of the Troodos Massif (Robertson and Hudson, 1974), which has a
134 bearing on the regional tectonic setting.

135 2.2. Mamonía Complex

136 The Mamonía Complex of western Cyprus is relevant here because it
137 represents a likely source of terrigenous sediment to the late Cretaceous
138 Kannaviou Formation. The Mamonía Complex is dominated by two different
139 tectono-stratigraphic units (Fig. 1b) of late Triassic to early Cretaceous age: (1)
140 Sandstone gravity-flow deposits, pelagic and redeposited limestone, chert,
141 mudstone and radiolarite of the sedimentary Ayios Photios Group (Lapierre,
142 1975; Robertson and Woodcock, 1979; Swarbrick and Robertson, 1980; Torley

143 and Robertson, 2018); and (2) basaltic volcanics, together with volumetrically
144 subordinate shallow-water carbonate, hemipelagic calcilutite, chert and
145 mudstone of the Dhiarizos Group (Lapierre, 1975; Robertson and Woodcock,
146 1979; Swarbrick and Robertson, 1980; Malpas et al., 1992; Lapierre et al.,
147 2007). The two stratigraphic groups are separated by tectonic contacts, and the
148 Mamonia Complex as a whole has been juxtaposed with the Troodos Massif by
149 a combination of thrusting and strike-slip faulting along steep arcuate fault
150 lineaments during the late Cretaceous (Robertson and Woodcock, 1979;
151 Swarbrick, 1980; Robertson, 1990; Morris et al., 1990; Bailey et al., 2000). The
152 Mamonia Complex is restored as a part of the earliest-formed oceanic crust
153 (Dhiarizos Group) and adjacent passive margin (Ayios Photios Group) of the
154 Southern Neotethys that rifted from the northern margin of Gondwana
155 (Robertson and Woodcock, 1979; Torley and Robertson, 2018). The volcanic
156 rocks are also relevant to the composition of the source mantle lithosphere that
157 may have affected the composition of subsequent arc magmatism in the region.

158 2.3. Transform faulting

159 Oceanic transform faulting is relevant to the Kannaviou Formation because it is
160 inferred to have created a sea-floor topography that greatly influenced the
161 deposition of the Kannaviou Formation during the late Cretaceous. The
162 Troodos ophiolite in central-south Cyprus is cut by the east-west-trending South
163 Troodos Transform Fault Zone, up to c. 15 km wide (Moore and Vine, 1971;
164 Murton, 1986; MacLeod, 1990; Morris et al., 1990; MacLeod and Murton, 1993)
165 (Fig. 1a). Transform faulting was active during the late Cretaceous genesis of
166 the Troodos ophiolite at a spreading axis (Murton and Gass, 1986; MacLeod
167 and Murton, 1993). Critically, the transform fault extends westwards beneath

168 the late Cretaceous-Cenozoic sedimentary cover and links with the arcuate
169 fault-bounded lineaments in western Cyprus (Robertson, 1977a; Malpas et al.,
170 1992, 1993; Morris et al., 1998) (Fig. 1b). The lineaments entrain fragments of
171 late Cretaceous ophiolitic rocks and their sedimentary cover including the
172 Kannaviou Formation (Robertson, 1977a; Gilbert and Robertson, 2013),
173 together with slivers of late Cretaceous amphibolite facies and greenschist
174 facies metamorphic rocks (Lapierre, 1975; Swarbrick, 1980, 1993; Malpas et
175 al., 1992). The Troodos Massif including the Kannaviou Formation was
176 tectonically juxtaposed with the Mamonia Complex during the late Cretaceous
177 (pre- to syn-Maastrichtian) (Robertson and Woodcock, 1979; Swarbrick, 1980,
178 1993; Malpas et al., 1992, 1993; Morris et al., 1998; Bailey et al., 2000).

179 2.4. Cenozoic-recent development

180 The post-depositional geological development needs to be taken into account
181 to understand the sedimentary development of the Kannaviou Formation. In
182 particular, western Cyprus was affected by extension along a c. north-south
183 axis during late Miocene to recent, related to formation of the Polis graben
184 (Robertson, 1977c; Payne and Robertson, 1995, 2000; Balmer et al., 2019).
185 The main Kannaviou Formation outcrop lies within the eastern part of the
186 graben. The formation together with the Troodos Massif as a whole was uplifted
187 and exposed mainly during the Pleistocene (Robertson, 1977c; Poole and
188 Robertson, 1998; Morag et al., 2016). The effects of the Cenozoic faulting (e.g.,
189 relative movement of fault blocks) and the Pleistocene uplift (e.g., landslipping)
190 were taken account of when interpreting the Kannaviou Formation.

191 2.5. Kyrenia Range

192 The Kyrenia Range in northern Cyprus is mentioned in this paper mainly
193 because it is a possible source of the volcanoclastic sands that supplied the
194 Kannaviou Formation. If correct, the tectonic setting of the Kyrenia Range
195 during the late Cretaceous has a direct bearing on the provenance and tectonic-
196 magmatic setting of the volcanism represented by the Kannaviou Formation.
197 The Kyrenia Range is dominated by Triassic-Cretaceous platform carbonates
198 that were metamorphosed under greenschist facies conditions during the late
199 Cretaceous (Baroz, 1979). Late Cretaceous felsic volcanics (Fourkovouno
200 (Selvilitepe) Formation) (Robertson and Woodcock, 1986; Huang et al., 2007;
201 Robertson et al., 2012; Chen, 2018) have been suggested as the source of the
202 Kannaviou Formation volcanoclastic sediments (Robertson, 1977a; Gilbert and
203 Robertson, 2013). The succession continues with Maastrichtian-early Cenozoic
204 basaltic volcanics and both pelagic and redeposited carbonates. The Kyrenia
205 Range is interpreted as part of the northern active continental margin of the
206 Southern Neotethys (Robertson and Woodcock, 1986; Robertson et al., 2012)
207 that was juxtaposed with the Troodos Massif, possibly by the late Eocene and
208 certainly by the late Miocene (Robertson et al., 2012, 2014). The Kyrenia Range
209 escaped the major anticlockwise tectonic rotation of the Troodos Massif (Morris
210 et al., 2015), and effectively forms the southern limit of Tauride continental crust
211 (Fig. 1a).

212

213 3. Methods

214 3.1. Fieldwork and sampling

215 Previous geological maps (Lapierre, 1975; Robertson, 1977a) were compared
216 and field checked. The type area of the Kannaviou Formation was remapped
217 to illustrate the structure and sediment distribution (Fig. 3). More northerly
218 exposures in the Sarama-Peristerona and Kinousa areas, and in the southern
219 part of the Akamas Peninsula, were studied for comparison (see
220 Supplementary material) (Robertson, 1977a). In addition, sedimentary logs of
221 well-exposed local successions were measured to shed light on depositional
222 processes and to aid sampling (Fig. 4). Fault distribution and kinematic studies
223 were carried out to determine regional stress regimes during different time
224 periods (see Supplementary material). During this study we used a combination
225 of new and previously collected samples (n=20 and 18, respectively), and also
226 new and existing laboratory data, as summarised in Table 1.

227 3.2. Petrography

228 Sandstones of medium to coarse grain size were studied using an optical
229 microscope to determine their mineralogy and petrography. Scanning electron
230 microscopy (SEM) was used to study grain fabric and texture. Fourteen
231 medium-grained sandstones with well-preserved textures were selected for
232 point counting (Table 1). At least 400 points was counted for each sample using
233 a Swift Automatic point-counter, which gave a statistically meaningful result with
234 95% confidence limits (Van der Plas and Tobi, 1965). The Gazzi-Dickinson
235 point-counting method was utilised to maximise source rock data while
236 minimising the effects of grain size variation (Graham et al., 1976; Dickinson
237 and Suczek, 1979; Ingersoll et al., 1984). The recorded components (with

238 explanatory notes) are listed in Table 2. The raw data (by percentage), and the
239 calculated framework parameters are given in the Supplementary material.

240 3.3. Whole-rock major, trace, and rare earth element geochemistry

241 Whole-rock major and trace element concentrations of the sandstones (both
242 new and previous samples) were analysed by X-ray fluorescence (XRF) at the
243 School of GeoSciences, University of Edinburgh, using the methods of Fitton
244 et al. (1998) and Fitton and Godard (2004) (see Table 1). Accuracy and
245 precision estimates are comparable to those of these authors.

246 Ten newly collected samples (Table 1) were analysed at the ACME
247 Laboratories, Vancouver for trace and rare-earth elements (REEs) by
248 inductively coupled plasma mass spectrometer, following lithium
249 metaborate/tetraborate fusion and nitric acid digestion. As an indication of
250 precision, the major intra-lab standard (Reference Material STD SO-18/19) was
251 analysed together with the samples, resulting in standard deviations ($\leq 6\%$) for
252 all trace and rare earth elements. For further information on the procedures,
253 geostandards and precision for the elements analysed see <http://acmelab.com>.
254 All of the analytical data for the major, trace and rare earth elements are listed
255 in the Supplementary material.

256 3.4. Glass and mineral chemistry

257 Two polished thin sections (nos. 1074 and 2164 of Robertson, 1977a) that
258 contain abundant well-preserved undevitrified volcanic glass and feldspar were
259 selected for analysis of major elements, using a Cameca SX100 electron
260 microprobe (EMPA) at the School of GeoSciences, University of Edinburgh.
261 Previous analyses of glass, feldspar and pyroxene used the same method
262 (Gilbert and Robertson, 2013) (Table 1). Details of the analytical conditions and

263 methods are given by Hayward (2011) and by Hartley and Thordarson (2013).
264 The accuracy of major element determinations is better than ± 1 % of total value.
265 All analytical data for glass, feldspar and pyroxene are given in the
266 Supplementary material.

267 Trace-element analyses of undevitrified volcanic glass were performed on
268 four new polished thin sections (nos. 14-11, 14-14, 16-20, 16-22) (Table 1)
269 using a Cameca IMS-4f ion probe at the School of GeoSciences, University of
270 Edinburgh. The analytical data, standardization protocols and errors are given
271 in the Supplementary material.

272 3.5. U-Th-Pb secondary ion microscopy (SIMS) geochronology

273 Zircon crystals were selected from the 50-125 μm fraction that was extracted
274 from c. 20 kg of medium to coarse-grained sandstone (sample nos. 14-04, 14-
275 11, 14-14) (Table 1). A Wilfley table, Frantz Isodynamic magnetic separator and
276 a high density solution (lithium polytungstate; 2.85 g/ml) were used to aid
277 separation. Zircon grains ($n=18$) were randomly picked under a binocular
278 microscope and finally mounted in epoxy resin and polished down to expose
279 the grain interior. Internal structures were studied with the SEM using
280 cathodoluminescence (CL) at the School of GeoSciences, University of
281 Edinburgh. U-Pb analysis was then performed on a Cameca ims-1270 SIMS at
282 the School of GeoSciences, University of Edinburgh, using the methods
283 detailed by Kelly et al. (2008) and Ustaömer et al. (2012). Errors on the reported
284 ages are $\pm 1\sigma$. Geochronological plots were produced using the Excel Macro
285 program ISOPLOT (Ludwig, 2012). Analytical results are listed in the
286 Supplementary material.

287

288 4. Results

289 4.1. Field relationships

290 4.1.1. Structure

291 Structural analysis was required to understand the stratigraphy of the
292 Kannaviou Formation. The main part of the outcrop southeast of Kannaviou
293 village is deformed into a large-scale syncline with a c. east-west-trending axis,
294 as inferred by the presence of outcrops of ophiolitic basement both to the north
295 and south (Fig. 3a-b). The core of the fold is made of variably folded mudstones
296 and volcanoclastic sandstones, typically up to hundreds of metres in scale.
297 Locally, the sandstone is structurally inverted, as indicated by overturned cross-
298 bedding and normal grading. West of Kannaviou village, the succession is
299 deformed into a large anticline (Fig. 3c). The core of this structure comprises
300 thick-bedded, medium to coarse-grained volcanoclastic sandstone, siltstone
301 and calcareous claystone. The Troodos ophiolitic lavas north of Kannaviou
302 village (near Ezousa River) are affected by top-to-the northeast thrusting (Fig.
303 3). In the south, the main Kannaviou Formation outcrop is overthrust by arcuate
304 lineaments of highly sheared ophiolitic serpentinite, as well exposed west of
305 Statos (Fig. 3). Also, in the south of the Akamas Peninsula, ophiolitic rocks are
306 thrust westwards over the Kannaviou Formation (Lapierre, 1975; Robertson,
307 1977a) (Fig. 1b).

308 The Kannaviou Formation is affected by two main generations of faulting.
309 Overall, compression-related faulting relates to latest Cretaceous
310 (Maastrichtian) emplacement of the Mesozoic continental margin and oceanic
311 rocks of the Mamonia Complex (Robertson, 1977a; Swarbrick and Naylor,
312 1980). This was followed by mainly extensional faulting related to formation of

313 the Neogene Polis graben (Payne and Robertson, 1995, 2000). Mapping and
314 kinematic analysis (see Supplementary material) show that faulting offsets
315 parts of the succession but does not greatly disrupt the stratigraphy of the
316 Kannaviou Formation.

317 4.1.2. Sedimentary succession

318 The lower part of the Kannaviou Formation (c. 100 m) is dominated by non-
319 calcareous to variably calcareous claystone (Fig. 4a-b), interbedded with thin-
320 bedded volcanoclastic mudstone (Figs. 4c, 5a). Several fine-grained, lenticular
321 volcanoclastic sandstone packages, up to 10 m thick, are locally present (Figs.
322 4a-d, 5b). Bioturbation (<3 cm long) is commonly well developed (Fig. 5c). The
323 mudstone and sandstone locally contain basalt, hyaloclastite breccia and/or
324 palagonite clasts, 3-45 cm in diameter, with a matrix-supported fabric, as seen
325 near the Troodos extrusive rock contact (Figs. 4b, 5d).

326 The middle part of the succession is characterised by thick-bedded,
327 medium to coarse-grained volcanoclastic sandstone (Fig. 4a, e-h). The
328 individual sandstone depositional unit is much thicker (up to 30 m), more
329 massive and virtually structureless compared to those beneath. A prominent c.
330 25 m thick nearly homogeneous tabular sandstone northeast of Kannaviou
331 village (Fig. 4a) exhibits occasional planar lamination, low-angle cross
332 lamination and indistinct normal grading. Convolute lamination (up to 25 cm
333 thick) and evidence of slumping occur locally (Figs. 4h, 5e). Cross-bedding
334 measurements from small outcrops (e.g., near Istinjo) show a general preferred
335 orientation of foreset lamination towards the southeast (Robertson, 1977a).
336 This is consistent with the absence of the Kannaviou Formation farther east,

337 where pelagic chalks of the Lefkara Formation directly overlie the Perapedhi
338 Formation or the Troodos ophiolitic lavas (Robertson, 1977a).

339 The upper part of the succession is dominated by claystone and
340 volcanoclastic mudstone (Fig. 4e-g, i-j). Lenticular sandstone units (up to 20 m
341 thick) are interbedded with structureless claystone and weakly-bedded
342 volcanoclastic mudstone, for example around Sarama-Lasa (Figs. 4e-f, 5f).
343 Sandstone, where present, is generally thin to medium-bedded, and forms
344 lenses up to c. 300 m long. Individual sandstones are fine to medium-grained,
345 well-laminated and normal-graded. Elsewhere, low-angle cross-bedding,
346 planar cross-bedding and horizontal stratification are present. Mud rip-up clasts
347 are locally present near the base of individual beds, and some beds are rich in
348 plant material (i.e., branches, twigs and leaf debris). Dark epiclastic grains of
349 basalt are commonly visible in hand specimen (<1 mm in size).

350 4.2. Petrography and detrital modes

351 Framework grains are characterised by sub-angular to sub-rounded
352 morphologies and poorly to moderately-sorted fabrics. Quartz (2-18 modal %) and
353 feldspar (6-21 modal %; up to 1200 μm) are common. Abundant
354 volcanoclastic material is present, mostly as transparent volcanic glass with only
355 rare phenocrysts (see Section 4.2.2). In contrast, volcanic grains (mostly
356 angular) range in composition from mafic to intermediate (dark coloured; <4%),
357 to felsic (pale coloured; 2-15%) and commonly contain phenocrysts (see
358 Section 4.2.2) (Fig. 6a). Grains of pyroxene (<3%, up to 500 μm), biotite (<2%)
359 and hornblende (<2%) occur variably. Clasts of radiolarian chert, mica-schist
360 and foraminiferal pelagic limestone also occur locally (Fig. 6b-c). Microfossils
361 are widespread, mostly radiolarians, planktic foraminifera and sponge spicules

362 (Fig. 6d). The sandstones are generally matrix-supported and carbonate-
363 cemented. The matrix constitutes 6-48 modal %, and mainly comprises clay
364 minerals, together with minor tiny detrital fragments of volcanic glass, feldspar
365 and mica.

366 4.2.1. Compositional variation

367 The sandstones show considerable compositional variation from the base of
368 the succession upwards. The lowermost sandstones (sample nos. 14-14, 19.1)
369 are relatively fine-grained (c. 150-300 μm), generally non-calcareous, rich in
370 quartz (including polycrystalline quartz; QFL%Q=17-19) but low in feldspar
371 (QFL%F=13-15). Mica-schist is common and also locally chert. A medium to
372 coarse-grained sandstone sample (no. 18.5) from near the Paleomylon River
373 contains abundant feldspar (QFL%F=24) and lithic fragments (QFL%L=70) that
374 are mostly of volcanic origin (97%). Where the Kannaviou Formation is exposed
375 along the arcuate tectonic lineaments (Fig. 1b) only the base of the succession
376 is exposed restricted to fine-grained, thin-bedded sandstone (Gilbert and
377 Robertson, 2013). A typical sandstone (no. 14.5) from the lineament south of
378 Episkopi is fine to medium-grained, carbonate-bearing litharenite with abundant
379 polycrystalline quartz and metamorphic lithics (e.g., mica-schist).

380 In the middle part of the succession (sample nos. 14-12, 14-13, 21.2, 22.1),
381 the grain size of the sandstone is typically c. 180-250 μm but reaches 400 μm
382 locally (e.g., south of Kannaviou village; no. 22.1). Quartz (including
383 polycrystalline quartz) decreases (QFL%Q=6-13), whereas feldspar increases
384 (QFL%F=10-32). Volcanic lithics slightly increase and chert becomes common.
385 Dolomite and carbonate cements become more abundant. Sandstones from
386 the upper part of the succession (sample nos. 14-11, 23.1) are generally

387 coarse-grained (c. 300-500 μm) with more abundant volcanic lithics
388 (LmLvLs%Lv=96-99). Polycrystalline quartz and mica-schist are sparse.
389 Devitrified volcanic glass and recrystallised limestone are rarely present.

390 Four medium-grained, thick-bedded sandstones from the middle to upper
391 part of the succession in the Sarama-Lasa area are characterised by marked
392 compositional variation, with generally low textural maturity. Two sandstones
393 (nos. 2124, 2158) have abundant lithic fragments (QFL%L=72-80) but few
394 quartz grains (QFL%Q<5). Two other sandstones (nos. 2141, 2156) have a
395 higher abundance of quartz, especially polycrystalline quartz (QFL%Q=15-20)
396 and subhedral feldspar (QFL%F=26) but less lithic fragments (QFL%L=54-59).
397 Volcanic lithics predominate (LmLvLs%Lv=92-96) in these two sandstones,
398 with subordinate metamorphic (no. 2141; LmLvLs%Lm=6) and sedimentary (no.
399 2156; LmLvLs%Ls=4) fractions.

400 4.2.2. Glass morphology

401 The grain size is typically c. 100-700 μm but reaches 1200 μm locally (Fig. 7).
402 Colourless glass is mainly felsic (Robertson, 1977a; Gilbert and Robertson,
403 2013), constituting over 75% of the grains analysed (see Section 4.3.1). Pinkish
404 or brownish glass is of mafic to intermediate composition (Robertson, 1977a)
405 (see Supplementary material). Taken together, the relative abundances of
406 glass morphologies, glass colour (related to composition), textures and vesicle
407 abundances allow four general glass groups to be recognised (Fig. 7): (1)
408 transparent, highly vesicular pumiceous glass with a common fluid-like or rarely
409 frothy texture; (2) colourless glass as blocky shards, cusped bubble wall, and
410 rarely tubular or spindle-shaped glass, all of up to moderate vesicularity; (3)

411 pinkish glass composed of generally vesicular cusped shards and blocky
412 shards; and (4) brownish glass with a microlitic texture.

413 4.2.3. Modal proportions

414 On the QFL diagram of McBride (1963) (Fig. 8a), sandstones from all sample
415 localities are feldspathic litharenite. An undissected arc basin is indicated on
416 the QFL diagram (e.g., Dickinson et al., 1983) (Fig. 8b) as the dominant
417 provenance, especially for the Kannaviou and Paleomylon River area
418 sandstones. Two samples from Sarama-Lasa (nos. 2141, 2156) and one from
419 south of Episkopi (no. 14.5) plot in the transitional arc field. Plotted on the QFL
420 and LmLvLs diagrams of Marsaglia and Ingersoll (1992) (Fig. 8c-d), the
421 Kannaviou and Paleomylon River area samples plot in the continental arc field.
422 The average Kannaviou Formation composition falls in the continental arc field
423 ($Q_{12}F_{21}L_{67}$) (Fig. 8c) or the overlapping field of intra-oceanic and continental
424 arcs ($Lm_2Lv_{94}Ls_4$) (Fig. 8d).

425 4.3. Glass and mineral chemistry

426 4.3.1. Volcanic glass

427 Volcanic glass of different morphology and from different localities shows
428 considerable compositional variation (Fig. 9). The volcanic glass analysed
429 (n=102) is divisible into two main chemical groups according to silica content:
430 i.e., mafic/intermediate (<57 wt. % SiO_2), and felsic (>70 wt. % SiO_2). All of the
431 glass samples have moderate Na_2O+K_2O contents (2.3-8.1 wt. %), typical of
432 the subalkaline/tholeiitic series (Fig. 9). Glass from the Lempa (no. 4.2),
433 Paleomylon (no. 18.5) and Sarama-Lasa (no. 2164) areas is felsic. Glass from
434 the Kannaviou area (nos. 19.1, 21.1, 21.2, 23A.1) is largely felsic (91%), rarely

435 trending towards intermediate/mafic (9%). Glass from the Akamas area (no.
436 1074) is bimodal, mostly mafic (88%) and to a lesser extent felsic (12%).

437 Oxides such as TiO_2 , Al_2O_3 , CaO and FeO are tightly grouped and exhibit
438 positive correlations with MgO (see Supplementary material). MgO contents
439 cluster around 0-1 wt. % and 4-6 wt. %. FeO exhibits a wide range (0.6-13.7
440 wt. %), as does CaO (0.7-10.9 wt. %). Al_2O_3 content is relatively high (c. 10.1-
441 19.5 wt. %), whereas TiO_2 is typically low (0.1-1.6 wt. %). Na_2O , K_2O and P_2O_5
442 are scattered.

443 The trace-element composition of the glass was also plotted on a normal
444 mid-ocean ridge basalt (N-MORB)-normalised multi-element spider diagram
445 (Fig. 10). Glass from near Kannaviou (nos. 14-11, 14-14) and from south of
446 Lapithiou (nos. 16-20, 16-22) is compositionally similar, characterised by
447 relative enrichment in Ba and Th (10-200×N-MORB), and also in Ta, Nb and
448 La (1-10×N-MORB). Concentrations of Zr and Sm lie nearly parallel to N-MORB.
449 Ti and Y are relatively depleted at 0.05-1×N-MORB concentrations.

450 4.3.2. Feldspar

451 Eighty-one feldspar grains were analysed from samples from five different
452 localities (Table 1) (Fig. 11a). All of the feldspar grains have low orthoclase
453 contents (<4.8%). Feldspar from the Akamas area (no. 1074; n=9) shows a
454 wide range in anorthite content (55-91%; labradorite-bytownite to anorthite),
455 whereas feldspar grains from the Kannaviou area (nos. 19.1, 21.1, 21.2, 23A.1;
456 n=37) are more variable (40-95%; andesine-anorthite). A bimodal distribution
457 of feldspar compositions exists in samples from the Lempa (no. 4.2; n=10),

458 Paleomylon (no. 18.5; n=12) and Sarama-Lasa (no. 2164; n=13) areas, with
459 anorthite contents of mainly 30-50% (andesine) and 70-90% (bytownite).

460 4.3.3. Clinopyroxene

461 Forty-two clinopyroxene grains were analysed from the Kannaviou (nos. 19.1,
462 21.1, 21.2, 23A.1; n=24), Lempa (no. 4.2; n=8) and Paleomylon (no. 18.5; n=10)
463 areas. Clinopyroxene grains show relatively uniform compositional proportions
464 and are mainly augite (Morimoto, 1988) with one exception from the Lempa
465 area (Fig. 11b).

466 4.3.4. Amphibole

467 Eight grains of amphibole from the Kannaviou (nos. 19.1, 21.1, 23A.1), Lempa
468 (no. 4.2) and Paleomylon (no. 18.5) areas have relatively uniform
469 magnesiohornblende compositions (Leake et al., 1997) (Fig. 11c).

470 4.4. Zircon U-Pb dating

471 Zircon grains are generally sparse and commonly poorly preserved. Most are
472 euhedral and 50-100 μm long (Fig. 12). The crystals display variable internal
473 structures including magmatic oscillatory zoning (zircon 1), inherited
474 (xenocrystic) cores (zircon 5) and metamict structures (zircon 8). The zircon
475 grains have high Th/U ratios (0.18-1.47), suggestive of a magmatic origin
476 (Rubatto, 2002). The 18 analysed zircon grains have concordance levels
477 ranging from 99-106%. The calculated $^{206}\text{Pb}/^{238}\text{U}$ age with the generally lowest
478 possible error was used for age determination.

479 Zircon grains from the Armou area (no. 14-4; n=6) have a dominant age
480 population of 81.9-85.7 Ma (n=5) (Fig. 13a), together with one grain of 578.9
481 Ma (zircon 6). Zircon grains from sandstones near Kannaviou village (nos. 14-

482 12, 14-14; n=12) have a significant zircon population of 78.1-83.6 Ma (n=11)
483 (Fig. 13b). One grain was dated at 560.8 Ma (zircon 12). The only concordant
484 or near concordant data (99-102%) within the dominant (relatively young) age
485 distribution are represented by magmatic-textured euhedral zircon grains (nos.
486 4, 7, 9, 10, 13, 14, 16, 17) (Fig. 13c). These analyses yield a mean weighted
487 mean $^{206}\text{Pb}/^{238}\text{U}$ age of 80.1 ± 1.1 Ma (MSWD=1.7) (Fig. 13d), which is assumed
488 to be the maximum age of the sandstone deposition, and also the probable age
489 of the volcanic source.

490 Some of the zircon age data were excluded from the weighted age for the
491 following reasons: The older zircon grains (nos. 6, 12) are rounded with a
492 patchy xenocrystic texture that is suggestive of recycled origin (Fig. 12). Five
493 zircon grains (nos. 1, 3, 8, 15, 18) show slightly reverse discordance, possibly
494 due to slight loss of U and/or variable excess radiogenic Pb (e.g., Söderlund et
495 al., 2010). Zircon grains 2 and 11 have relatively high common ^{204}Pb at 2.9 and
496 3.5 ppb, respectively. Zircon grain 5 that has an inherited core with a slightly
497 older age (85.7 Ma) and zircon 7 with a relatively old age (83.6 Ma) were also
498 excluded.

499 4.5. Whole-rock geochemistry

500 4.5.1. Major-element variation

501 The Kannaviou Formation sandstones show a wide compositional range (SiO_2
502 contents of 32-63 wt. %) (Fig. 14), characterised by low TiO_2 (<0.7 wt. %), Na_2O
503 (0.9-2.9 wt. %), K_2O (0.4-1.8 wt. %) and Fe_2O_3 (2.8-5.4 wt. %). Al_2O_3 values are
504 relatively high (typically 11-18 wt. %), as are CaO (5.0-26.6 wt. %) (see
505 Supplementary material). Loss on ignition values are high (3-22 wt. %), as

506 expected given the common carbonate cement. As a result, we focus on trace
507 element contents and inter-element ratios.

508 4.5.2. Trace-element variation

509 Selected trace element concentrations for the Kannaviou Formation
510 sandstones are shown in multi-element diagrams (Fig. 15), normalised to upper
511 continental crust (UCC). Patterns of sandstones from Armou, Lempa, Sarama-
512 Lasa and south of Lapithiou are similar. Their trace element concentrations are
513 well below UCC with the exceptions of Y, Tm and Yb. The Armou, Sarama-
514 Lasa and south of Lapithiou area sandstones are mainly highly depleted in Th,
515 U, Nb and La, whereas the Lempa samples (nos. 4.1, 4.2) are relatively
516 enriched in these elements (with a more restricted range). In addition, one
517 sample (no. 21.1) from the Kannaviou area is characterised by positive
518 anomalies of Th, U, La and Ce but pronounced depletions in Ba and Sr,
519 whereas others (e.g., nos. 14-12, 19.1, 23A.1) are similar to Lempa (no. 4.2) or
520 Sarama-Lasa (no. 16-39). In contrast, the Paleomylon River area sandstones
521 are highly depleted in all trace elements, with pronounced positive anomalies
522 of Sr and wide ranges of U, K, Nb and La. However, Sr and probably also Y
523 (no. 16-04) are slightly enriched. A sample from near Ezousa River (no. 16-30)
524 is strongly depleted in U and has moderate negative anomalies of Ba, Sr and
525 Zr.

526 Positive anomalies generally exist compared to UCC, especially for Sr, Ba
527 and probably also for K, controlled by feldspar and/or K-bearing clay mineral
528 content (e.g., illite, mica) (Nesbitt et al., 1980; McLennan et al., 1983; Feng and
529 Kerrich, 1990). In contrast, negative anomalies of Zr, Hf, Th and U can be
530 explained by a reduced detrital heavy mineral fraction (Taylor and McLennan,

531 1985) and/or relatively mafic provenance (Bauluz et al., 2000). The generally
532 positive anomalies of Y and probably also of P, especially from the Sarama-
533 Lasa area samples (nos. 16-33, 16-34), imply weathering enrichment of Y
534 related to phosphatic clay and/or a detrital heavy minerals (Wronkiewicz and
535 Condie, 1987).

536 4.5.3. Rare earth element variation

537 Chondrite-normalised rare earth element (REE) patterns of selected
538 sandstones from the Kannaviou Formation and reference data from UCC
539 (Rudnick and Gao, 2003; Hu and Gao, 2008) and deep-sea sands from various
540 settings (McLennan et al., 1990) are shown in Figure 16. Sandstones from the
541 Kannaviou area (nos. 14-11, 14-12, 14-14) show moderately fractionated REE
542 patterns with $(La/Yb)_N=1.83-3.93$ and $(Gd/Yb)_N=0.99-1.16$, generally negative
543 Eu anomalies (0.73-1.0) and relatively low total REE contents (45.1-67.9 ppm).
544 Sandstones from the Paleomylon River area (nos. 16-04, 16-13, 16-14) are
545 comparatively enriched in LREE, have negative Eu anomalies (0.81-0.83) and
546 flatten out towards HREEs. Sandstone from Sarama-Lasa (no. 16-34) has a
547 fractionated REE pattern with a moderate $(La/Yb)_N=2.01$, a negative Eu
548 anomaly (0.71) and relative HREE enrichment. Sandstones from south of
549 Lapithiou (nos. 16-22, 16-23, 16-29) are similar to the Kannaviou area, but with
550 considerably more pronounced REE fractionation and lower HREE
551 concentrations. In contrast, the reference data (McLennan et al., 1990) show
552 much less variation. In general, the average Kannaviou Formation sandstone
553 parallels average forearc basin sand composition.

554

555 5. Discussion

556 5.1. Local geological influences

557 The thickness and facies variation of the sandstone, especially in the lower part
558 of the Kannaviou Formation, were strongly influenced by the contemporaneous
559 sea-floor topography. The northeasterly limit of the Kannaviou Formation
560 coincides with the tectonically controlled relief that was created by the westward
561 extension of the c. east-west-trending South Troodos Transform Fault
562 (Robertson, 1977a) (Fig. 17). The transform fault zone formed a bathymetric
563 depression with a strongly rising fault-controlled topography to the north and
564 northeast of the type area around Kannaviou. Fault scarp-derived (epiclastic)
565 lava breccia and relatively coarse-grained, thick-bedded sandstone and minor
566 conglomerate accumulated near the northern limit of the transform, as seen in
567 the Paleomylon River valley (Fig. 4b). After its accumulation during the
568 Campanian (c. 80 Ma) the Kannaviou Formation was affected by north to
569 northeast-directed compression in its type area around Kannaviou. The
570 compression relates to docking of the relatively allochthonous Triassic-
571 Cretaceous continental margin and oceanic rocks of the Mamonia Complex
572 (Robertson and Woodcock, 1979; Malpas et al., 1992; Bailey et al., 2000) (Fig.
573 4d). During the Paleogene, the Kannaviou Formation was covered by the
574 pelagic chalks of the Lefkara Formation (Figs. 3, 4e). The formation was later
575 transected by c. northwest-southeast-trending steep extensional faults related
576 to the Polis graben during late Miocene-Pliocene (Payne and Robertson, 1995,
577 2000; Balmer et al., 2019) (see Supplementary material). The present-day
578 exposure is locally influenced by landsliding, triggered by the Pleistocene uplift
579 of Cyprus and related earthquakes (Mercier et al., 1973; Robertson, 1977c;

580 Poole and Robertson, 1998; Morag et al., 2016). It was necessary to take
581 account of all of these features to understand the primary deposition of the
582 volcanoclastic sediments.

583 5.2. Deposition of the volcanoclastic sandstone

584 The non-calcareous claystone and radiolarian mudstone in the lower part of the
585 succession (e.g., Fig. 4a-b) accumulated relatively slowly, near or beneath the
586 carbonate compensation depth (CCD) based mainly on the carbonate and
587 microfossil content of the interbedded fine-grained sediments (Robertson,
588 1977a). The near-basal matrix-supported basaltic clasts and occasional
589 lenticular, amalgamated sandstone packages with composite bedding (Figs. 4b,
590 5b) are indicative of relatively rapid, channelised emplacement by mass flows.
591 The petrographic evidence of basaltic epiclasts near the base of the succession
592 (no. 18.5) (Fig. 4b), partially degraded hyaloclastite (Gilbert and Robertson,
593 2013), and the high abundance of fine-grained matrix (see Supplementary
594 material), indicate derivation from the adjacent, then submerged Troodos
595 ophiolite.

596 Upwards, the increased occurrence of calcareous claystone, mudstone
597 and volcanoclastic sandstone, with local evidence of convolute lamination,
598 record relatively high sedimentation rates and common tectonic instability (see
599 Section 4.1.2) (e.g., Figs. 4h, 5e). Sporadic, indistinct planar and low-angle
600 cross-lamination are indicative of subordinate turbidity current deposition in
601 parts of the succession (Robertson, 1977a) (Fig. 4a). The relatively coarse
602 grain size, the increase in subhedral feldspar grains, and the occurrence of
603 subangular chert and mica-schist grains (see Section 4.2.1), together suggest
604 that source lithologies were being rapidly degraded and reworked.

605 The relatively thick (up to 20 m thick by c. 300 m long), lenticular
606 volcanoclastic sandstones, locally rich in mud rip-up clasts (see Section 4.1.2)
607 are indicative of rapid, pulsed, channelised accumulation (Robertson, 1977a),
608 similar to that reported from comparable sediments elsewhere (e.g., Nishimura
609 et al., 1991). The appearance of locally abundant although fragmentary plant
610 material indicates input from land (see Section 4.1.2). The upward presence of
611 calcareous mudstone interbeds (e.g., Fig. 4e-g, i-j) with calcareous microfossils
612 indicates a change to deposition above the CCD.

613 The vast amount of vesicular pyroclastic material (Fig. 7) is interpreted to
614 have originated from explosive volcanic eruptions (Robertson, 1977a; Gilbert
615 and Robertson, 2013), similar to many volcanoclastic deposits elsewhere
616 (Schindlbeck et al., 2013; Kutterolf et al., 2014). Excellent examples were
617 recently documented from the northwest Pacific region (Busby et al., 2017;
618 Kutterolf et al., 2018; Robertson et al., 2018). The restriction of the pyroclastic
619 material to sand-sized or smaller (see Section 4.2.2) points to initial explosive
620 eruption, followed by dominantly aeolian ash transport. The eruptions are likely
621 to have been subaerial but could also have been in shallow water (< c. 300 m)
622 where hydrostatic pressure was insufficient to prevent explosive release of ash
623 into the atmosphere. Such phreatic eruptions are for example known from the
624 1965 eruption of Taal Volcano, Philippines (Moore et al., 1966), and the 1975-
625 1977 activity of La Soufrière de Guadeloupe (Lesser Antilles) (Boichu et al.,
626 2011). After initial ash fallout, and probable local current reworking, the
627 volcanoclastic sediment represented by the Kannaviou Formation was carried
628 downslope by mass flows in submarine channels, individually up to 25 m deep
629 by up to 300 m wide (Figs. 4b, 5f). Sequences of repeated turbidites are not

630 developed in contrast to many deep-sea successions in modern and ancient
631 forearc basins (Dickinson, 1995; Pickering and Hiscott, 2016). Also,
632 undisturbed primary ash fallout deposits are effectively absent. The lack of
633 conglomeratic or pyroclastic debris-flows deposits within the Kannaviou
634 Formation hints at long-distance aeolian transport that left such coarse-grained
635 material behind. Alternatively, a topographic barrier (e.g., ocean floor fault zone)
636 (Fig. 17) could have isolated the depositional area from coarser-grained supply.
637 The dominance of thick, channelised mass-flow (Fig. 4), relative to classical
638 turbidites points, points to relatively proximal deposition in an upper to mid-fan
639 setting (Howell and Normark, 1982). It is therefore unlikely that the sands were
640 transported very long distances (hundreds to thousands of km) by axial flow as
641 in some modern trench settings, such as the Peru-Chile trench (Schweller et
642 al., 1981) or the Aleutian trench (Piper et al., 1973). However, initial long-
643 distance sediment transport by wind and currents is not precluded, as
644 discussed further below.

645 5.3. Factors affecting sandstone composition

646 5.3.1. Alteration of mineral and glass grains

647 In thin section, calcium is relatively abundant in the form of foraminifera, calcite
648 spar (cement), clay minerals and feldspar (up to 14.5 modal %). Relatively high
649 values of CaO, together with positive correlations of CaO and loss on ignition
650 (LOI) values, are consistent with the carbonate content (Fig. 18a). Dissolved
651 feldspar grains are relatively common. Some detrital pyroxene grains show
652 superficial alteration to chlorite. In places, secondary porosity including small
653 late-stage cracks is infilled by clay minerals or calcite spar. Only rarely are glass

654 shards partly devitrified, in which case they typically have thin clay or carbonate
655 cement coatings.

656 The relatively unaltered nature of the glass (c. 86% of the grains) is
657 supported by the analytical totals of typically >92 wt. % (see Supplementary
658 material). A few glass grains, mainly from Sarama (no. 2164), gave totals of 89-
659 91 wt. %. The typically high average totals of c. 95 wt. % are similar to those
660 reported from a range of Pleistocene deep-sea sediments, including tephra
661 from the Mediterranean Sea (90-99 wt. %) (Clift and Blusztajn, 1999), Central
662 America (c. 93 wt. %) (Kutterolf et al., 2008a, b), New Zealand (92-99 wt. %)
663 (Lowe et al., 2008) and also Neogene tephra from the northwest Pacific (90-
664 100 wt. %) (Bryant et al., 2003; Kutterolf et al., 2018). A possible explanation of
665 the relatively unaltered nature of the Kannaviou Formation sandstones,
666 especially the volcanic glass, is because of the protective effects of diagenetic
667 carbonate cement (e.g., Ulmer-Scholle et al., 2015).

668 A few glass grains (especially two from the Kannaviou area) have
669 unusually low analytical totals (89-90 wt. %) and high silica contents (61-71
670 wt. %); this could have several explanations: (1) loss of Na and K during
671 analysis (Nielsen and Sigurdsson, 1981; Clift and Fitton, 1998); (2) relatively
672 high eruptive volatile contents, following crystal fractionation (Burnham and
673 Jahns, 1962); and (3) secondary hydration (Clift and Dixon, 1994). The majority
674 of the glass grains have high silica contents similar, for example, to
675 Mediterranean tephra (Clift and Blusztajn, 1999). The relationship between
676 measured volatile-loss (100%-Total) and silica content (Clift and Dixon, 1994)
677 (Fig. 18b) suggests that little secondary hydration of the Kannaviou Formation
678 glass has generally taken place.

679 5.3.2. Grain-size, weathering, sorting and recycling

680 Several factors can affect sandstone chemical composition, including grain-size
681 variation, weathering, sorting and recycling (e.g., Wronkiewicz and Condie,
682 1987; Cullers, 1995). Some elemental concentrations and ratios can be
683 selectively affected by grain-size variation. However, MnO, CaO, K₂O and Sr
684 concentrations, and also La/Co, Th/Co, La/Ni and Th/Cr ratios are normally not
685 much affected (Cullers, 1995). Finer-grained fractions typically comprise
686 relatively homogeneous detritus and therefore generally have relatively
687 consistent elemental concentrations and ratios (Cullers, 1995, 2000). These
688 fractions are typically characterised by relatively high Al₂O₃, Fe₂O₃, MgO, TiO₂,
689 Th, Sc, Nb, Y and REE, low SiO₂, Na₂O and Ba, and relatively low Eu/Eu*,
690 La/Sc and Th/Sc (Taylor and McLennan, 1985; Cullers, 1995). In the Kannaviou
691 Formation sandstones Na₂O (correlation coefficient $r=0.83$), TiO₂ ($r=0.67$), Sc
692 ($r=0.68$), Be ($r=0.61$), Ga ($r=0.92$), Hf ($r=0.70$), V ($r=0.47$), Zr ($r=0.48$), Eu
693 ($r=0.90$) and HREE ($r=0.4-0.6$) all correlate with Al₂O₃ (see Supplementary
694 material), which suggests a clay mineral influence (e.g., clayey matrix, illite,
695 kaolinite) on chemical composition (e.g., Roser and Korsch, 1986; Feng and
696 Kerrich, 1990). To overcome these effects, trace element ratios, namely La/Co,
697 Th/Co, Th/Cr, Eu/Eu*, La/Sc, Th/Sc, Zr/Sc and La/Th were used to characterise
698 provenance and tectonic setting (Taylor and McLennan, 1985; Bhatia and
699 Crook, 1986; Condie and Wronkiewicz, 1990; Cullers, 1995, 2000). However,
700 caution is required because some plots (e.g., La-Th-Sc, Th-Sc-Zr) can be
701 influenced by local sorting, and by mafic/heavy mineral variation (Bhatia and
702 Crook, 1986; Floyd et al., 1991).

703 Th/U ratios can indicate source area weathering and sedimentary recycling
704 (e.g., Taylor and McLennan, 1985; McLennan et al., 1993). The majority of the
705 Kannaviou Formation sandstones have Th/U ratios of 1.83-4.0, generally
706 similar to active margin-derived turbidites (McLennan et al., 1990). The low
707 values suggest derivation from little weathered magmatic arc-related source
708 rocks (McLennan et al., 1993). In contrast, relatively elevated Th/U ratios (5-28)
709 in some samples (nos. 16-16, 16-20, 16-25, 16-39, 21.1) point to enhanced
710 subaerial weathering.

711 The absence of significant zircon enrichment (37-99 ppm) precludes
712 marked sediment recycling or sorting effects (McLennan et al., 1993). The
713 depositional age from microfossils (Campanian-early Maastrichtian; 84-72 Ma)
714 (Urquhart and Banner, 1994; Bragina and Bragin, 1995) is broadly coeval with
715 the related volcanism as indicated by zircon geochronology (c. 80 Ma). This
716 evidence rules out chemical differentiation resulting from long-term
717 sedimentary recycling.

718 5.4. Source rock characteristics

719 5.4.1. Petrographic constraints

720 The QFL diagram (Fig. 8b) illustrates entire grain populations and emphasises
721 grain stability, weathering, transport mechanisms and source rocks. All of the
722 samples plot near the lithic apex with the main contribution being from volcanic
723 glass, consistent with a magmatic arc source (e.g., Dickinson et al., 1983).
724 Sandstones from south of Episkopi (no. 14.5) and near Sarama-Lasa (nos.
725 2141, 2156) cluster towards the recycled field, with relatively high quartz
726 abundances (especially polycrystalline quartz at 2-3 modal %). These clastic
727 materials were probably supplied from petrographically similar quartzose

728 sandstones in the adjacent Mamonia Complex, especially those of late Triassic
729 age (Robertson, 1977a). The mean composition of the Kannaviou Formation
730 plots in the area of overlapping fields (Fig. 8d) in the LmLvLs diagram is
731 explained by the high volcanic glass content (15-47 modal %). Despite this, the
732 relatively high average quartz content ($QFL\%Q=12$) in the Kannaviou
733 Formation sandstones supports input from a continental margin arc (Marsaglia
734 and Ingersoll, 1992; Marsaglia et al., 2016).

735 5.4.2. Constraints from glass composition

736 The volcanic glass has relatively low abundances of Na_2O (1.9-4.4 wt. %), K_2O
737 (0.2-4.6 wt. %), TiO_2 (0.1-1.6 wt. %) and P_2O_5 (<0.2 wt. %), typical of incipient
738 subduction-related volcanism (Woodhead et al., 1993; Straub, 2003).
739 Enrichment in Ba and Th, together with depletion in Ti and Nb, support an arc
740 origin (e.g., Pearce, 1983). The glass compositions plot close to the tholeiitic
741 trend on the ternary $Na_2O+K_2O-FeO-MgO$ (AFM) diagram (Fig. 19a). The trend
742 towards the alkaline apex likely represents arc magmatic maturity (Kuno, 1966;
743 Geringer et al., 1986), and is consistent with differentiation of a single parental
744 basaltic magma (Gilbert and Robertson, 2013).

745 Volcanic glass composition is critical to evaluate continental versus
746 oceanic sediment provenance (Bryant et al., 2003; Kutterolf et al., 2014).
747 Elevated U/Th, Ba/La and Sm/La ratios indicate pelagic sediment and/or fluid
748 influence on magmatic composition (Patino et al., 2000; Straub and Layne,
749 2003; Plank, 2005; Carr et al., 2007). Elevated ratios of Th/La, Rb/Hf and Th/Nb
750 suggest continental crust and/or subducted terrigenous sediment influence
751 (Hannah et al., 2002; Bryant et al., 2003; Stern et al., 2003). The relatively
752 elevated Th/Nb and Th/La ratios in the Kannaviou Formation glass (Fig. 19b-c)

753 therefore support the involvement of continental crust and/or subducted
754 terrigenous sediment in magma genesis.

755 5.4.3. Constraints from mineral analysis

756 The dominance of augite, with one rare diopside (Fig. 11b), suggests a mafic
757 igneous source (Deer et al., 2013). The clinopyroxene compositions, as shown
758 in the ternary $\text{TiO}_2\text{-MnO-Na}_2\text{O}$ discriminant plot (after Nisbet and Pearce, 1977)
759 (Fig. 19d), indicate a volcanic arc affinity for all of the grains analysed. In
760 addition, the two Ediacaran zircon grains (560 and 578 Ma) originated from
761 older continental crust. The Triassic-Cretaceous sedimentary succession of the
762 adjacent Mamonia Complex is a likely source for the grains of these ages based
763 on detrital zircon geochronology (Chen, 2018).

764 5.4.4. Constraints from whole-rock geochemistry

765 The relatively uniform ratios of La/Co, Th/Co and Th/Cr, together with La/Sc
766 and Th/Sc in the Kananviou Formation sandstones, are consistent with
767 derivation from predominantly mafic source rocks, with a subordinate variable
768 input from felsic rocks (Cullers, 1995, 2000) (Table 3). Sandstones with unusual
769 La/Sc or Th/Sc represent locally increased detrital felsic input (e.g., feldspar,
770 muscovite) or reduced mafic contribution (Taylor and McLennan, 1985; Condie
771 and Wronkiewicz, 1990; Cullers, 2000). Th/Sc vs. Zr/Sc and La/Th vs. Hf
772 diagrams indicate similar compositional variations (Fig. 20a-b).

773 Moderately fractionated REE patterns, low ΣREE abundances (45-79 ppm)
774 and low $(\text{La/Yb})_N$ (1.8-6.2), together indicate dominant derivation from mafic to
775 intermediate-composition rocks. Slight HREE enrichment in one sample (no.
776 16-34) from directly beneath the Kathikas Formation in the Sarama-Lasa area
777 (Fig. 4f) probably resulted from heavy mineral enrichment (e.g., zircon) and/or

778 input of relatively degraded fine-grained material (Taylor and McLennan, 1985),
779 both of which could have been derived from the Mamonia Complex. Negative
780 Eu anomalies of 0.71-1.00 are slightly higher than those in craton-derived post-
781 Archean Australia Shale (PAAS) (0.66; Taylor and McLennan, 1985) and UCC
782 (0.70; Rudnick and Gao, 2003). These ratios are comparable to those of
783 sandstones derived from mafic sources (0.71-0.95; Cullers, 2000) and/or
784 magmatic arcs (0.79-1.04; Bhatia, 1985) associated with active margin settings
785 (McLennan et al., 1990). Overall, the linear array of sandstone data (Fig. 20c)
786 is consistent with a mixture of compositionally variable young arc-derived
787 material and upper crust-sourced material (e.g., McLennan and Taylor, 1984)
788 that was probably derived from the adjacent Mamonia Complex.

789 5.5. Provenance

790 The trace element ratios of the volcanic glass, coupled with the presence of
791 some terrigenous sediment, support a continental arc affinity (Fig. 19b-c).
792 Despite this, the trace-element ratios of the sandstones generally fingerprint an
793 oceanic island arc setting. Specifically, the ratios of La/Sc (0.58 ± 0.18), Th/Sc
794 (0.17 ± 0.06) and La/Th (4.08 ± 0.77) are generally comparable to those of
795 sandstones derived from an oceanic island arc setting (0.55 ± 0.22 , 0.15 ± 0.08 ,
796 4.26 ± 1.2). However, several ratios (e.g., Eu/Eu*) suggest a continental
797 contribution. The scattering towards the continental island arc field is consistent
798 with locally reduced mafic contribution or increased felsic input (Bhatia and
799 Crook, 1986; Cullers, 1995, 2000; Cullers and Podkovyrov, 2000). On the
800 ternary Th-Sc-Zr diagram (Bhatia and Crook, 1986) (Fig. 21a) all of the
801 sandstones plot in or near the oceanic island arc field.

802 The average Kannaviou Formation sandstone has negative Nb-Ta
803 anomalies compared to the UCC-normalised multi-element patterns of average
804 greywacke from several different tectonic environments (Floyd et al., 1991) (Fig.
805 21b). The negative anomalies are comparable to those of oceanic island arc-
806 sourced greywackes, suggestive of sediment sources involving subduction-
807 related magmatic rocks (Floyd et al., 1991). The variable enrichments in V-Cr-
808 Ni-Sc and the slightly positive Ti anomalies are also consistent with arc
809 provenance (either continental or oceanic). In addition, the pronounced
810 depletion in Zr and Hf precludes significant enrichment in heavy minerals (e.g.,
811 zircon). The patterns are generally consistent with a source composed
812 predominantly of subduction-related rocks of oceanic island arc affinity, plus a
813 minor continental input (McLennan et al., 1990, 1993; Floyd et al., 1991).

814

815 5.6. Tectonic-magmatic setting

816 5.6.1. Continental arc magmatism on thinned, depleted continental crust?

817 The most likely explanation of the apparent discrepancy between the
818 continental margin arc setting inferred from the glass trace element chemistry
819 and the mainly oceanic arc origin suggested by the trace and REE data is that
820 the arc magmas represented by the Kannaviou Formation were not extracted
821 from fertile asthenosphere above normal-thickness continental crust. Arc-type
822 signatures could instead result if magma was extracted from crust that was
823 relatively thin and/or depleted by previous melt extraction (Fitton et al., 1997;
824 Condie, 2003). In the case of the Kannaviou Formation, both of these situations
825 are likely to have occurred because the region was affected by Triassic rift-
826 related magmatism to form the Southern Neotethys. Early spreading of this

827 ocean basin is represented by the late Triassic MORB (Dhiarizos Group) of the
828 Mamonia Complex (Robertson and Woodcock, 1979; Malpas et al., 1992, 1993;
829 Chan et al., 2008). Active continental margins in several other regions are
830 known to have relatively primitive oceanic arc-type signatures, as indicated by
831 the chemistry of derived volcanoclastic sediments and related tuffaceous
832 deposits, for example the Brook Street Terrane in southern New Zealand
833 (Robertson et al., in press).

834 5.6.2. Arc-volcanoclastic sediment comparisons

835 Despite their inferred continental margin arc provenance, as mainly inferred
836 from the glass composition, the Kannaviou Formation sandstones accumulated
837 on oceanic crust. Examples of volcanic arc-sourced successions overlying
838 oceanic crust are well represented in the southwest and north Pacific regions
839 (e.g., Horn et al., 1969; Marsaglia, 1992; Clift et al., 1998; Kutterolf et al., 2018;
840 Robertson et al., 2018). Ancient examples of oceanic arc-derived volcanoclastic
841 sediments that accumulated on oceanic crust include the late Cretaceous
842 Nindam Formation in northwest India (Robertson and Degnan, 1994; Clift et al.,
843 2000, 2002), the Jurassic Talkeetna Volcanic Formation in Alaska (Plafker et
844 al., 1989; Clift et al., 2005; Greene et al., 2006), the Permian Takitimu Group in
845 southern New Zealand (Houghton and Landis, 1989; Spandler et al., 2005;
846 Robertson and Palamakumbura, in press; Robertson et al., in press), the
847 Jurassic Gran Cañon Formation (Critelli et al., 2002; Busby, 2004) and the
848 Cretaceous Alisitos Group (Busby et al., 2006; Marsaglia et al., 2016) in Mexico.
849 In addition, there are many instances of arc-derived successions overlying
850 continental crust (Dickinson, 1995), to name one well-documented example,

851 the late Cenozoic Central American Volcanic Arc (Carr, 1984; Kutterolf et al.,
852 2008a, b; Schindlbeck et al., 2016).

853 A key requirement for the genesis of the Kannaviou Formation sandstones
854 is for supra-subduction zone oceanic lithosphere, represented by the Troodos
855 ophiolite, to collide with an adjacent continental margin arc, following
856 subduction of intervening Neotethyan oceanic crust. The tectonic-magmatic
857 setting of the Kannaviou Formation can be broadly compared to the intersection
858 of the Mariana-Bonin forearc (counterpart of the Troodos ophiolite) with the
859 Japanese continental island arc, as exposed in the Miura and Boso Peninsulas
860 (Ogawa et al., 1985, 2008). However, no exact counterpart is known elsewhere
861 for the complex microplate setting of Cyprus during the latest Cretaceous.

862 5.6.3. Implications for late Cretaceous arc magmatism in the eastern 863 Mediterranean

864 The previously suggested source (Robertson, 1977a; Gilbert and Robertson,
865 2013) of the Kannaviou Formation is the Fourkovouno (Selvilitepe) Formation
866 of the Kyrenia Range. This is characterised by a c. 400 m thick late Cretaceous
867 subduction-related volcanogenic succession that encompasses felsic
868 tuffaceous rocks, felsic debris-flow deposits and rhyolitic lava flows (Moore,
869 1960; Poisson, 1977; Baroz, 1979, 1980; Robertson and Woodcock, 1986;
870 Huang et al., 2007; Robertson et al., 2012; Chen, 2018). However, there are
871 differences between the Kannaviou Formation source volcanism and that of the
872 Kyrenia Range continental margin arc magmatism: (1) the Kannaviou
873 Formation sandstones were derived from an incipient continental margin arc,
874 whereas the Kyrenia Range volcanic rocks represent a more evolved Andean-
875 type active continental margin; and (2) the Kannaviou Formation volcanism is

876 significantly older (80.1 ± 1.1 Ma) than that of the Kyrenia Range ($^{206}\text{Pb}/^{238}\text{U}$ age
877 of 72.9 ± 1.0 Ma) (Chen, 2018). A possible explanation for these differences is
878 that older, immature arc volcanism originally existed in the Kyrenia Range area
879 but has been concealed by subsequent subduction and/or continental collision,
880 consistent with the evidence of southward thrusting during the Middle Eocene
881 and Late Miocene-earliest Pliocene (Baroz, 1979; Robertson et al., 2012, 2014;
882 McCay and Robertson, 2013; Robertson and Kinnaird, 2016).

883 The northerly active continental margin of the Southern Neotethys,
884 represented in north Cyprus by the Kyrenia Range (Robertson et al., 2012),
885 extended eastwards through the Misis-Andırın lineament of southern Turkey
886 into southeast Turkey (e.g., Robertson, 2002) (Fig. 1a). Late Cretaceous
887 continental margin arc magmatism in southeast Turkey is also interpreted to
888 relate to northward subduction of the Southern Neotethys beneath a northerly-
889 located Tauride continental unit (e.g., Robertson, 2002; Parlak, 2006; Rızaoğlu
890 et al., 2009; Robertson et al., 2006, 2007, 2012). There are two potential
891 sources of felsic ash in southeast Turkey: (1) tholeiitic oceanic arc magmatism
892 dated at 83-75 Ma (Aktaş and Robertson, 1984, 1990; Robertson et al., 2007;
893 Karaoğlu et al., 2013); and (2) I-type, calc-alkaline Andean-type intrusive rocks,
894 dated at 88-82 Ma (Santonian-Campanian) (Parlak, 2006; Robertson et al.,
895 2006; Rızaoğlu et al., 2009; Karaoğlu et al., 2016). Unfortunately, any
896 extrusive equivalents of the continental arc magmatism were eroded or are not
897 exposed. Of the two occurrences of arc magmatism, based on the geochemical
898 evidence, only the continental margin arc volcanism could be a source for the
899 Kannaviou Formation volcanic ash, assuming long-distance transport by winds
900 and/or currents. Prevailing easterly winds and currents have been modelled for

901 the late Cretaceous (e.g., Hay, 2011), such that a source well to the east of
902 Cyprus should be considered.

903 5.6.4. Pyroclastic fallout dispersal efficiency

904 Pyroclastic fallout components such as glass shards, feldspar crystals, mafic
905 crystals, lithic grains and pumice can be dispersed substantial distances by
906 wind (Carey and Sigurdsson, 1982, 2000; Fisher and Schmincke, 1984; Pyle,
907 1989). In general, the dispersal distance is mainly controlled by a combination
908 of grain size, prevailing wind strength and eruptive volume (i.e., column height)
909 (Pyle, 1989; Carey, 1996). Relatively recent (<0.5 Ma) ash of grain size 32-500
910 μm that was derived from the continental margin Japan arc can be correlated
911 with tuffaceous sediments of the oceanic Izu-Bonin forearc, up to 1000 km away
912 (Kutterolf et al., 2018). Maximum grain size versus distance from source
913 relationships are, for example, known for ash layers that were produced by the
914 Toba eruption in Sumatra (75 ka; Ninkovich et al., 1978), the Campanian
915 ignimbrite eruption in Italy (33 ka; Cornell et al., 1983) and the Minoan eruption
916 of Santorini (1620 B.C.; Watkins et al., 1978). The maximum sizes of the
917 feldspar/glass crystals and the mafic crystals (e.g., pyroxene) of the Kannaviou
918 Formation sandstones are up to 1200 μm and c. 500 μm , respectively.
919 Assuming the crystals were sourced from a common eruptive centre, these
920 sizes are compatible with eruptions on the approximate scale of the Minoan
921 eruption of Santorini (28 km³; Watkins et al., 1978), with a likely distance of c.
922 100 km from the source arc (Fig. 22). This distance is significantly less than
923 that of the known continental margin arc volcanism in southeast Turkey (c. 300
924 km). Also, to achieve the up to 750 m thickness of the Kannaviou Formation,
925 repeated Santorini-scale eruptions would be needed over a relatively short time

926 period (c. 0.3 Ma), followed by channelised sediment transport of up to c. 300
927 km (e.g., Mason et al., 2004; Deline et al., 2011). The volcanoclastic
928 sandstones are found only in western Cyprus and not overlying the Troodos
929 ophiolite as a whole, which points to a relatively local source, followed by
930 bathymetrically controlled (channelised) deposition. The most likely scenario is
931 that the Kannaviou Formation source eruptions were located close to the
932 Kyrenia Range but have since been concealed tectonically, as a result of the
933 crustal contraction that took place in response to subduction or collision.

934 5.6.5. Tectonic-magmatic model

935 Our proposed model (Fig. 23) builds on a previously proposed double
936 subduction scenario (e.g., Robertson, 2002; Parlak, 2006; Karaođlan et al.,
937 2016), in which the Troodos ophiolite formed above an intra-oceanic subduction
938 zone (c. 90 Ma) (Mukasa and Ludden, 1987), and then moved northwards
939 related to subduction beneath Tauride microcontinent crust. Resulting early-
940 stage (incipient) continental margin arc volcanism supplied pyroclastic fallout
941 deposits to a deep-marine forearc basin to the south, coupled with gravity flow
942 reworking. In addition, terrigenous sediment, mostly siliciclastic and
943 recrystallised carbonate, was supplied from the adjacent continental margin,
944 represented by the Triassic-Cretaceous terrigenous-derived sedimentary rocks
945 of the Mamonia Complex (Robertson and Woodcock, 1979; Torley and
946 Robertson, 2018).

947

948 6. Conclusions

949 In this study we have used a combination field-based sedimentology and
950 structural geology, optical petrography, whole-rock, glass and mineral
951 chemistry, and also U-Pb zircon dating to infer that the late Cretaceous
952 (80.1 ± 1.0 Ma) arc volcanism of the Kannaviou Formation in western Cyprus
953 was derived from an incipient continental margin arc. A similar integrated multi-
954 technique approach has the potential to shed new light on a range of modern
955 and ancient arc-related sediments elsewhere. The presence of terrigenous
956 material within some of the volcanoclastic sandstones initially suggested a
957 continental margin arc setting. The SIMS trace element analysis of relatively
958 unaltered volcanic glass confirmed a continental influence. Despite this, several
959 conventional trace element tectonic discriminant diagrams point to an oceanic
960 arc source. The likely solution of this apparent discrepancy is that the
961 continental margin arc was constructed on magmatically depleted lithosphere
962 that was thinned during regional late Permian-early Jurassic rifting of the
963 Southern Neotethys. Effective interpretation of comparable arc-derived
964 volcanoclastic sandstones elsewhere therefore depends on a multi-technique
965 approach, especially glass trace element analysis (where possible) and should
966 not rely on interpretation of whole-rock chemical data alone.

967

968 Acknowledgements

969 We particularly thank Richard Hinton, Steffen Kutterolf and Dick Kroon for
970 scientific discussion. Edinburgh University undergraduates helped transport the
971 large volumes of rocks required for the U-Pb zircon dating back to Edinburgh.
972 Linda Kirstein kindly advised on zircon separation and made laboratory

973 preparation facilities available for the U-Pb dating. Mike Hall is thanked for thin
974 section preparation and polishing blocks for zircon analysis. Nick Odling kindly
975 assisted with the XRF analysis. The first author gratefully acknowledges the
976 receipt of a joint studentship of the Principal's Career Development PhD
977 Scholarship and Edinburgh Global Research Scholarship. The authors are
978 grateful for financial support from the Natural Environment Research Council-
979 Ion Microprobe Facility (to A. H. F. Robertson) to carry out SIMS U-Pb dating
980 of detrital zircon. Fieldwork and geochemical analysis were aided by financial
981 support from the International Association of Sedimentologists [Postgraduate
982 Grant Scheme], the Mineralogical Society of Great Britain and Ireland
983 [Postgraduate Student Bursary Awards], and the Edinburgh Geological Society
984 [Clough Fund]. Additional financial support for fieldwork was provided by the
985 John Dixon Memorial Fund.

986

987 Reference

- 988 Aktaş, G., Robertson, A.H.F., 1984. The Maden Complex, SE Turkey: evolution
989 of a Neotethyan active margin. In: Dixon, J.E., Robertson, A.H.F. (Eds.),
990 The Geological Evolution of the Eastern Mediterranean. Geological
991 Society of London, Special Publications 17, pp. 375-402.
- 992 Aktaş, G., Robertson, A.H.F., 1990. Tectonic evolution of the Tethys suture
993 zone in SE Turkey: evidence from the petrology and geochemistry of
994 Late Cretaceous and Middle Eocene extrusives. In: Malpas, J., Moores,
995 E.M., Panayiotou, A., Xenophontos, C. (Eds.), Ophiolites-Oceanic
996 Crustal Analogues. Proceedings of the International Symposium
997 'Troodos 1987'. Geological Survey Department, Nicosia, Cyprus, pp.
998 311-329.
- 999 Bailey, W., Holdsworth, R., Swarbrick, R., 2000. Kinematic history of a
1000 reactivated oceanic suture: the Mamonia Complex Suture Zone, SW
1001 Cyprus. *Journal of the Geological Society* 157, 1107-1126.
- 1002 Balmer, E.M., Robertson, A.H.F., Raffi, I., Kroon, D., 2019. Pliocene–
1003 Pleistocene sedimentary development of the syntectonic Polis graben,
1004 NW Cyprus: evidence from facies analysis, nannofossil biochronology
1005 and strontium isotope dating. *Geological Magazine* 156, 889-917.
- 1006 Baroz, F., 1979. Etude géologique dans le Pentadaktylos et la Mesaoria
1007 (Chypre Septentrionale). Doctor of Science Thesis (published).
1008 Université de Nancy, France, 434 pp.
- 1009 Baroz, F., 1980. Volcanism and continent-island arc collision in the
1010 Pentadaktylos range, Cyprus. In: Panayiotou, A. (Ed.), Ophiolites:
1011 Proceedings of the International Ophiolite Symposium. Cyprus Ministry

1012 of Agriculture and Natural Resources, Geology Survey Department,
1013 Nicosia, Cyprus, pp. 73-85.

1014 Bauluz, B., Mayayo, M.J., Fernandez-Nieto, C., Lopez, J.M.G., 2000.
1015 Geochemistry of Precambrian and Paleozoic siliciclastic rocks from the
1016 Iberian Range (NE Spain): implications for source-area weathering,
1017 sorting, provenance, and tectonic setting. *Chemical Geology* 168, 135-
1018 150.

1019 Bhatia, M.R., 1985. Rare earth element geochemistry of Australian Paleozoic
1020 graywackes and mudrocks: provenance and tectonic control.
1021 *Sedimentary Geology* 45, 97-113.

1022 Bhatia, M.R., Crook, K.A., 1986. Trace element characteristics of graywackes
1023 and tectonic setting discrimination of sedimentary basins. *Contributions*
1024 *to Mineralogy and Petrology* 92, 181-193.

1025 Boichu, M., Villemant, B., Boudon, G., 2011. Degassing at La Soufrière de
1026 Guadeloupe volcano (Lesser Antilles) since the last eruptive crisis in
1027 1975–77: Result of a shallow magma intrusion? *Journal of Volcanology*
1028 *and Geothermal Research* 203, 102-112.

1029 Bragina, L.G., Bragin, N.Y., 1995. Radiolarians and stratigraphy of Campanian-
1030 Maestrichtian deposits of southwestern Cyprus. *Stratigraphic and*
1031 *Geological Correlation* 3, 147-155.

1032 Bryant, C., Arculus, R., Eggins, S., 2003. The geochemical evolution of the Izu-
1033 Bonin arc system: A perspective from tephra recovered by deep-sea
1034 drilling. *Geochemistry, Geophysics, Geosystems* 4, 1094,
1035 doi:10.1029/2002GC000427.

- 1036 Burnham, C.W., Jahns, R.H., 1962. A method for determining the solubility of
1037 water in silicate melts. *American Journal of Science* 260, 721-745.
- 1038 Busby, C., 2004. Continental growth at convergent margins facing large ocean
1039 basins: a case study from Mesozoic convergent-margin basins of Baja
1040 California, Mexico. *Tectonophysics* 392, 241-277.
- 1041 Busby, C., Adams, B.F., Mattinson, J., Deoreo, S., 2006. View of an intact
1042 oceanic arc, from surficial to mesozonal levels: Cretaceous Alisitos arc,
1043 Baja California. *Journal of Volcanology and Geothermal Research* 149,
1044 1-46.
- 1045 Busby, C.J., Tamura, Y., Blum, P., Guèrin, G., Andrews, G.D.M., Barker, A.K.,
1046 Berger, J.L.R., Bongiolo, E.M., Bordiga, M., DeBari, S.M., Gill, J.B.,
1047 Hamelin, C., Jia, J., John, E.H., Jonas, A.S., Jutzeler, M., Kars, M.A.C.,
1048 Kita, Z.A., Konrad, K., Mahony, S.H., Martini, M., Miyazaki, T., Musgrave,
1049 R.J., Nascimento, D.B., Nichols, A.R.L., Ribeiro, J.M., Sato, T.,
1050 Schindlbeck, J.C., Schmitt, A.K., Straub, S.M., Vautravers, M.J., Yang,
1051 Y., 2017. The missing half of the subduction factory: shipboard results
1052 from the Izu rear arc, IODP Expedition 350. *International Geology*
1053 *Review* 59, 1677-1708.
- 1054 Carey, S.N., 1996. Modeling of tephra fallout from explosive eruptions. In:
1055 Scarpa, R., Tilling, R. (Eds.), *Monitoring and mitigation of volcano*
1056 *hazards*. Springer, Berlin, pp. 429-461.
- 1057 Carey, S.N., Schneider, J.-L., 2011. Volcaniclastic processes and deposits in
1058 the deep-sea. In: Huneke, H., Mulder, T. (Eds.), *Developments in*
1059 *Sedimentology* 63. Elsevier, Amsterdam, pp. 457-515.

1060 Carey, S.N., Sigurdsson, H., 1982. Influence of particle aggregation on
1061 deposition of distal tephra from the May 18, 1980, eruption of Mount St.
1062 Helens volcano. *Journal of Geophysical Research: Solid Earth* 87, 7061-
1063 7072.

1064 Carey, S.N., Sigurdsson, H., 2000. Grain size of Miocene volcanic ash layers
1065 from Sites 998, 999, and 1000: Implications for source areas and
1066 dispersal. In: Leckie, R.M., Sigurdsson, H., Acton, G.D., Draper, G.
1067 (Eds.), *Proceedings of the Ocean Drilling Program, Scientific Results*
1068 165. Ocean Drilling Program, College Station, TX, pp. 101-113.

1069 Carr, M.J., 1984. Symmetrical and segmented variation of physical and
1070 geochemical characteristics of the Central American volcanic front.
1071 *Journal of Volcanology and Geothermal Research* 20, 231-252.

1072 Carr, M.J., Patino, L.C., Feigenson, M.D., 2007. Petrology and geochemistry of
1073 lavas. In: Jochen Bundschuh, G.E.A. (Ed.), *Central America-geology,*
1074 *resources and hazards.* A. A. Balkema, Rotterdam, Netherlands, pp.
1075 565-577.

1076 Chan, G.H.-N., Malpas, J., Xenophontos, C., Lo, C.-H., 2008. Magmatism
1077 associated with Gondwanaland rifting and Neo-Tethyan oceanic basin
1078 development: evidence from the Mamonia Complex, SW Cyprus.
1079 *Journal of the Geological Society* 165, 699-709.

1080 Chen, G., 2018. Provenance-related studies of Triassic-Miocene Tethyan
1081 sedimentary and igneous rocks from Cyprus. Unpublished PhD thesis.
1082 University of Edinburgh, UK, 484 pp.

- 1083 Clift, P.D., Blusztajn, J., 1999. The trace-element characteristics of Aegean and
1084 Aeolian volcanic arc marine tephra. *Journal of Volcanology and*
1085 *Geothermal Research* 92, 321-347.
- 1086 Clift, P.D., Degnan, P.J., Hannigan, R., Blusztajn, J., 2000. Sedimentary and
1087 geochemical evolution of the Dras forearc basin, Indus suture, Ladakh
1088 Himalaya, India. *Geological Society of America Bulletin* 112, 450-466.
- 1089 Clift, P.D., Dixon, J.E., 1994. Variations in arc volcanism and sedimentation
1090 related to rifting of the Lau Basin (southwest Pacific). In: Hawkins, J.W.,
1091 Parson, L.M., Allan, J.F., Resig, J., Weaver, P. (Eds.), *Proceedings of*
1092 *the Ocean Drilling Program, Scientific Results* 135. Ocean Drilling
1093 Program, College Station, TX, pp. 23-50.
- 1094 Clift, P.D., Draut, A.E., Kelemen, P.B., Blusztajn, J., Greene, A., 2005.
1095 Stratigraphic and geochemical evolution of an oceanic arc upper crustal
1096 section: The Jurassic Talkeetna Volcanic Formation, south-central
1097 Alaska. *Geological Society of America Bulletin* 117, 902-925.
- 1098 Clift, P.D., Fitton, J.G., 1998. Trace and rare earth element chemistry of
1099 volcanic ashes from sites 918 and 919: implications for Icelandic
1100 volcanism. In: Saunders, A.D., Larsen, H.C., Wise, S.H. (Eds.),
1101 *Proceedings of the Ocean Drilling Program, Scientific Results* 152.
1102 Ocean Drilling Program, College Station, TX, pp. 67-84.
- 1103 Clift, P.D., Hannigan, R., Blusztajn, J., Draut, A.E., 2002. Geochemical
1104 evolution of the Dras–Kohistan Arc during collision with Eurasia:
1105 evidence from the Ladakh Himalaya, India. *Island Arc* 11, 255-273.
- 1106 Clift, P.D., MacLeod, C.J., Tappin, D.R., Wright, D.J., Bloomer, S.H., 1998.
1107 Tectonic controls on sedimentation and diagenesis in the Tonga Trench

1108 and forearc, southwest Pacific. Geological Society of America Bulletin
1109 110, 483-496.

1110 Clube, T.M.M., Creer, K., Robertson, A., 1985. Palaeorotation of the Troodos
1111 microplate, Cyprus. Nature 317, 522-525.

1112 Clube, T.M.M., Robertson, A.H.F., 1986. The palaeorotation of the Troodos
1113 microplate, Cyprus, in the Late Mesozoic-Early Cenozoic plate tectonic
1114 framework of the Eastern Mediterranean. Survey in Geophysics 8, 375-
1115 437.

1116 Condie, K.C., 1993. Chemical composition and evolution of the upper
1117 continental crust: contrasting results from surface samples and shales.
1118 Chemical Geology 104, 1-37.

1119 Condie, K.C., 2003. Incompatible element ratios in oceanic basalts and
1120 komatiites: tracking deep mantle sources and continental growth rates
1121 with time. Geochemistry, Geophysics, Geosystems 4, 1005,
1122 doi:10.1029/2002GC000333.

1123 Condie, K.C., Wronkiewicz, D., 1990. The Cr/Th ratio in Precambrian pelites
1124 from the Kaapvaal Craton as an index of craton evolution. Earth and
1125 Planetary Science Letters 97, 256-267.

1126 Cornell, W., Carey, S., Sigurdsson, H., 1983. Computer simulation of transport
1127 and deposition of the Campanian Y-5 ash. Journal of Volcanology and
1128 Geothermal Research 17, 89-109.

1129 Critelli, S., Marsaglia, K.M., Busby, C.J., 2002. Tectonic history of a Jurassic
1130 backarc-basin sequence (the Gran Cañon Formation, Cedros Island,

1131 Mexico), based on compositional modes of tuffaceous deposits.
1132 Geological Society of America Bulletin 114, 515-527.

1133 Cullers, R.L., 1995. The controls on the major-and trace-element evolution of
1134 shales, siltstones and sandstones of Ordovician to Tertiary age in the
1135 Wet Mountains region, Colorado, USA. *Chemical Geology* 123, 107-131.

1136 Cullers, R.L., 2000. The geochemistry of shales, siltstones and sandstones of
1137 Pennsylvanian–Permian age, Colorado, USA: implications for
1138 provenance and metamorphic studies. *Lithos* 51, 181-203.

1139 Cullers, R.L., Podkovyrov, V.N., 2000. Geochemistry of the Mesoproterozoic
1140 Lakhanda shales in southeastern Yakutia, Russia: implications for
1141 mineralogical and provenance control, and recycling. *Precambrian
1142 Research* 104, 77-93.

1143 Deer, W.A., Howie, R.A., Zussman, J., 2013. An introduction to the rock-forming
1144 minerals. Mineralogical Society, London, 494 pp.

1145 Deligne, N., Coles, S., Sparks, R., 2010. Recurrence rates of large explosive
1146 volcanic eruptions. *Journal of Geophysical Research: Solid Earth* 115,
1147 B06203, doi:10.1029/2009JB006554.

1148 Dickinson, W.R., 1995. Forearc Basins. In: Busby, C., Ingersoll, R. (Eds.),
1149 *Tectonics of Sedimentary Basins*. Blackwell Science, Oxford, pp. 221-
1150 262.

1151 Dickinson, W.R., Beard, L.S., Brakenridge, G.R., Erjavec, J.L., Ferguson, R.C.,
1152 Inman, K.F., Knepp, R.A., Lindberg, F.A., Ryberg, P.T., 1983.
1153 Provenance of North American Phanerozoic sandstones in relation to
1154 tectonic setting. *Geological Society of America Bulletin* 94, 222-235.

- 1155 Dickinson, W.R., Suczek, C.A., 1979. Plate tectonics and sandstone
1156 compositions. American Association of Petroleum Geologists Bulletin 63,
1157 2164-2182.
- 1158 Feng, R., Kerrich, R., 1990. Geochemistry of fine-grained clastic sediments in
1159 the Archean Abitibi greenstone belt, Canada: implications for
1160 provenance and tectonic setting. *Geochimica et Cosmochimica Acta* 54,
1161 1061-1081.
- 1162 Fisher, R.V., Schmincke, H.-U., 1984. *Pyroclastic rocks*. Springer-Verlag, Berlin
1163 Heidelberg, 472 pp.
- 1164 Fitton, J.G., Godard, M., 2004. Origin and evolution of magmas on the Ontong
1165 Java Plateau. In: Fitton, J.G., Mahoney, J.J., Wallace, P.J., Saunders,
1166 A.D. (Eds.), *Origin and Evolution of the Ontong Java Plateau*. Geological
1167 Society of London, Special Publications 229, pp. 151-178.
- 1168 Fitton, J.G., Saunders, A., Larsen, L., Hardarson, B., Norry, M., 1998. Volcanic
1169 rocks from the southeast Greenland margin at 63°N: composition,
1170 petrogenesis and mantle sources. In: Saunders, A.D., Larsen, H.C.,
1171 Wise, S.W., Jr. (Eds.), *Proceedings of the Ocean Drilling Program*,
1172 *Scientific Results 152*. Ocean Drilling Program, College Station, TX, pp.
1173 331-350.
- 1174 Fitton, J.G., Saunders, A.D., Norry, M.J., Hardarson, B.S., Taylor, R.N., 1997.
1175 Thermal and chemical structure of the Iceland plume. *Earth and*
1176 *Planetary Science Letters* 153, 197-208.
- 1177 Floyd, P., Leveridge, B., 1987. Tectonic environment of the Devonian
1178 Gramscatho basin, south Cornwall: framework mode and geochemical

1179 evidence from turbiditic sandstones. *Journal of the Geological Society*
1180 144, 531-542.

1181 Floyd, P., Shail, R., Leveridge, B., Franke, W., 1991. Geochemistry and
1182 provenance of Rhenohercynian synorogenic sandstones: implications
1183 for tectonic environment discrimination. In: Morton, A.C., Todd, S.P.,
1184 Haughton, P.D.W. (Eds.), *Developments in Sedimentary Provenance*
1185 *Studies*. Geological Society of London, Special Publication 57, pp. 173-
1186 188.

1187 Gass, I.G., 1968. Is the Troodos Massif of Cyprus a Fragment of Mesozoic
1188 Ocean Floor? *Nature* 220, 39-42.

1189 Geringer, G., Botha, B., Pretorius, J., Ludick, D., 1986. Calc-alkaline volcanism
1190 along the eastern margin of the Namaqua Mobile Belt, South Africa-a
1191 possible middle Proterozoic volcanic arc. *Precambrian Research* 33,
1192 139-170.

1193 Gilbert, M.F., Robertson, A.H.F., 2013. Field relations, geochemistry and origin
1194 of the Upper Cretaceous volcanoclastic Kannaviou Formation in western
1195 Cyprus: evidence of a southerly Neotethyan volcanic arc. In: Robertson,
1196 A.H.F., Parlak, O., Ünlügenç, U.C. (Eds.), *Geological Development of*
1197 *Anatolia and the Easternmost Mediterranean Region*. Geological
1198 Society of London, Special Publications 372, pp. 273-298.

1199 Graham, S.A., Ingersoll, R.V., Dickinson, W.R., 1976. Common provenance for
1200 lithic grains in Carboniferous sandstones from Ouachita Mountains and
1201 Black Warrior Basin. *Journal of Sedimentary Research* 46, 620-632.

- 1202 Greene, A.R., Debari, S.M., Kelemen, P.B., Blusztajn, J., Clift, P.D., 2006. A
1203 detailed geochemical study of island arc crust: the Talkeetna arc section,
1204 south–central Alaska. *Journal of Petrology* 47, 1051-1093.
- 1205 Hannah, R.S., Vogel, T.A., Patino, L.C., Alvarado, G.E., Pérez, W., Smith, D.R.,
1206 2002. Origin of silicic volcanic rocks in Central Costa Rica: a study of a
1207 chemically variable ash-flow sheet in the Tiribi Tuff. *Bulletin of*
1208 *Volcanology* 64, 117-133.
- 1209 Hartley, M.E., Thordarson, T., 2013. The 1874-1876 volcano-tectonic episode
1210 at Askja, North Iceland: Lateral flow revisited. *Geochemistry,*
1211 *Geophysics, Geosystems* 14, 2286-2309.
- 1212 Hay, W.W., 2011. Can humans force a return to a ‘Cretaceous’ climate?
1213 *Sedimentary Geology* 235, 5-26.
- 1214 Hayward, C., 2011. High spatial resolution electron probe microanalysis of
1215 tephtras and melt inclusions without beam-induced chemical modification.
1216 *The Holocene* 22, 119-125.
- 1217 Horn, D.R., Delach, M.N., Horn, B.M., 1969. Distribution of volcanic ash layers
1218 and turbidites in the North Pacific. *Geological Society of America Bulletin*
1219 80, 1715-1724.
- 1220 Houghton, B., Landis, C., 1989. Sedimentation and volcanism in a Permian arc-
1221 related basin, southern New Zealand. *Bulletin of Volcanology* 51, 433-
1222 450.
- 1223 Howell, D.G., Normark, W.R., 1982. Sedimentology of submarine fans. In:
1224 Scholle, P.A., D., S. (Eds.), *Sandstone depositional environments.*
1225 *American Association of Petroleum Geologists, Memoir* 31, pp. 365-404.

- 1226 Hu, Z., Gao, S., 2008. Upper crustal abundances of trace elements: a revision
1227 and update. *Chemical Geology* 253, 205-221.
- 1228 Huang, K., Malpas, J., Xenophontos, C., 2007. Geological studies of igneous
1229 rocks and their relationships along the Kyrenia Range. In: Moumani, K.,
1230 Shawabkeh, K., Al-Malabeh, A., Abdelghafoor, M. (Eds.), 6th
1231 International Congress of Eastern Mediterranean Geology, Amman,
1232 Jordan, pp. 53.
- 1233 Ingersoll, R.V., Bullard, T.F., Ford, R.L., Grimm, J.P., Pickle, J.D., Sares, S.W.,
1234 1984. The effect of grain size on detrital modes: a test of the Gazzi-
1235 Dickinson point-counting method. *Journal of Sedimentary Research* 54,
1236 103-116.
- 1237 Inwood, J., Anderson, M.W., Morris, A., Robertson, A.H.F., 2009. Successive
1238 structural events in the Hatay ophiolite of southeast Turkey:
1239 Distinguishing oceanic, emplacement and post-emplacement phases of
1240 faulting. *Tectonophysics* 473, 208-222.
- 1241 Irvine, T., Baragar, W., 1971. A guide to the chemical classification of the
1242 common volcanic rocks. *Canadian Journal of Earth Sciences* 8, 523-548.
- 1243 Karaođlan, F., Parlak, O., Hejl, E., Neubauer, F., Kloetzli, U., 2016. The
1244 temporal evolution of the active margin along the Southeast Anatolian
1245 Orogenic Belt (SE Turkey): Evidence from U–Pb, Ar–Ar and fission track
1246 chronology. *Gondwana Research* 33, 190-208.
- 1247 Karaođlan, F., Parlak, O., Robertson, A., Thöni, M., Klötzli, U., Koller, F., Okay,
1248 A.İ., 2013. Evidence of Eocene high-temperature/high-pressure
1249 metamorphism of ophiolitic rocks and granitoid intrusion related to
1250 Neotethyan subduction processes (Dođanşehir area, SE Anatolia). In:

1251 Robertson, A.H.F., Parlak, O., Ünlügenç, U.C. (Eds.), Geological
1252 Development of Anatolia and the Easternmost Mediterranean Region.
1253 Geological Society of London, Special Publications 372, pp. 249-272.

1254 Kelly, N., Hinton, R., Harley, S., Appleby, S., 2008. New SIMS U–Pb zircon
1255 ages from the Langavat Belt, South Harris, NW Scotland: implications
1256 for the Lewisian terrane model. *Journal of the Geological Society* 165,
1257 967-981.

1258 Kuno, H., 1966. Lateral variation of basalt magma type across continental
1259 margins and island arcs. *Bulletin of Volcanology* 29, 195-222.

1260 Kutterolf, S., Freundt, A., Perez, W., Mörz, T., Schacht, U., Wehrmann, H.,
1261 Schmincke, H.U., 2008a. Pacific offshore record of plinian arc volcanism
1262 in Central America: 2. Tephra volumes and erupted masses.
1263 *Geochemistry, Geophysics, Geosystems* 9, Q02S02,
1264 doi:10.1029/2007GC001791.

1265 Kutterolf, S., Freundt, A., Pérez, W., Mörz, T., Schacht, U., Wehrmann, H.,
1266 Schmincke, H.U., 2008b. Pacific offshore record of plinian arc volcanism
1267 in Central America: 1. Along-arc correlations. *Geochemistry,*
1268 *Geophysics, Geosystems* 9, Q02S01, doi:10.1029/2007GC001631.

1269 Kutterolf, S., Schindlbeck, J., Robertson, A., Avery, A., Baxter, A., Petronotis,
1270 K., Wang, K.L., 2018. Tephrostratigraphy and Provenance From IODP
1271 Expedition 352, Izu-Bonin Arc: Tracing Tephra Sources and Volumes
1272 From the Oligocene to Recent. *Geochemistry, Geophysics, Geosystems*
1273 19, 150-174.

1274 Kutterolf, S., Schindlbeck, J.C., Scudder, R.P., Murray, R.W., Pickering, K.T.,
1275 Freundt, A., Labanieh, S., Heydolph, K., Saito, S., Naruse, H.,

1276 Underwood, M.B., Wu, H., 2014. Large volume submarine ignimbrites in
1277 the Shikoku Basin: An example for explosive volcanism in the Western
1278 Pacific during the Late Miocene. *Geochemistry, Geophysics,*
1279 *Geosystems* 15, 1837-1851.

1280 Lapierre, H., 1968. Découverte d'une série volcanosédimentaire probablement
1281 d'âge Crétacé supérieur au SW de l'île de Chypre. *Comptes Rendus de*
1282 *l'Académie des Sciences* D266, 1876-1878.

1283 Lapierre, H., 1975. Les Formations Sédimentaires et Éruptives Des Nappes de
1284 Mamonía et Leurs Relations Avec Le Massif Du Troodos (Chypre
1285 Occidentale). *Mémoires de la Société géologique de France* 123, Paris,
1286 131 pp.

1287 Lapierre, H., Bosch, D., Narros, A., Mascle, G., Tardy, M., Demant, A., 2007.
1288 The Mamonía Complex (SW Cyprus) revisited: remnant of Late Triassic
1289 intra-oceanic volcanism along the Tethyan southwestern passive margin.
1290 *Geological Magazine* 144, 1-19.

1291 Le Bas, M.J., Le Maitre, R., Streckeisen, A., Zanettin, B., 1986. A chemical
1292 classification of volcanic rocks based on the total alkali-silica diagram.
1293 *Journal of Petrology* 27, 745-750.

1294 Leake, B.E., Woolley, A.R., Arps, C.E.S., Birch, W.D., Gilbert, M.C., Grice, J.D.,
1295 Hawthorne, F.C., Kato, A., Kisch, H.J., Krivovichev, V.G., Linthout, K.,
1296 Laird, J., Mandarino, J.A., Maresch, W.V., Nickel, E.H., Rock, N.M.S.,
1297 Schumacher, J.C., Smith, D.C., Stephenson, N.C.N., Ungaretti, L.,
1298 Whittaker, E.J.W., Youzhi, G., 1997. Nomenclature of amphiboles:
1299 report of the subcommittee on amphiboles of the International

1300 Mineralogical Association, Commission on New Minerals and Mineral
1301 Names. *Mineralogical Magazine* 61, 295-321.

1302 Lord, A.R., Panayides, I., Urquhart, E., Xenophontos, C., 2000. A
1303 biochronostratigraphical framework for the Late Cretaceous-Recent
1304 circum-Troodos sedimentary sequence, Cyprus. In: Panayides, I.,
1305 Xenophontos, C., Malpas, J. (Eds.), *Proceedings of the Third
1306 International Conference on the Geology of the Eastern Mediterranean*.
1307 Cyprus Geological Survey Department, Nicosia, Cyprus, pp. 289-298.

1308 Lowe, D.J., Shane, P.A., Alloway, B.V., Newnham, R.M., 2008. Fingerprints
1309 and age models for widespread New Zealand tephra marker beds
1310 erupted since 30,000 years ago: a framework for NZ-INTIMATE.
1311 *Quaternary Science Reviews* 27, 95-126.

1312 Ludwig, K.R., 2012. Users manual for Isoplot 3.75. Berkeley Geochronology
1313 Centre Special Publication No. 5, 75 pp.

1314 MacLeod, C.J., 1990. Role of the Southern Troodos Transform Fault in the
1315 rotation of the Cyprus microplate: evidence from the Eastern Limassol
1316 Forest Complex. In: Malpas, J., Moores, E.M., Panayiotou, A.,
1317 Xenophontos, C. (Eds.), *Ophiolites oceanic crustal analogues:
1318 proceedings of the symposium 'Troodos 1987'*. Cyprus Geological
1319 Survey Department, Nicosia, Cyprus, pp. 75-86.

1320 MacLeod, C.J., Murton, B.J., 1993. Structure and tectonic evolution of the
1321 Southern Troodos Transform Fault Zone, Cyprus. In: Prichard, H.M.,
1322 Alabaster, T., Harris, N.B., Neary, C.R. (Eds.), *Magmatic Processes and
1323 Plate Tectonics*. Geological Society of London, Special Publications 76,
1324 pp. 141-176.

- 1325 Malpas, J., Calon, T., Squires, G., 1993. The development of a late Cretaceous
1326 microplate suture zone in SW Cyprus. In: Prichard, H.M., Alabaster, T.,
1327 Harris, N.B., Neary, C.R. (Eds.), *Magmatic Processes and Plate*
1328 *Tectonics*. Geological Society of London, Special Publications 76, pp.
1329 177-195.
- 1330 Malpas, J., Xenophontos, C., Williams, D., 1992. The Ayia Varvara Formation
1331 of SW Cyprus: A product of complex collisional tectonics.
1332 *Tectonophysics* 212, 193-211.
- 1333 Marsaglia, K.M., 1992. Petrography and provenance of volcanoclastic sands
1334 recovered from the Izu-Bonin Arc, Leg 126. In: Taylor, B., Fujioka, K., et
1335 al. (Eds.), *Proceedings of the Ocean Drilling Program, Scientific Results*
1336 *126*. Ocean Drilling Program, College Station, TX, pp. 139-154.
- 1337 Marsaglia, K.M., Barone, M., Critelli, S., Busby, C., Fackler-Adams, B., 2016.
1338 Petrography of volcanoclastic rocks in intra-arc volcano-bounded to fault-
1339 bounded basins of the Rosario segment of the Lower Cretaceous Alisitos
1340 oceanic arc, Baja California, Mexico. *Sedimentary Geology* 336, 138-
1341 146.
- 1342 Marsaglia, K.M., Ingersoll, R.V., 1992. Compositional trends in arc-related,
1343 deep-marine sand and sandstone: a reassessment of magmatic-arc
1344 provenance. *Geological Society of America Bulletin* 104, 1637-1649.
- 1345 Mason, B.G., Pyle, D.M., Oppenheimer, C., 2004. The size and frequency of
1346 the largest explosive eruptions on Earth. *Bulletin of Volcanology* 66, 735-
1347 748.

- 1348 McBride, E.F., 1963. A classification of common sandstones. *Journal of*
1349 *Sedimentary Research* 33, 664-669.
- 1350 McCay, G.A., Robertson, A.H.F., 2013. Upper Miocene–Pleistocene
1351 deformation of the Girne (Kyrenia) Range and Dar Dere (Ovgos)
1352 lineaments, northern Cyprus: role in collision and tectonic escape in the
1353 easternmost Mediterranean region. In: Robertson, A.H.F., Parlak, O.,
1354 Ünlügenç, U.C. (Eds.), *Geological Development of Anatolia and the*
1355 *Easternmost Mediterranean Region*. Geological Society, London,
1356 *Special Publications* 372, pp. 421-445.
- 1357 McLennan, S.M., Hemming, S., McDaniel, D., Hanson, G., 1993. Geochemical
1358 approaches to sedimentation, provenance, and tectonics. In: Johnsson,
1359 M.J., Basu, A. (Eds.), *Processes Controlling the Composition of Clastic*
1360 *Sediments*. Geological Society of America, *Special Paper* 284, pp. 21-
1361 40.
- 1362 McLennan, S.M., Taylor, S., Eriksson, K., 1983. Geochemistry of Archean
1363 shales from the Pilbara Supergroup, western Australia. *Geochimica et*
1364 *Cosmochimica Acta* 47, 1211-1222.
- 1365 McLennan, S.M., Taylor, S., McCulloch, M., Maynard, J., 1990. Geochemical
1366 and Nd-Sr isotopic composition of deep-sea turbidites: crustal evolution
1367 and plate tectonic associations. *Geochimica et Cosmochimica Acta* 54,
1368 2015-2050.
- 1369 McLennan, S.M., Taylor, S.R., 1984. Archean sedimentary rocks and their
1370 relation to the composition of the Archean continental crust. In: Kröner,
1371 A., Hanson, G.N., Goodwin, A.M. (Eds.), *Archean geochemistry: the*

1372 origin and evolution of the Archaean continental crust. Springer-Verlag,
1373 Berlin, pp. 47-72.

1374 Mercier, J., Vergely, P., Delibassis, N., 1973. Comparison between deformation
1375 deduced from the analysis of recent faults and from focal mechanisms
1376 of earthquakes (an example: the Paphos region, Cyprus).
1377 Tectonophysics 19, 315-332.

1378 Moore, J.G., Nakamura, K., Alcaraz, A., 1966. The 1965 Eruption of Taal
1379 Volcano. Science 151, 955-960.

1380 Moore, T.A., 1960. The geology and mineral resources of the Astromeritis-
1381 Kormakiti area. Geological Survey Department, Memoir 6, Nicosia,
1382 Cyprus, 96 pp.

1383 Moores, E.M., Vine, F.J., 1971. The Troodos Massif, Cyprus and other
1384 ophiolites as oceanic crust: evaluation and implications. Philosophical
1385 Transactions of the Royal Society of London. Series A, Mathematical
1386 and Physical Sciences 268, 443-466.

1387 Morag, N., Haviv, I., Katzir, Y., 2016. From ocean depths to mountain tops:
1388 Uplift of the Troodos ophiolite (Cyprus) constrained by low-temperature
1389 thermochronology and geomorphic analysis. Tectonics 35, 622-637.

1390 Morimoto, N., 1988. Nomenclature of pyroxenes. Mineralogy and Petrology 39,
1391 55-76.

1392 Morris, A., 1996. A review of palaeomagnetic research in the Troodos ophiolite,
1393 Cyprus. In: Morris, A., Tarling, D.H. (Eds.), Palaeomagnetism and
1394 Tectonics of the Mediterranean Region. Geological Society of London,
1395 Special Publications 105, pp. 311-324.

- 1396 Morris, A., Anderson, M.W., Robertson, A.H.F., 1998. Multiple tectonic rotations
1397 and transform tectonism in an intraoceanic suture zone, SW Cyprus.
1398 *Tectonophysics* 299, 229-253.
- 1399 Morris, A., Creer, K.M., Robertson, A.H.F., 1990. Palaeomagnetic evidence for
1400 clockwise rotations related to dextral shear along the southern Troodos
1401 transform fault, Cyprus. *Earth and Planetary Science Letters* 99, 250-
1402 262.
- 1403 Morris, A., Robertson, A.H.F., Anderson, M.W., Hodgson, E., 2015. Did the
1404 Kyrenia Range of northern Cyprus rotate with the Troodos–Hatay
1405 microplate during the tectonic evolution of the eastern Mediterranean?
1406 *International Journal of Earth Sciences* 105, 399-415.
- 1407 Mukasa, S.B., Ludden, J.N., 1987. Uranium-lead isotopic ages of
1408 plagiogranites from the Troodos ophiolite, Cyprus, and their tectonic
1409 significance. *Geology* 15, 825-828.
- 1410 Murton, B., 1986. Anomalous oceanic lithosphere formed in a leaky transform
1411 fault: evidence from the Western Limassol Forest Complex, Cyprus.
1412 *Journal of the Geological Society* 143, 845-854.
- 1413 Murton, B.J., Cass, I.G., 1986. Western Limassol Forest complex, Cyprus: part
1414 of an Upper Cretaceous leaky transform fault. *Geology* 14, 255-258.
- 1415 Nesbitt, H.W., Markovics, G., Price, R.C., 1980. Chemical processes affecting
1416 alkalis and alkaline earths during continental weathering. *Geochimica et*
1417 *Cosmochimica Acta* 44, 1659-1666.
- 1418 Nielsen, C.H., Sigurdsson, H., 1981. Quantitative methods for electron
1419 microprobe analysis of sodium in natural and synthetic glasses.
1420 *American Mineralogist* 66, 547-552.

1421 Ninkovich, D., Sparks, R., Ledbetter, M., 1978. The exceptional magnitude and
1422 intensity of the Toba eruption, Sumatra: an example of the use of deep-
1423 sea tephra layers as a geological tool. *Bulletin of Volcanology* 41, 286-
1424 298.

1425 Nisbet, E.G., Pearce, J.A., 1977. Clinopyroxene composition in mafic lavas
1426 from different tectonic settings. *Contributions to Mineralogy and*
1427 *Petrology* 63, 149-160.

1428 Nishimura, A., Marsaglia, K.M., Rodolfo, K.S., Colella, A., Hiscott, R.N., Tazaki,
1429 K., Gill, J.B., Janecek, T., Firth, J., Isiminger-Kelso, M., Herman, Y.,
1430 Taylor, R.N., Taylor, B., Fujioka, K., Leg 126 Scientific Party, 1991.
1431 Pliocene-quaternary submarine pumice deposits in the Sumisu Rift area,
1432 Izu-Bonin Arc. In: Fisher, R.V., Smith, G.A. (Eds.), *Sedimentation in*
1433 *Volcanic Settings. Society of Economic Paleontologists and*
1434 *Mineralogists Special Publication* 45, pp. 201-208.

1435 Ogawa, Y., Horiuchi, K., Taniguchi, H., Naka, J., 1985. Collision of the Izu arc
1436 with Honshu and the effects of oblique subduction in the Miura-Boso
1437 Peninsulas. *Tectonophysics* 119, 349-379.

1438 Ogawa, Y., Takami, Y., Takazawa, S., 2008. Oblique subduction in an island
1439 arc collision setting: unique sedimentation, accretion, and deformation
1440 processes in the Boso TTT-type triple junction area, NW Pacific. In:
1441 Draut, A.E., Clift, P.D., Scholl, W.D. (Eds.), *Formation and Applications*
1442 *of the Sedimentary Record in Arc Collision Zones. Geological Society of*
1443 *America, Special Paper* 436, pp. 155-170.

1444 Parlak, O., 2006. Geodynamic significance of granitoid magmatism in the
1445 southeast Anatolian orogen: geochemical and geochronological evidence

1446 from Göksun–Afşin (Kahramanmaraş, Turkey) region. *International*
1447 *Journal of Earth Sciences* 95, 609-627.

1448 Patino, L.C., Carr, M.J., Feigenson, M.D., 2000. Local and regional variations
1449 in Central American arc lavas controlled by variations in subducted
1450 sediment input. *Contributions to Mineralogy and Petrology* 138, 265-283.

1451 Payne, A.S., Robertson, A.H.F., 1995. Neogene supra-subduction zone
1452 extension in the Polis graben system, west Cyprus. *Journal of the*
1453 *Geological Society* 152, 613-628.

1454 Payne, A.S., Robertson, A.H.F., 2000. Structural evolution and regional
1455 significance of the Polis graben system, western Cyprus. In: Panayides,
1456 I., Xenophontos, C., Malpas, J. (Eds.), *Proceedings of the Third*
1457 *International Conference on the Geology of the Eastern Mediterranean*.
1458 Cyprus Geological Survey Department, Nicosia, Cyprus, pp. 45-60.

1459 Pearce, J.A., 1983. Role of the sub-continental lithosphere in magma genesis
1460 at active continental margins. In: Hawkersworth, C.J., Norry, M.J. (Eds.),
1461 *Continental Basalts and Mantle Xenoliths*. Shiva, Cheshire, UK, pp. 230-
1462 249.

1463 Pearce, J.A., Robinson, P.T., 2010. The Troodos ophiolitic complex probably
1464 formed in a subduction initiation, slab edge setting. *Gondwana Research*
1465 18, 60-81.

1466 Pickering, K., Hiscott, R., 2016. *Deep Marine Systems: Processes, Deposits,*
1467 *Environments, Tectonics and Sedimentation*. Wiley, Chichester, UK, 672
1468 pp.

1469 Piper, D.J., von Huene, R., Duncan, J.R., 1973. Late Quaternary sedimentation
1470 in the active eastern Aleutian Trench. *Geology* 1, 19-22.

- 1471 Plafker, G., Nokleberg, W., Lull, J., 1989. Bedrock geology and tectonic
1472 evolution of the Wrangellia, Peninsular, and Chugach terranes along the
1473 Trans-Alaska Crustal Transect in the Chugach Mountains and southern
1474 Copper River Basin, Alaska. *Journal of Geophysical Research: Solid*
1475 *Earth* 94, 4255-4295.
- 1476 Plank, T., 2005. Constraints from Thorium/Lanthanum on Sediment Recycling
1477 at Subduction Zones and the Evolution of the Continents. *Journal of*
1478 *Petrology* 46, 921-944.
- 1479 Poisson, A., 1977. *Récherches Géologiques dans les Taurides Occidentales,*
1480 *Turquie. Doctor of Science Thesis (published). Université Paris-Sud,*
1481 *France, 795 pp.*
- 1482 Poole, A.J., Robertson, A.H.F., 1998. Pleistocene fanglomerate deposition
1483 related to uplift of the Troodos Ophiolite, Cyprus. In: Robertson, A.H.F.,
1484 Emeis, K., Richter, C., Camerlenghi, A. (Eds.), *Proceedings of the*
1485 *Ocean Drilling Program, Scientific Results 160. Ocean Drilling Program,*
1486 *College Station, TX, pp. 544-568.*
- 1487 Pyle, D.M., 1989. The thickness, volume and grainsize of tephra fall deposits.
1488 *Bulletin of Volcanology* 51, 1-15.
- 1489 Rızaoğlu, T., Parlak, O., Höck, V., Koller, F., Hames, W.E., Billor, Z., 2009.
1490 Andean-type active margin formation in the eastern Taurides:
1491 Geochemical and geochronological evidence from the Baskil granitoid
1492 (Elazığ, SE Turkey). *Tectonophysics* 473, 188-207.
- 1493 Robertson, A.H.F., 1975. Cyprus umbers: basalt-sediment relationships on a
1494 Mesozoic ocean ridge. *Journal of the Geological Society* 131, 511-531.

- 1495 Robertson, A.H.F., 1976. Pelagic chalks and calciturbidites from the lower
1496 Tertiary of the Troodos Massif, Cyprus. *Journal of Sedimentary*
1497 *Research* 46, 1007-1016.
- 1498 Robertson, A.H.F., 1977a. The Kannaviou Formation, Cyprus: volcanoclastic
1499 sedimentation of a probable Late Cretaceous volcanic arc. *Journal of the*
1500 *Geological Society* 134, 269-292.
- 1501 Robertson, A.H.F., 1977b. The Moni Melange, Cyprus: an olistostrome formed
1502 at a destructive plate margin. *Journal of the Geological Society* 133, 447-
1503 466.
- 1504 Robertson, A.H.F., 1977c. Tertiary uplift history of the Troodos massif, Cyprus.
1505 *Geological Society of America Bulletin* 88, 1763-1772.
- 1506 Robertson, A.H.F., 1990. Tectonic evolution of Cyprus. In: Malpas, J., Moores,
1507 E.M., Panayiotou, A., Xenophontos, C. (Eds.), *Ophiolites-Oceanic*
1508 *Crustal Analogues: Proceedings of the International Symposium*
1509 *'Troodos 1987'*. Cyprus Geological Survey Department, Nicosia, Cyprus,
1510 pp. 235-250.
- 1511 Robertson, A.H.F., 2002. Overview of the genesis and emplacement of
1512 Mesozoic ophiolites in the Eastern Mediterranean Tethyan region. *Lithos*
1513 65, 1-67.
- 1514 Robertson, A.H.F., Degnan, P., 1994. The Dras arc complex: lithofacies and
1515 reconstruction of a Late Cretaceous oceanic volcanic arc in the Indus
1516 suture zone, Ladakh Himalaya. *Sedimentary Geology* 92, 117-145.
- 1517 Robertson, A.H.F., Hudson, J.D., 1974. Pelagic sediments in the Cretaceous
1518 and Tertiary history of the Troodos Massif, Cyprus. In: Hsü, K.J.,

1519 Jenkyns, H.C. (Eds.), *Pelagic Sediments: on Land and Under the Sea*.
1520 Blackwell Scientific Publications, Oxford, pp. 403-436.

1521 Robertson, A.H.F., Kinnaird, T.C., 2016. Structural development of the central
1522 Kyrenia Range (north Cyprus) in its regional setting in the eastern
1523 Mediterranean region. *International Journal of Earth Sciences* 105, 417-
1524 437.

1525 Robertson, A.H.F., Kutterolf, S., Avery, A., Baxter, A.T., Petronotis, K., Acton,
1526 G.D., Carvallo, C., Schindlbeck, J.C., 2018. Depositional setting,
1527 provenance, and tectonic-volcanic setting of Eocene–Recent deep-sea
1528 sediments of the oceanic Izu–Bonin forearc, northwest Pacific (IODP
1529 Expedition 352). *International Geology Review* 60, 1816-1854.

1530 Robertson, A.H.F., McCay, G.A., Tasli, K., Yıldız, A., 2014. Eocene
1531 development of the northerly active continental margin of the Southern
1532 Neotethys in the Kyrenia Range, north Cyprus. *Geological Magazine*
1533 151, 692-731.

1534 Robertson, A.H.F., Palamakumbura, R.N., 2019. Geological development and
1535 regional significance of an oceanic magmatic arc and its sedimentary
1536 cover: Permian Brook Street Terrane, South Island, New Zealand. In:
1537 Robertson, A.H.F. (Ed.), *Paleozoic-Mesozoic Geology of South Island,*
1538 *New Zealand: Subduction-related Processes Adjacent to SE Gondwana.*
1539 *Geological Society of London, Memoirs* 49 (in press).

1540 Robertson, A.H.F., Palamakumbura, R.N., Campbell, H., 2019. Permian-
1541 Triassic felsic tuffs in South Island, New Zealand: significance for
1542 oceanic and active continental margin subduction. In: Robertson, A.H.F.
1543 (Ed.), *Paleozoic-Mesozoic Geology of South Island, New Zealand:*

1544 Subduction-related Processes Adjacent to SE Gondwana. Geological
1545 Society of London, Memoirs 49 (in press).

1546 Robertson, A.H.F., Parlak, O., Rizaoglu, T., Ünlügenç, Ü., İnan, N., Tasli, K.,
1547 Ustaömer, T., 2007. Tectonic evolution of the South Tethyan ocean:
1548 evidence from the Eastern Taurus Mountains (Elaziğ region, SE Turkey).
1549 In: Ries, A.C., Butler, R.W.H., Graham, R.H. (Eds.), Deformation of the
1550 Continental Crust: The Legacy of Mike Coward. Geological Society of
1551 London, Special Publications 272, pp. 231-270.

1552 Robertson, A.H.F., Tasli, K., İnan, N., 2012. Evidence from the Kyrenia Range,
1553 Cyprus, of the northerly active margin of the Southern Neotethys during
1554 Late Cretaceous–Early Cenozoic time. Geological Magazine 149, 264-
1555 290.

1556 Robertson, A.H.F., Ustaömer, T., Parlak, O., Ünlügenç, U.C., Taşlı, K., İnan, N.,
1557 2006. The Berit transect of the Tauride thrust belt, S Turkey: Late
1558 Cretaceous–Early Cenozoic accretionary/collisional processes related
1559 to closure of the Southern Neotethys. Journal of Asian Earth Sciences
1560 27, 108-145.

1561 Robertson, A.H.F., Woodcock, N.H., 1979. Mamonía Complex, southwest
1562 Cyprus: Evolution and emplacement of a Mesozoic continental margin.
1563 Geological Society of America Bulletin 90, 651-665.

1564 Robertson, A.H.F., Woodcock, N.H., 1986. The role of the Kyrenia Range
1565 Lineament, Cyprus, in the geological evolution of the eastern
1566 Mediterranean area. Philosophical Transactions of the Royal Society of
1567 London. Series A, Mathematical and Physical Sciences 317, 141-177.

1568 Robertson, A.H.F., Xenophontos, C., 1993. Development of concepts
1569 concerning the Troodos ophiolite and adjacent units in Cyprus. n:
1570 Prichard, H.M., Alabaster, T., Harris, N.B.W., Neary, C.R. (Eds.),
1571 Magmatic Processes and Plate Tectonics. Geological Society of London,
1572 Special Publications 76, pp. 85-119.

1573 Robinson, P.T., Malpas, J., 1990. The Troodos ophiolite of Cyprus: new
1574 perspectives on its origin and emplacement. In: Malpas, J., Moores, E.M.,
1575 Panayiotou, A., Xenophontos, C. (Eds.), Ophiolites, Oceanic Crustal
1576 Analogues. Cyprus Geological Survey Department, Nicosia, Cyprus, pp.
1577 13-26.

1578 Roser, B.P., Korsch, R.J., 1986. Determination of tectonic setting of sandstone-
1579 mudstone suites using SiO₂ content and K₂O/Na₂O ratio. The Journal of
1580 Geology 94, 635-650.

1581 Rubatto, D., 2002. Zircon trace element geochemistry: partitioning with garnet
1582 and the link between U–Pb ages and metamorphism. Chemical Geology
1583 184, 123-138.

1584 Rudnick, R., Gao, S., 2003. Composition of the continental crust. In: Holland,
1585 H.D., Turekian, K.K. (Eds.), Treatise on Geochemistry 3, Elsevier-
1586 Pergamon, Oxford, pp. 1-64.

1587 Schindlbeck, J.C., Kutterolf, S., Freundt, A., Alvarado, G., Wang, K.L., Straub,
1588 S., Hemming, S., Frische, M., Woodhead, J., 2016. Late Cenozoic
1589 tephrostratigraphy offshore the southern Central American Volcanic Arc:
1590 1. Tephra ages and provenance. Geochemistry, Geophysics,
1591 Geosystems 17, 4641-4668.

1592 Schindlbeck, J.C., Kutterolf, S., Freundt, A., Scudder, R., Pickering, K.T.,
1593 Murray, R., 2013. Emplacement processes of submarine volcanoclastic
1594 deposits (IODP Site C0011, Nankai Trough). *Marine Geology* 343, 115-
1595 124.

1596 Schweller, W.J., Kulm, L.D., Prince, R.A., 1981. Tectonics, structure, and
1597 sedimentary framework of the Peru-Chile Trench. In: Kulm, L.V.D.,
1598 Dymond, J., Dasch, E.J., Hussong, D.M., Roderick, R. (Eds.), *Nazca
1599 Plate: Crustal Formation and Andean Convergence*. Geological Society
1600 of America Memoirs 154, pp. 323-349.

1601 Söderlund, U., Hofmann, A., Klausen, M.B., Olsson, J.R., Ernst, R.E., Persson,
1602 P.-O., 2010. Towards a complete magmatic barcode for the Zimbabwe
1603 craton: Baddeleyite U–Pb dating of regional dolerite dyke swarms and
1604 sill complexes. *Precambrian Research* 183, 388-398.

1605 Spandler, C., Worden, K., Arculus, R., Eggins, S., 2005. Igneous rocks of the
1606 Brook Street Terrane, New Zealand: implications for Permian tectonics
1607 of eastern Gondwana and magma genesis in modern intra-oceanic
1608 volcanic arcs. *New Zealand Journal of Geology and Geophysics* 48, 167-
1609 183.

1610 Stern, R.J., Fouch, M.J., Klemperer, S.L., 2003. An overview of the Izu-Bonin-
1611 Mariana subduction factory. In: Eiler, J. (Ed.), *Inside the Subduction
1612 Factory*. American Geophysical Union 138, Washington, D. C., pp. 175-
1613 222.

1614 Straub, S.M., 2003. The evolution of the Izu Bonin - Mariana volcanic arcs (NW
1615 Pacific) in terms of major element chemistry. *Geochemistry, Geophysics,
1616 Geosystems* 4, 1018, doi:10.1029/2002GC000357.

1617 Straub, S.M., Layne, G.D., 2003. Decoupling of fluids and fluid-mobile elements
1618 during shallow subduction: Evidence from halogen-rich andesite melt
1619 inclusions from the Izu arc volcanic front. *Geochemistry, Geophysics,*
1620 *Geosystems* 4, 9003, doi:10.1029/2002GC000349.

1621 Sun, S.-s., McDonough, W.F., 1989. Chemical and isotopic systematics of
1622 oceanic basalts: implications for mantle composition and processes. In:
1623 Saunders, A.D., Norry, M.J. (Eds.), *Magmatism in the Ocean Basins.*
1624 Geological Society of London, Special Publications 42, pp. 313-345.

1625 Swarbrick, R.E., 1980. The Mamonia complex of S.W. Cyprus: a Mesozoic
1626 continental margin and its relationship to the Troodos Complex. In:
1627 Panayiotou, A. (Ed.), *Ophiolites: Proceedings of the International*
1628 *Ophiolite Symposium.* Cyprus Ministry of Agriculture and Natural
1629 Resources, Geology Survey Department, Nicosia, Cyprus, pp. 86-92.

1630 Swarbrick, R.E., 1993. Sinistral strike-slip and transpressional tectonics in an
1631 ancient oceanic setting: the Mamonia Complex, southwest Cyprus.
1632 *Journal of the Geological Society* 150, 381-392.

1633 Swarbrick, R.E., Naylor, M.A., 1980. The Kathikas melange, SW Cyprus: late
1634 Cretaceous submarine debris flows. *Sedimentology* 27, 63-78.

1635 Swarbrick, R.E., Robertson, A.H.F., 1980. Revised stratigraphy of the Mesozoic
1636 rocks of southern Cyprus. *Geological Magazine* 117, 547-563.

1637 Taylor, S.R., McLennan, S.M., 1985. *The Continental Crust: its Composition*
1638 *and Evolution.* Blackwell Scientific Publications, United States, 312 pp.

1639 Torley, J.M., Robertson, A.H.F., 2018. New evidence and interpretation of
1640 facies, provenance and geochemistry of late Triassic-early Cretaceous
1641 Tethyan deep-water passive margin-related sedimentary rocks (Ayios

1642 Photios Group), SW Cyprus in the context of eastern Mediterranean
1643 geodynamics. *Sedimentary Geology* 377, 82-110.

1644 Ulmer-Scholle, D.S., Scholle, P.A., Schieber, J., Raine, R.J., 2015. A color
1645 guide to the petrography of sandstones, siltstones, shales and
1646 associated rocks. American Association of Petroleum Geologists,
1647 Memoir 109, Tulsa, 509 pp.

1648 Urquhart, E., Banner, F.T., 1994. Biostratigraphy of the supra-ophiolite
1649 sediments of the Troodos Massif, Cyprus: the Cretaceous Perapedhi,
1650 Kannaviou, Moni and Kathikas formations. *Geological Magazine* 131,
1651 499-518.

1652 Ustaömer, P.A., Ustaömer, T., Robertson, A., 2012. Ion probe U-Pb dating of
1653 the Central Sakarya basement: a peri-Gondwana terrane intruded by
1654 late Lower Carboniferous subduction/collision-related granitic rocks.
1655 *Turkish Journal of Earth Sciences* 21, 905-932.

1656 Van der Plas, L., Tobi, A., 1965. A chart for judging the reliability of point
1657 counting results. *American Journal of Science* 263, 87-90.

1658 Watkins, N., Sparks, R., Sigurdsson, H., Huang, T., Federman, A., Carey, S.,
1659 Ninkovich, D., 1978. Volume and extent of the Minoan tephra from
1660 Santorini Volcano: new evidence from deep-sea sediment cores. *Nature*
1661 271, 122-126.

1662 Woodhead, J., Eggins, S., Gamble, J., 1993. High field strength and transition
1663 element systematics in island arc and back-arc basin basalts: evidence
1664 for multi-phase melt extraction and a depleted mantle wedge. *Earth and*
1665 *Planetary Science Letters* 114, 491-504.

1666 Wronkiewicz, D.J., Condie, K.C., 1987. Geochemistry of Archean shales from
1667 the Witwatersrand Supergroup, South Africa: source-area weathering
1668 and provenance. *Geochimica et Cosmochimica Acta* 51, 2401-2416.

1669 Yamamoto, T., 2009. Sedimentary processes caused by felsic caldera-forming
1670 volcanism in the Late Miocene to Early Pliocene intra-arc Aizu basin, NE
1671 Japan arc. *Sedimentary Geology* 220, 337-348.

1672

1673 Listing of Figures

1674 Fig. 1. (a) Simplified map showing Cyprus in the eastern Mediterranean. The
1675 locations of the late Cretaceous volcanogenic sediments (FF; blue box) in the
1676 Kyrenia Range, northern Cyprus and the late Cretaceous arc-related rocks in
1677 southeast Turkey (green box) are indicated; (b) Outline geological map of
1678 western Cyprus, showing the main outcrops of the late Cretaceous Kannaviou
1679 Formation, and their relationship to the Troodos ophiolite and Mamonia
1680 Complex (modified after Robertson, 1977a; Robertson and Woodcock, 1979;
1681 Swarbrick, 1980). Abbreviations: STTFZ, South Troodos Transform Fault Zone;
1682 FF, Fourkovouno (Selvilitepe) Formation.

1683 Fig. 2. Main geological units in western Cyprus; see Fig. 4 for detailed
1684 sedimentary logs of local successions and keys (data from Robertson, 1977a,
1685 and this study).

1686 Fig. 3. Geological map of the main outcrop of the Kannaviou Formation near
1687 Kannaviou village (modified from Lapierre, 1975). Stratigraphic sections (a-d)
1688 are indicated. Dash lines for generalised sections; solid lines for measured
1689 sections.

1690 Fig. 4. Summary logs showing local facies and thickness variations. See Fig. 3
1691 for locations of sections a-d and the Supplementary material for e-j. Dash lines
1692 for generalised sections; solid lines for measured sections.

1693 Fig. 5. Field photographs of the Kannaviou Formation. (a) Volcanogenic clay
1694 and siltstone with interspersed lenticular volcanoclastic sandstone, 1 km ENE of
1695 Kannaviou village. Samples (nos. 16-04, 16-13) are from this outcrop; (b) Thick-
1696 bedded, lenticular sandstone, interbedded with claystone and mudstone;
1697 overlying the uppermost Troodos extrusives (lava breccias) near the
1698 Paleomylon River (see section in Fig. 4b). Samples 16-16, 18.4 and 18.5 are
1699 from this section; (c) Bioturbation on bedding surface (<3 cm long) (see Fig. 5a
1700 for location); (d) Matrix-supported basaltic breccia (hyaloclastite) with
1701 palagonite clasts; within lenticular volcanoclastic sandstone (see Fig. 5b for
1702 location); (e) Sandstone showing convolute lamination and slumping, 1 km
1703 WNW of Istinjo (see section in Fig. 4h); (f) Lenticular (channelised) sandstone,
1704 up to 20 m thick, occupying the upper part of the succession, 1 km NNW of
1705 Lasa.

1706 Fig. 6. Photomicrographs of the Kannaviou Formation sandstones. (a) Microlitic
1707 volcanic fragment (Lvf). Surrounding detrital grains include volcanic glass (Vg),
1708 pyroxene (Px) and feldspar (Fg) (cross-polarised light); (b) Foliated, detrital
1709 mica-schist fragments (Lm) composed of quartz and muscovite (cross-
1710 polarised light); (c) Angular chert fragment (Ls) (plane-polarised light); (d) Well-
1711 preserved radiolarians (R) and planktic foraminifera (F) from the upper part of
1712 the succession (plane-polarised light). Sandstone sample number is indicated
1713 in the top-left corner.

1714 Fig. 7. Optical micrographs (a-i) and scanning electron micrographs (j-l) of
1715 Kannaviou Formation sandstones illustrating glass shards: (a-f) and (j-l) near
1716 Kannaviou village; (g) near the Paleomylon River; (h-i) south of Lapithiou.
1717 Sandstone sample number is indicated in the top-left corner. (a) subangular,
1718 highly vesicular, pumiceous glass; (b) angular blocky and cusplate bubble-wall
1719 shards; (c) cusplate shard; (d) pinkish (mafic) blocky shard with tiny tubular
1720 vesicle; (e) pinkish (mafic) and colourless (felsic) cusplate bubble-wall glass and
1721 spindle-like glass; (f) subrounded, 'frothy' glass shard; (g) thin tubular vesicle;
1722 (h) subrounded, brownish glass (mafic); (i) subangular to subrounded blocky
1723 glass (felsic) with microlitic texture; (j) conchoidal glassy fracture surface of
1724 vesicular pumice; (k) blocky, pumiceous and cusplate glass; (l) highly vesicular
1725 bubble wall glass. Abbreviation: B, blocky; C, cusplate; F, frothy; P, pumiceous;
1726 S, spindle; T, tabular.

1727 Fig. 8. Point-count data of the Kannaviou Formation sandstones. (a) QFL
1728 (quartz-feldspar-lithic fragments) diagram for lithological classification (after
1729 McBride, 1963); (b) Ternary QFL (quartz-feldspar-lithic fragments) plot for
1730 discrimination of tectonic settings (after Dickinson et al., 1983); (c) QFL (quartz-
1731 feldspar-lithic fragments) plot with fields from Marsaglia and Ingersoll (1992) for
1732 comparison; also shown are the average data for the total dataset and the
1733 separate sample localities; (d) LmLvLs (metamorphic-volcanic-sedimentary
1734 lithic fragments) plot with fields from Marsaglia and Ingersoll (1992) for
1735 comparison; also shown are the average data for the total dataset and the
1736 separate sample localities.

1737 Fig. 9. Na₂O+K₂O vs. SiO₂ diagram for volcanic glass (after Le Bas et al., 1986).
1738 The alkaline-subalkaline boundary line is from Irvine and Baragar (1971).
1739 Values are in wt. % and recalculated on a volatile-free basis.

1740 Fig. 10. Normal mid-ocean ridge basalt (N-MORB)-normalised trace-element
1741 distributions of the volcanic glass from the Kannaviou Formation sandstones.
1742 N-MORB data after Sun and McDonough (1989).

1743 Fig. 11. Geochemical plots for mineral grains of the Kannaviou Formation
1744 sandstones. (a) Anorthite-Albite-Orthoclase ternary diagram (after Deer et al.,
1745 2013) for feldspar; (b) Pyroxene ternary diagram (after Morimoto, 1988); (c)
1746 Classification of amphibole (after Leake et al., 1997).

1747 Fig. 12. Selected cathodoluminescence images of zircon grains analysed from
1748 the Kannaviou Formation sandstones. Locations of the ion probe analysis spots
1749 and the corresponding ages ($^{206}\text{Pb}/^{238}\text{U} \pm 1\sigma$) are indicated. Scale bar=20 μm .

1750 Fig. 13. Zircon analysis from the Kannaviou Formation sandstones. (a) An
1751 enlarged plot showing 5 analyses of magmatic zircon grains from sample 14-
1752 04 near Armou village; (b) An enlarged plot showing 11 analyses of magmatic
1753 zircon grains from samples near the Kannaviou village; (c) Wetherill Concordia
1754 diagram for the combined 8 concordant analyses, yielding a $^{206}\text{Pb}/^{238}\text{U}$ age of
1755 80.44 ± 1.0 Ma. One analysis (zircon 7; black arrow) with an apparently old age
1756 was excluded for Fig. 13d; (d) $^{206}\text{Pb}/^{238}\text{U}$ weighted mean diagram for zircon.

1757 Fig. 14. Total alkali vs. silica diagram for the Kannaviou Formation sandstones
1758 (after Le Bas et al., 1986). The alkaline-subalkaline boundary line is from Irvine
1759 and Baragar (1971).

1760 Fig. 15. Upper continental crust (UCC)-normalised multi-element diagrams for
1761 sandstones from the Kannaviou Formation. Grey shaded areas indicate the
1762 total range of data. Normalising values from Rudnick and Gao (2003) and Hu
1763 and Gao (2008).

1764 Fig. 16. Chondrite-normalised REE diagrams for the Kannaviou Formation
1765 sandstones and deep-sea sands from various settings. Grey shaded areas
1766 indicate the total range of data from the Kannaviou Formation sandstones.
1767 Normalising values of chondrite are from Taylor and McLennan (1985). UCC
1768 and deep-sea sands of various settings data are from Rudnick and Gao (2003),
1769 Hu and Gao (2008) and McLennan et al. (1990), respectively.

1770 Fig. 17. Inferred palaeotopography of southwest Cyprus (see black box of inset
1771 for location) during the early Maastrichtian (in present geographical co-
1772 ordinates). The Kannaviou Formation transgresses an irregular fault-controlled
1773 ocean-floor topography, represented by the Troodos ophiolite. The fault scarps
1774 represent part of the westward extension of the South Troodos Transform Fault
1775 Zone (modified from Robertson, 1977a).

1776 Fig. 18. Geochemical plots of the Kannaviou Formation sandstones. (a)
1777 Correlation diagram of LOI vs. CaO for the whole-rock data; (b) Diagram
1778 showing the relationship between total silica contents of volcanic glass from all
1779 sites with their apparent volatile contents (100%-analytical total) (after Clift and
1780 Dixon, 1994).

1781 Fig. 19. Geochemical plots for glass and pyroxene of the Kannaviou Formation
1782 sandstones. (a) Ternary AFM ($\text{Na}_2\text{O}+\text{K}_2\text{O}-\text{FeO}-\text{MgO}$) plot showing the magma
1783 series and volcanic affinity of the glass; division between the calc-alkaline and

1784 the tholeiitic fields after Irvine and Baragar (1971); (b) U/Th vs. Th/Nb (after
1785 Bryant et al., 2003) for volcanic glass; (c) Th/La vs. Sm/La (after Plank, 2005)
1786 for volcanic glass; (d) Ternary TiO₂-MnO-Na₂O diagram for pyroxene (after
1787 Nisbet and Pearce, 1977). Abbreviations: VAB, volcanic arc basalt; OFB,
1788 ocean-floor basalt; WPA, within-plate alkali basalt; WPT, within-plate tholeiitic
1789 basalt.

1790 Fig. 20. Comparative plots for discriminating the provenance of the Kannaviou
1791 Formation sandstones. (a) Th/Sc vs. Zr/Sc diagram (after McLennan et al.,
1792 1993). Asterisks mark the average compositions of felsic volcanic rock,
1793 andesite and basalt (after Condie, 1993). Grey squares represent the average
1794 compositions of UCC (Rudnick and Gao, 2003; Hu and Gao, 2008); (b) La/Th
1795 vs. Hf diagram (after Floyd and Leveridge, 1987); (c) Ternary plot of La-Th-Sc.
1796 Values of potential source rocks (grey squares) are from McLennan and Taylor
1797 (1984).

1798 Fig. 21. Comparative chemical plots for the Kannaviou Formation. (a) Th-Sc-
1799 Zr/10 ternary plot (after Bhatia and Crook, 1986); (b) Normalised multi-element
1800 patterns for average Kannaviou Formation sandstone composition, and also for
1801 greywacke data (averaged) from different tectonic environments (after Floyd et
1802 al., 1991). Upper continental crust-normalisation values from Rudnick and Gao
1803 (2003) and from Hu and Gao (2008).

1804 Fig. 22. Variation in maximum grain size for the Toba, Campanian, and
1805 Santorini marine tephra fall layers (from Fisher and Schmincke, 1984).
1806 Horizontal lines with arrows show the maximum feldspar crystal sizes in the
1807 Kannaviou Formation. Vertical dashed line corresponds to the probable

1808 distance (c. 100 km) from the source arc to the Kannaviou Formation
1809 volcanoclastic sediments.

1810 Fig. 23. Plate tectonic model for the Campanian (c. 80 Ma) arc-type magmatism
1811 in Cyprus. (a) Map view showing the Kannaviou Formation accumulates in a
1812 deep-marine forearc basin setting to the south of Tauride continental crust. This
1813 is bordered by oceanic crust and also by continental crust, represented by the
1814 Mamonia Complex (to the west), which supplies small amounts of terrigenous
1815 material, especially to the upper part of the Kannaviou Formation. The Troodos
1816 ophiolite forms by incipient spreading above a separate subduction zone farther
1817 south. (b) Cross-sections showing the Kannaviou Formation being created by
1818 arc volcanism located in a distal (southerly) part of the Tauride microcontinent.
1819 Cross-section line is indicated in Fig. 23a.

1820

1821 Listing of Tables

1822 Table 1. GPS coordinates of sample locations and summary of the types of
1823 analysis carried out on the Kannaviou Formation.

1824 Table 2. Framework parameters (with explanatory notes) of point-counted
1825 sandstones from the Kannaviou Formation.

1826 Table 3. Range of elemental ratios of the Kannaviou Formation sandstones
1827 compared to the corresponding range of ratios in sediments derived from felsic
1828 and mafic rocks.

1829

1830

1831

1832

1833 Listing of Supplementary material

1834 Supplementary Appendix A. References, standardisation protocols and errors
1835 for SIMS analysis of glass trace elements in the Kannaviou Formation.

1836 Supplementary Appendix B. Fault distribution and kinematic analysis along the
1837 southwest margin of Troodos ophiolite.

1838 Supplementary Figure 1. Geological map of the Peristerona to Lasa region
1839 showing an additional outcrop of the Kannaviou Formation in western Cyprus
1840 (modified from Lapierre, 1975). Stratigraphic sections (e-j) are indicated.

1841 Supplementary Figure 2. Stereoplots showing the orientation of fault planes and
1842 kinematic results. (a-b) near Asproyia; (c) Kannaviou Dam area; (d) Ezousa
1843 River area; (e) near Kannaviou village; (f) near Kritou Marottou; (g) west of
1844 Istinjo; (h) Zakharia area.

1845 Supplementary Figure 3. Major element binary plots of glass shards in the
1846 Kannaviou Formation sandstones.

1847 Supplementary Figure 4. Major element binary plots of the Kannaviou
1848 Formation sandstones.

1849 Supplementary Table 1. Point-count data for the Kannaviou Formation,
1850 calculated from no less than 400 points. For framework parameters (with
1851 explanatory notes) see Table 2.

1852 Supplementary Table 2. Major element oxides and trace elements, analysed by
1853 XRF; also trace elements and rare earth elements analysed by ICP-MS for the
1854 Kannaviou Formation sandstones.

1855 Supplementary Table 3. Electron microprobe analyses of volcanic glass,
1856 feldspar, pyroxene and amphibole grains in the Kannaviou Formation
1857 sandstones. Major elements in wt. %.

1858 Supplementary Table 4. Analyses of trace elements in volcanic glass of the
1859 Kannaviou Formation sandstones; analysed by secondary ion mass
1860 spectrometry (SIMS). Trace elements in ppm.

1861 Supplementary Table 5. SIMS zircon U-Pb analyses of the zircon grains
1862 separated from the Kannaviou Formation sandstones.

1863 Supplementary Table 6. Table of correlation coefficients for the Kannaviou
1864 Formation sandstones.

1865

1866

1867

1868

1869

Fig. 1

[Click here to download high resolution image](#)

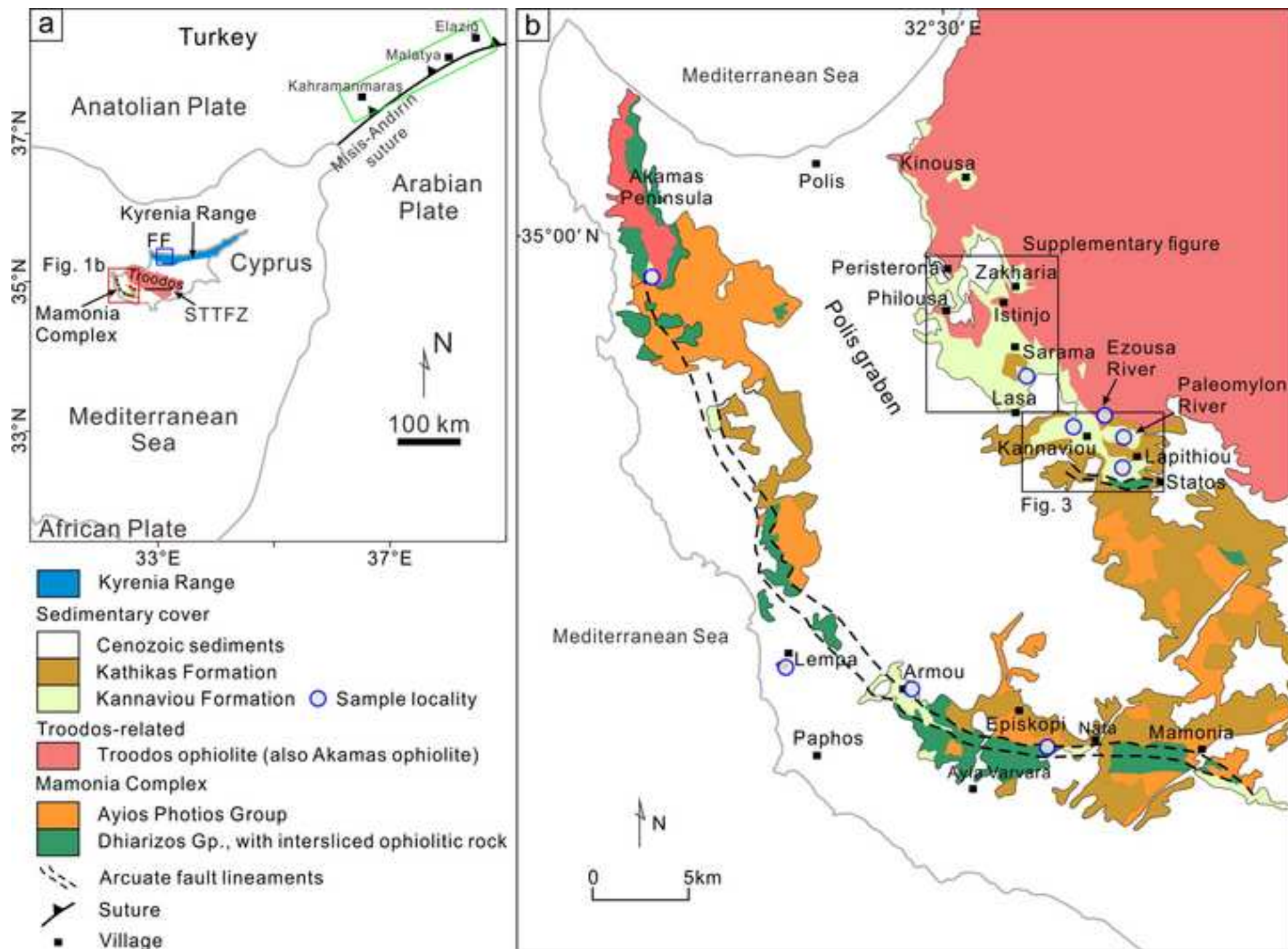


Fig. 2

[Click here to download high resolution image](#)

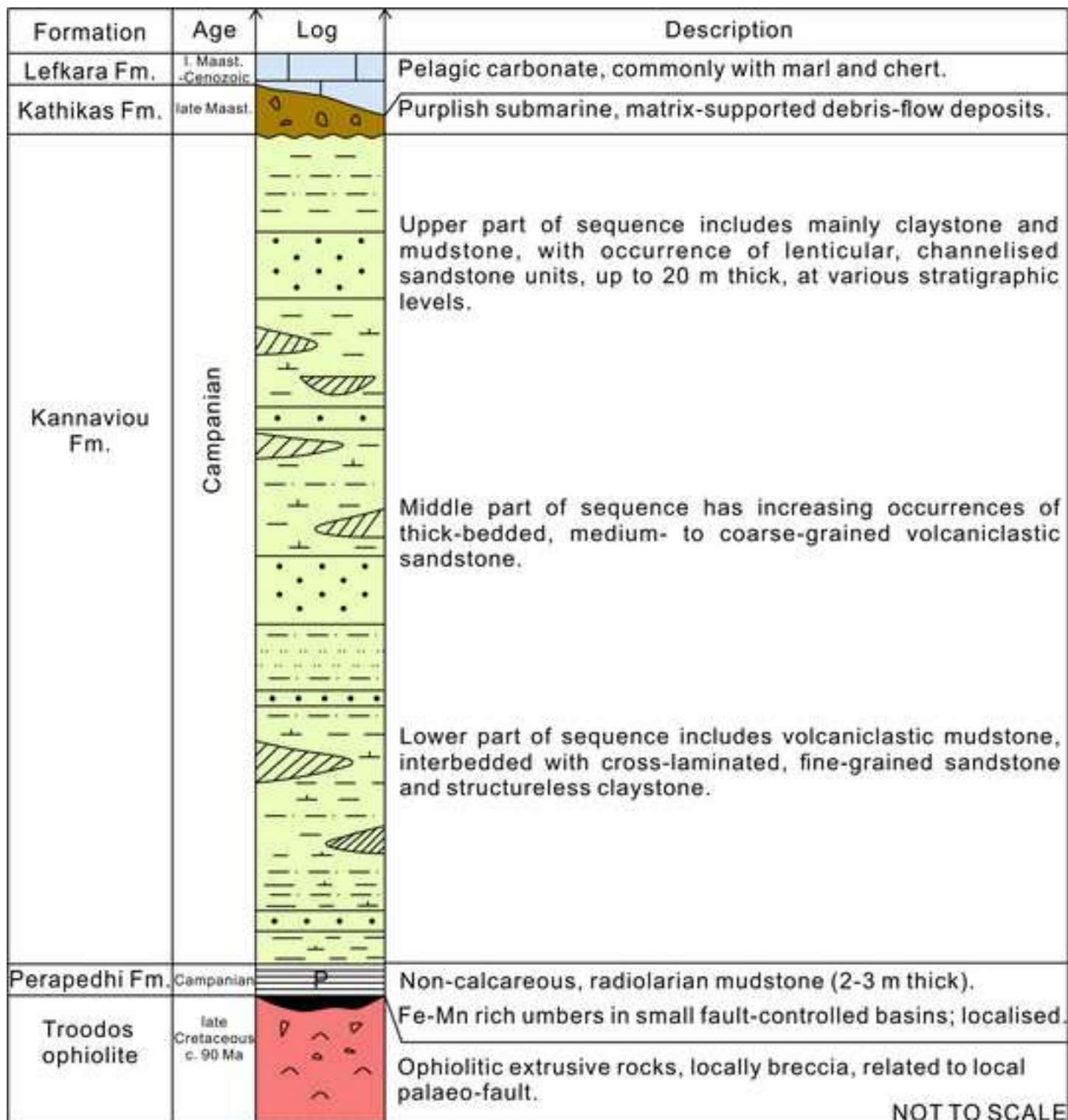
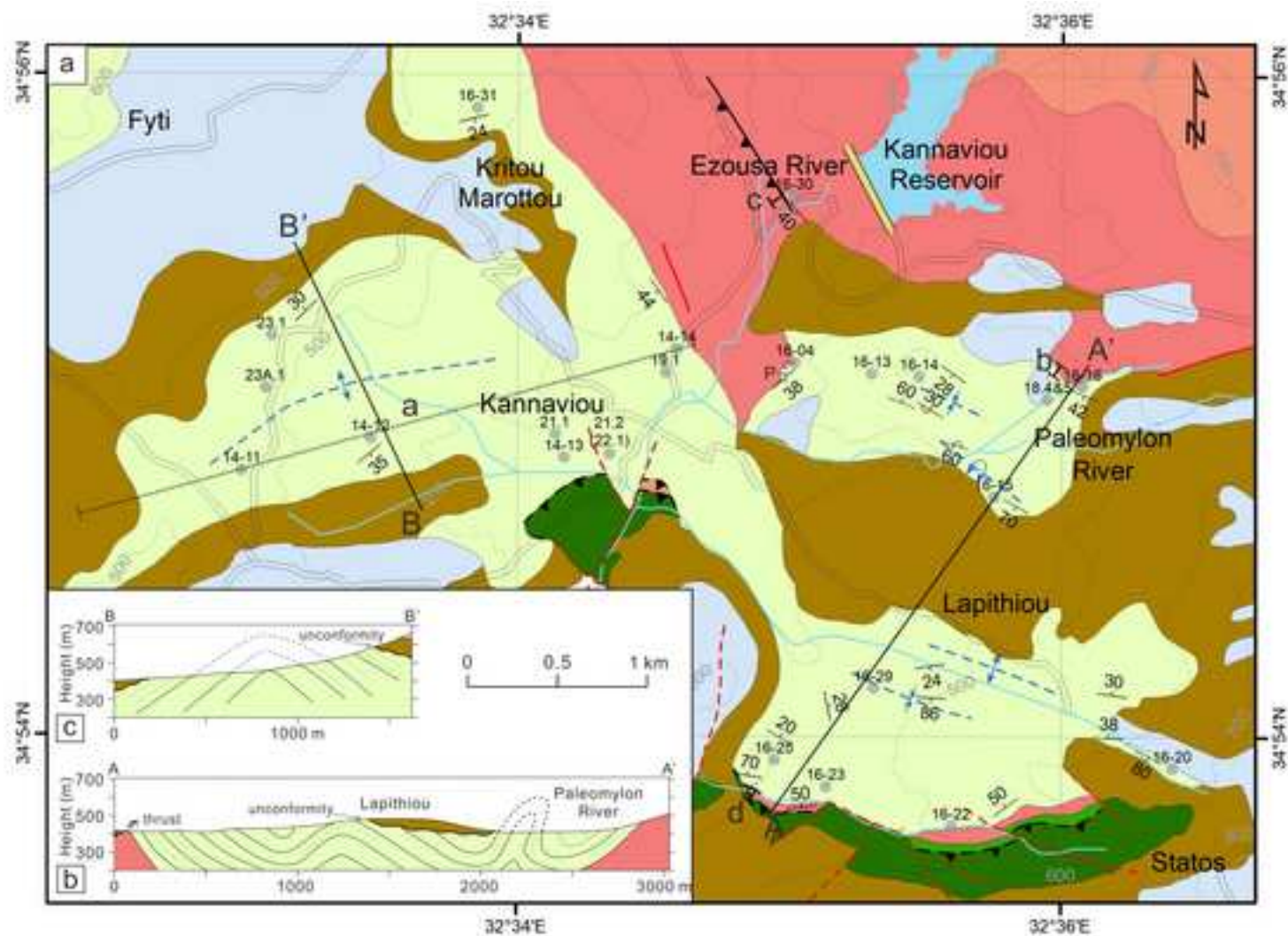


Fig. 3

[Click here to download high resolution image](#)



Legend

- | | | | |
|--|-------------------|--|--------------------|
| | Measured sections | | Fault |
| | Sample location | | Inferred fault |
| | Dam | | Thrust |
| | River or stream | | Inferred thrust |
| | Road | | Inferred anticline |
| | Inclined bedding | | Inferred syncline |
| | Overtured bedding | | Overturm anticline |

Sedimentary cover

- | | |
|--|--------------------|
| | Quaternary deposit |
| | Lefkara Fm. |
| | Kathikas Fm. |
| | Kannaviou Fm. |
| | Perapedhi Fm. |

Ophiolitic rocks

- | | |
|--|--------------|
| | Pillow lava |
| | Diabase |
| | Gabbro |
| | Serpentinite |

Fig. 4

[Click here to download high resolution image](#)

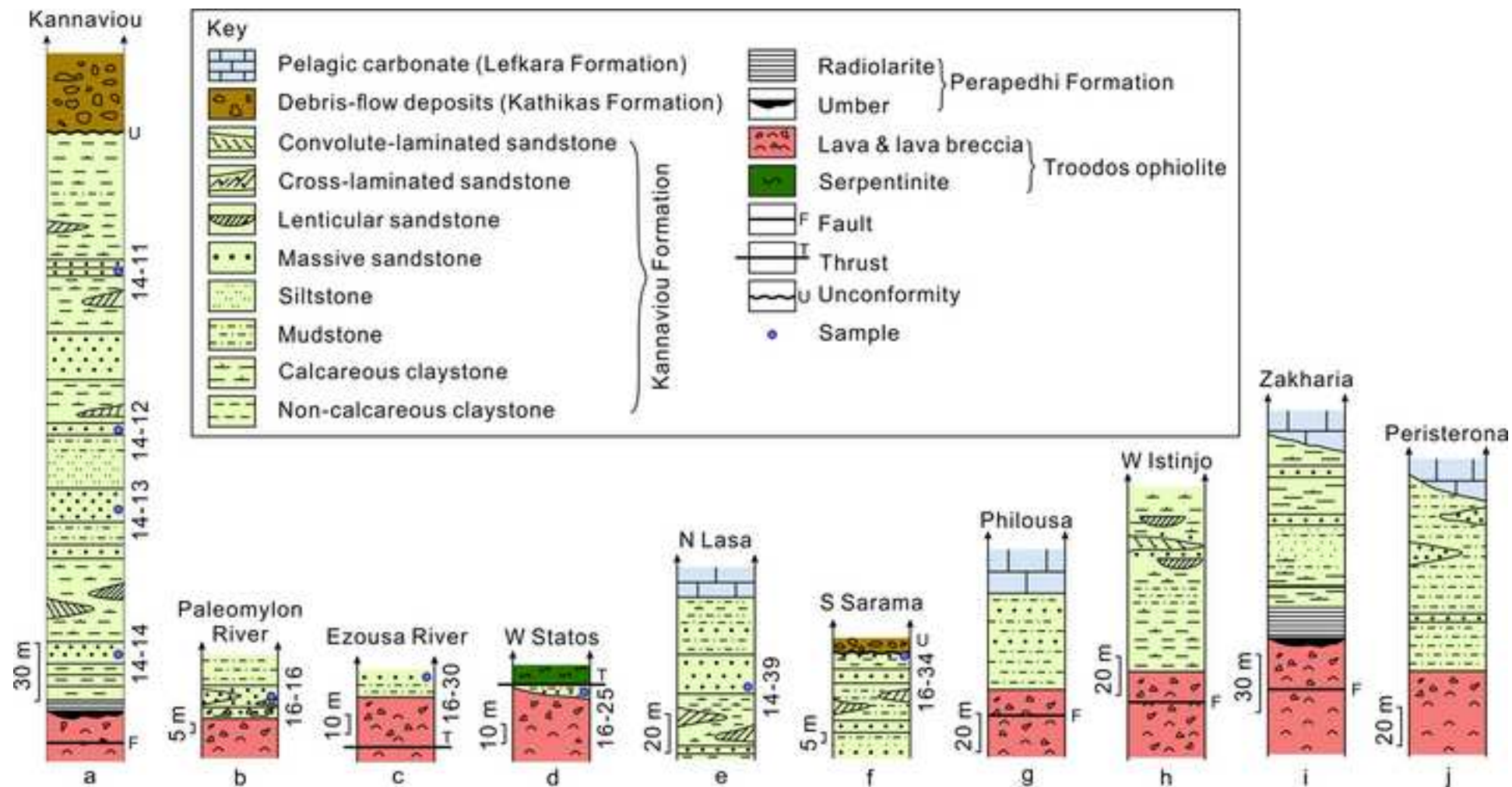


Fig. 5
[Click here to download high resolution image](#)



Fig. 6

[Click here to download high resolution image](#)

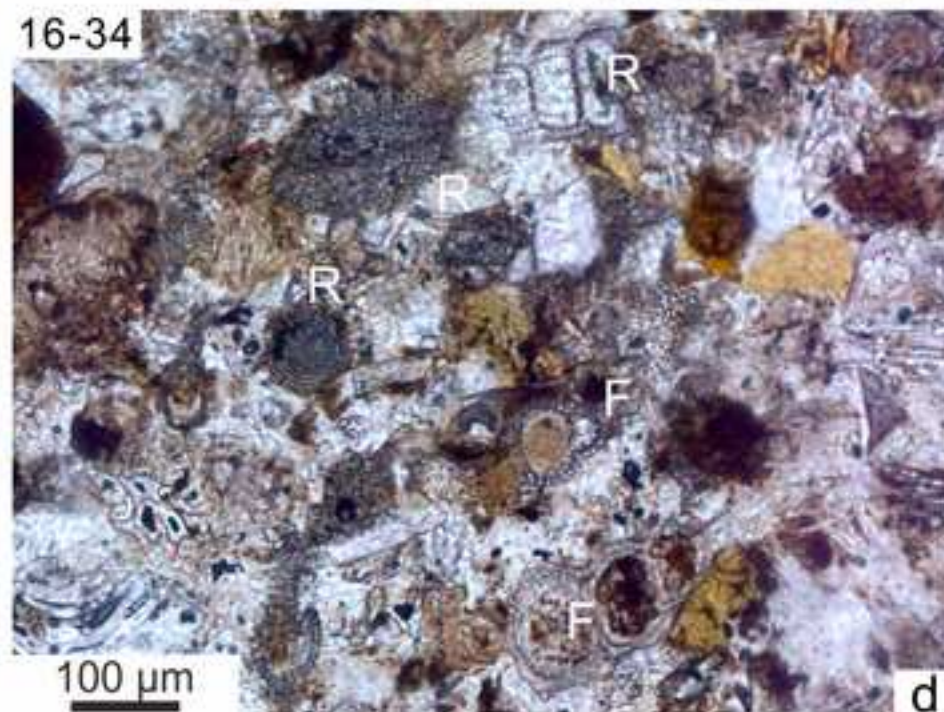
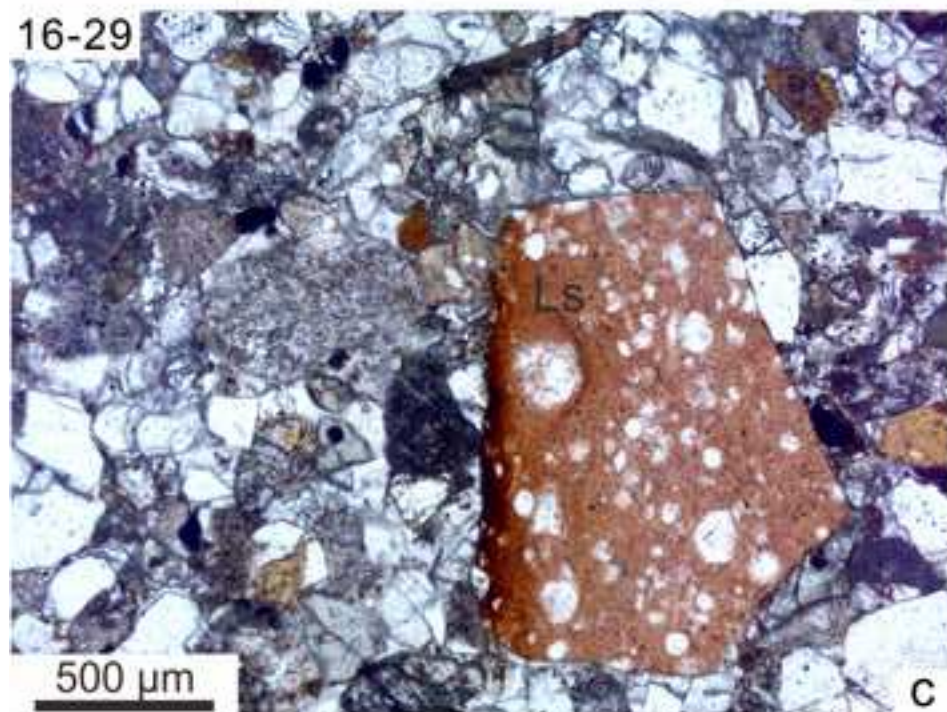
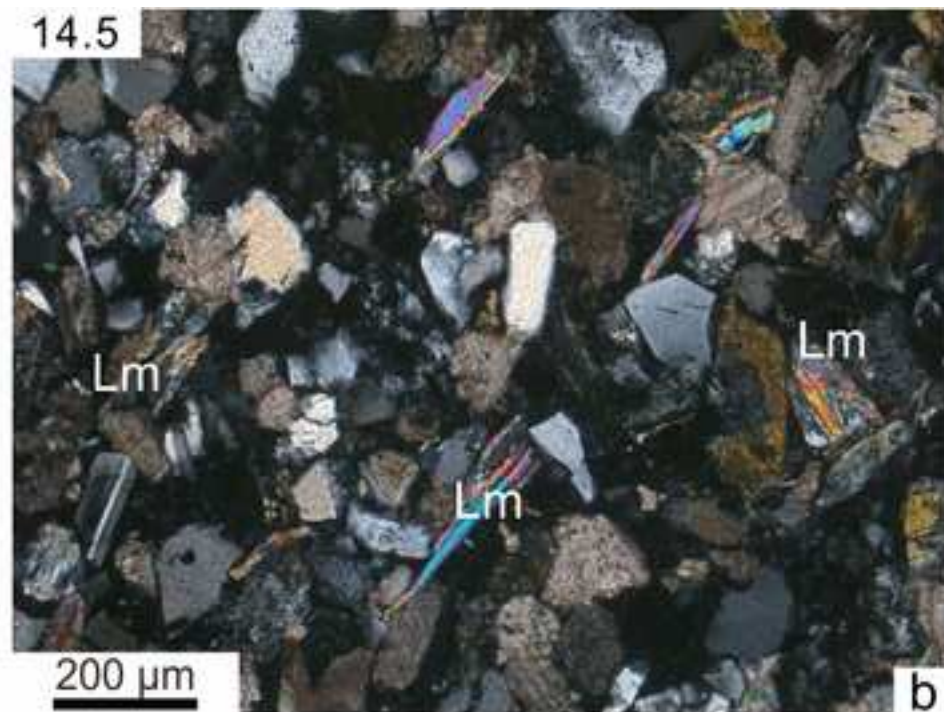
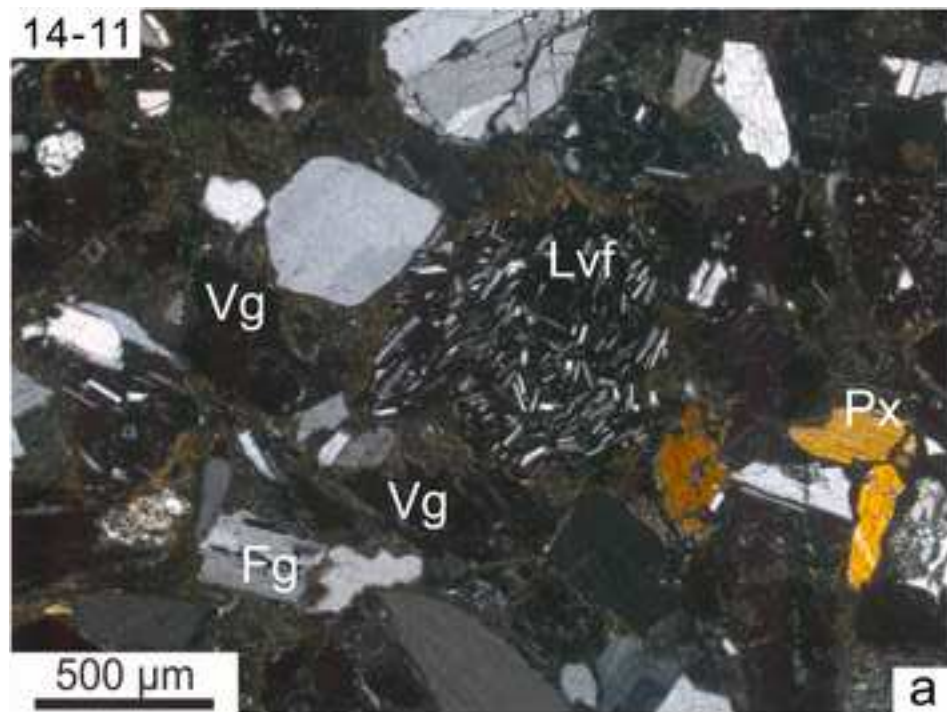


Fig. 7
[Click here to download high resolution image](#)

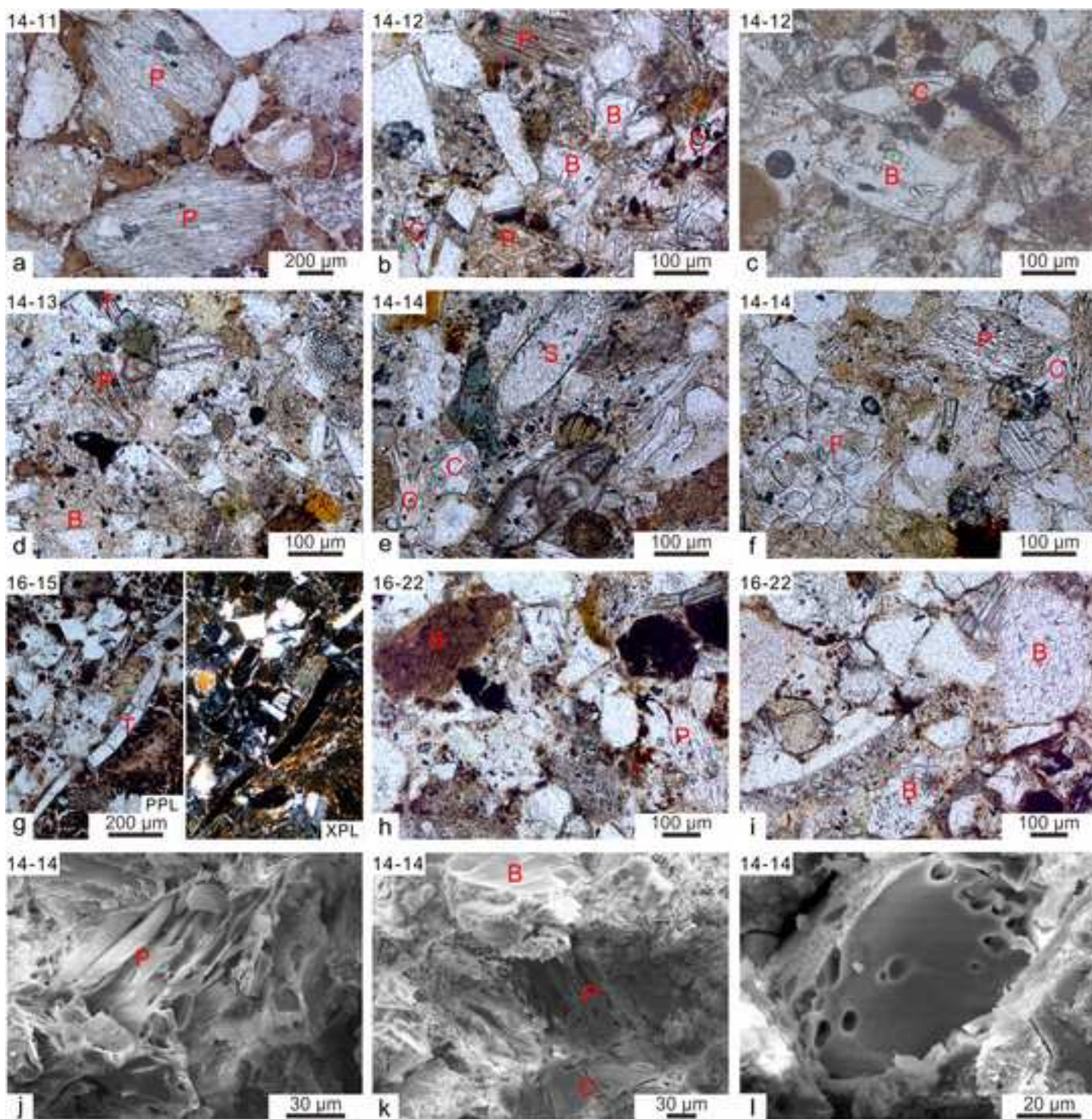


Fig. 8

[Click here to download high resolution image](#)

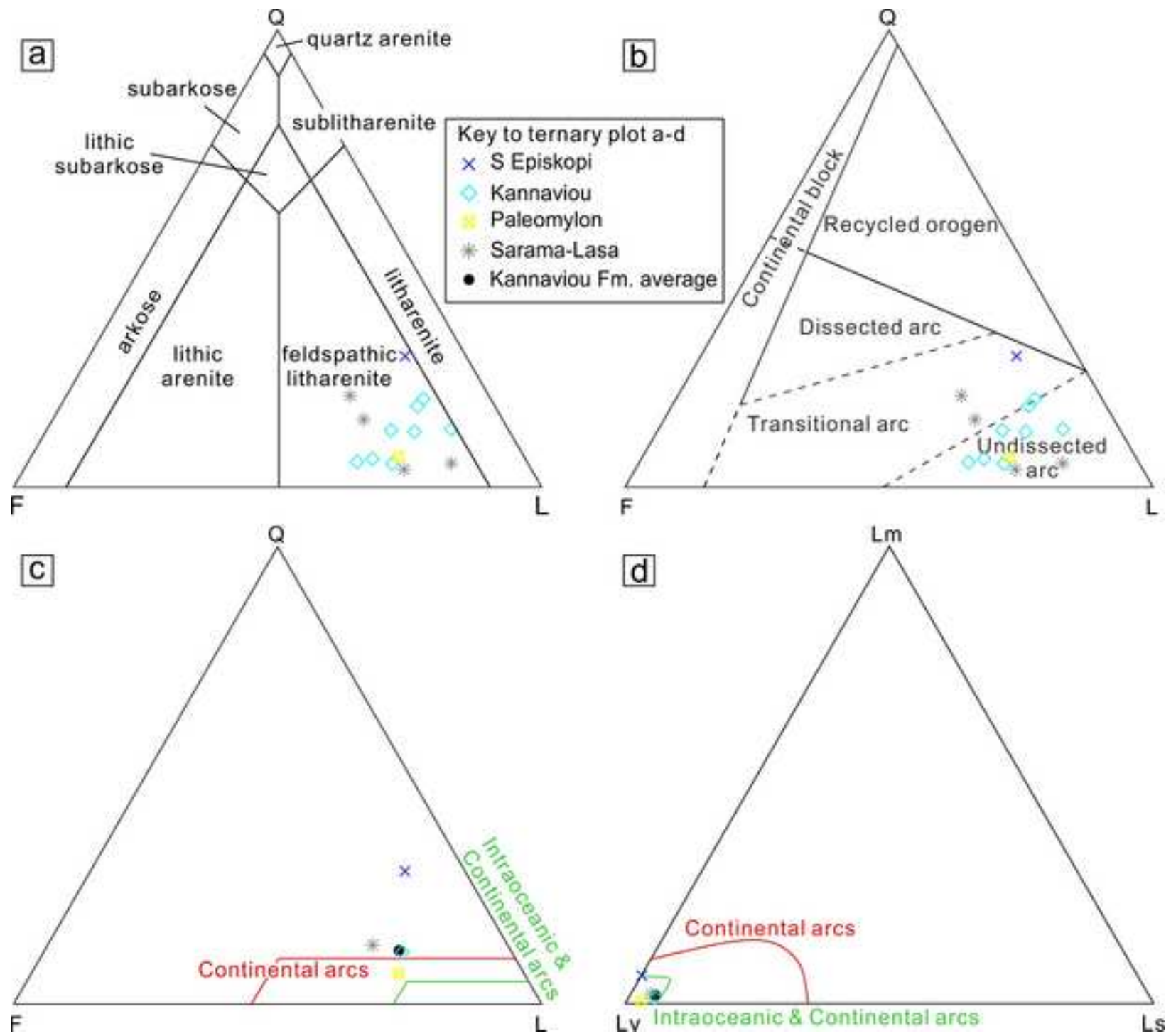


Fig. 9

[Click here to download high resolution image](#)

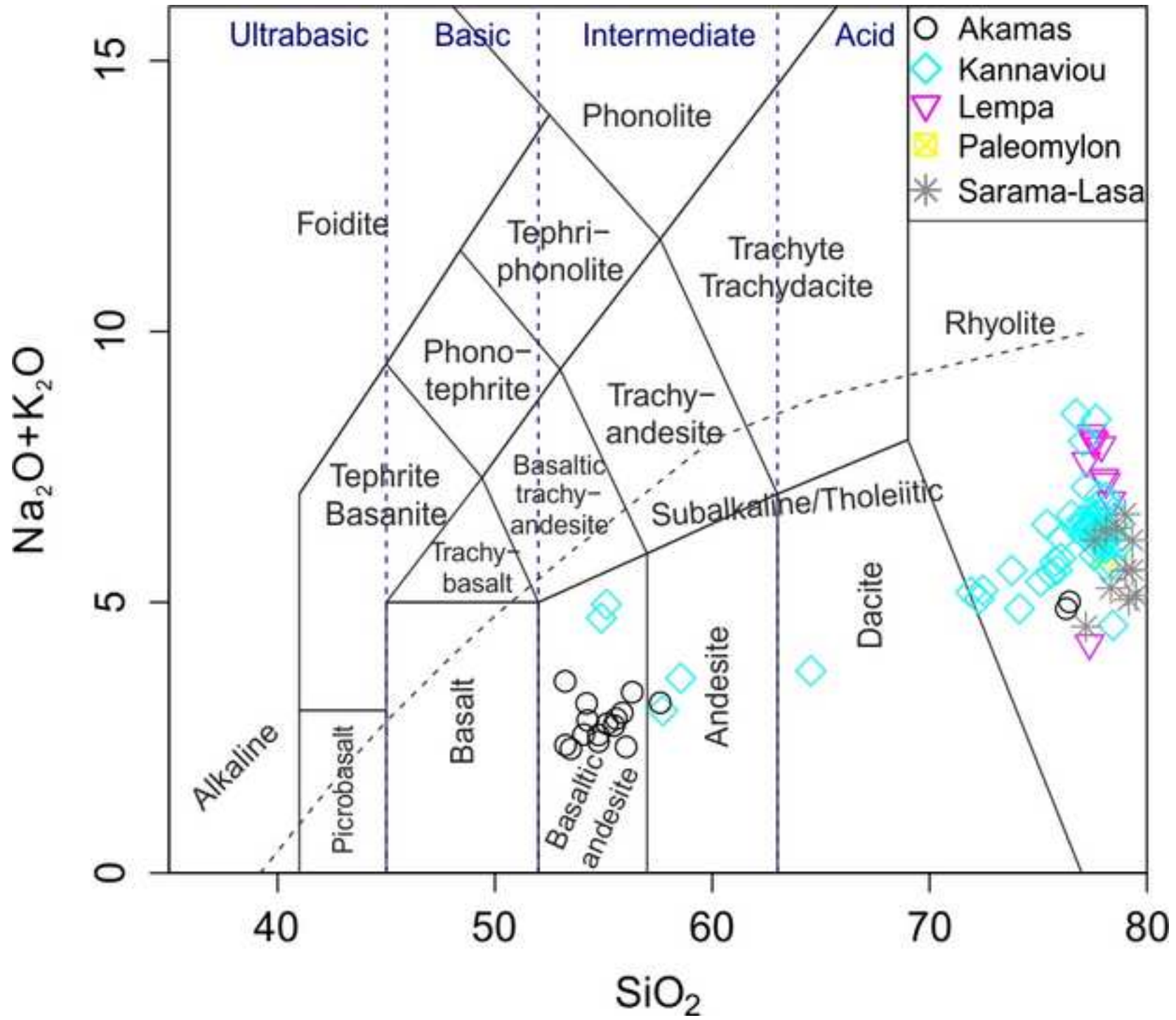


Fig. 10
[Click here to download high resolution image](#)

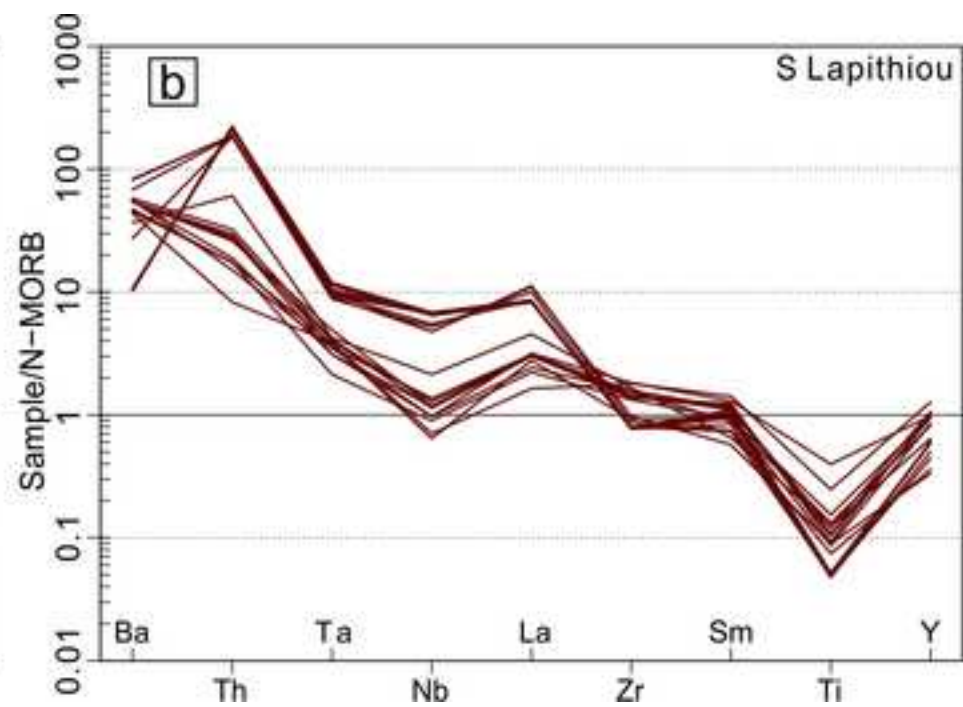
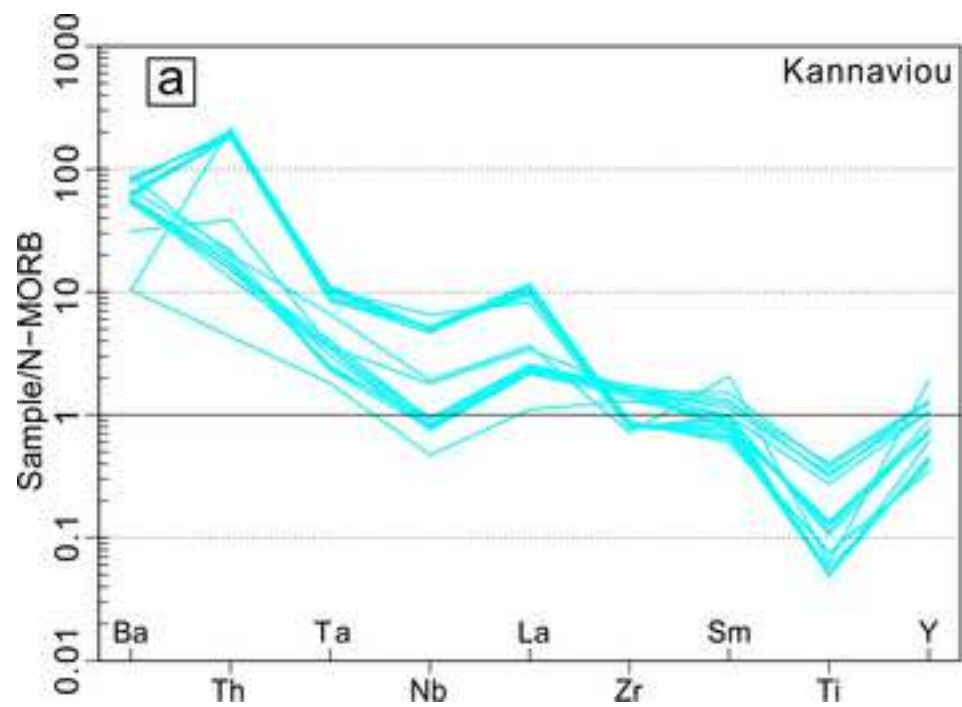


Fig. 11

[Click here to download high resolution image](#)

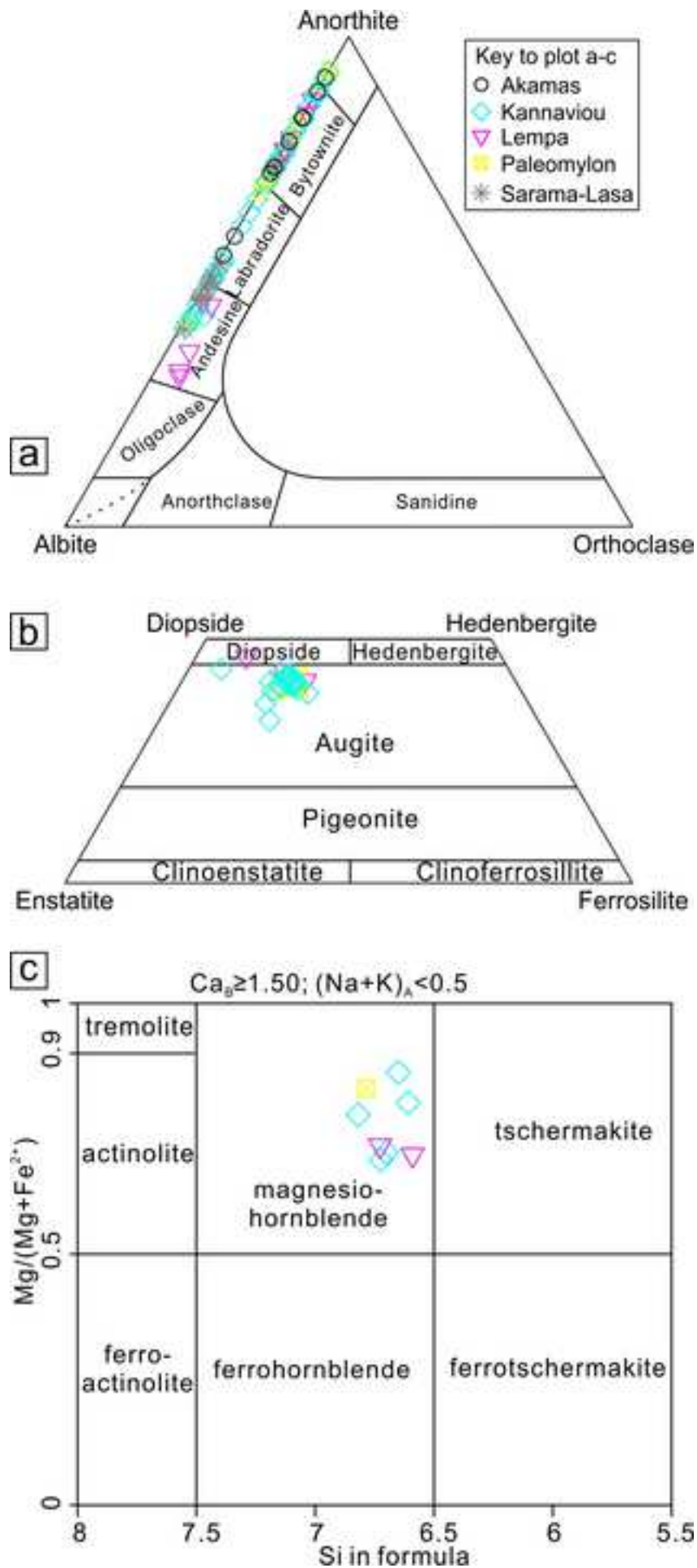


Fig. 12
[Click here to download high resolution image](#)

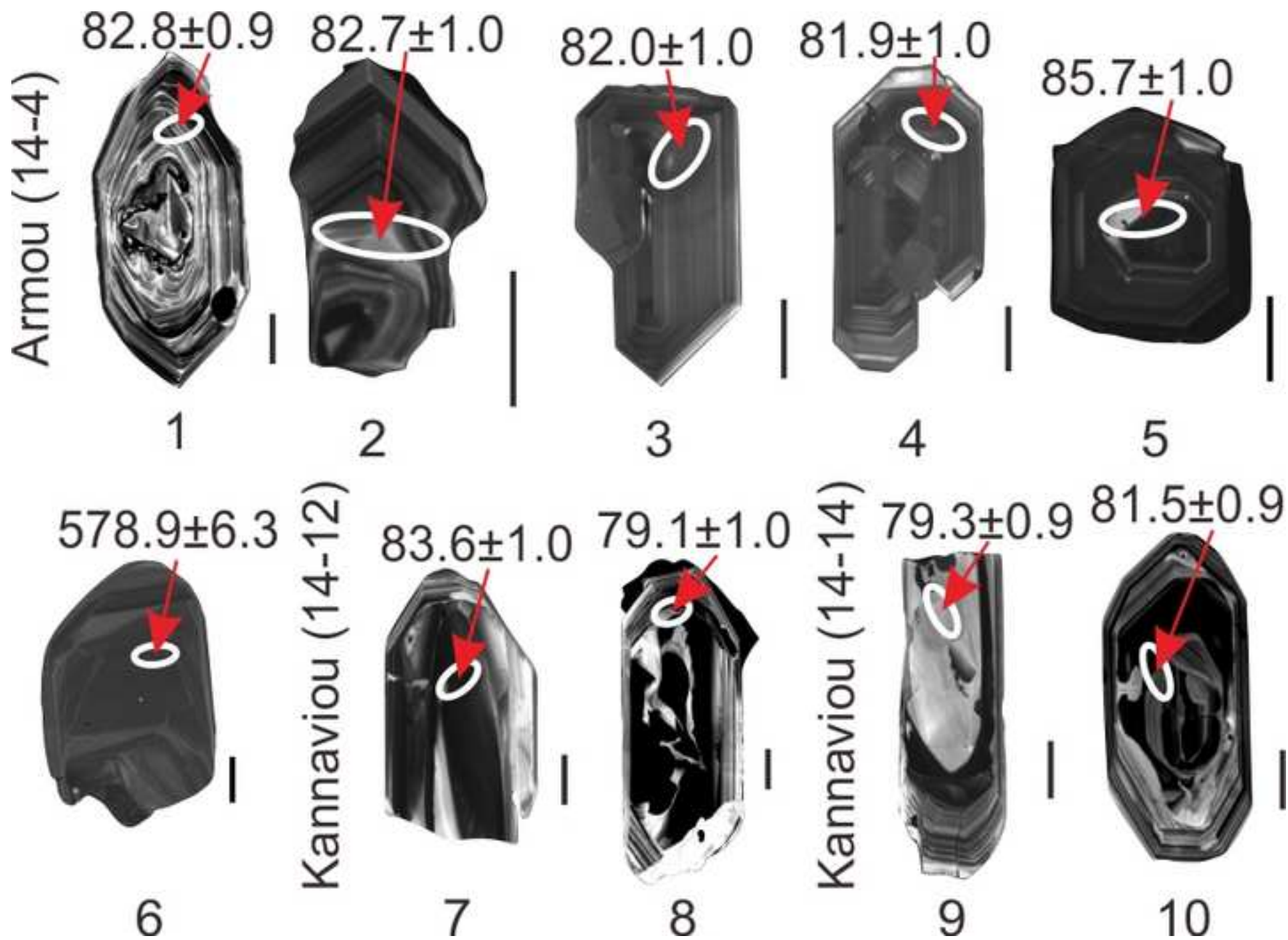


Fig. 13

[Click here to download high resolution image](#)

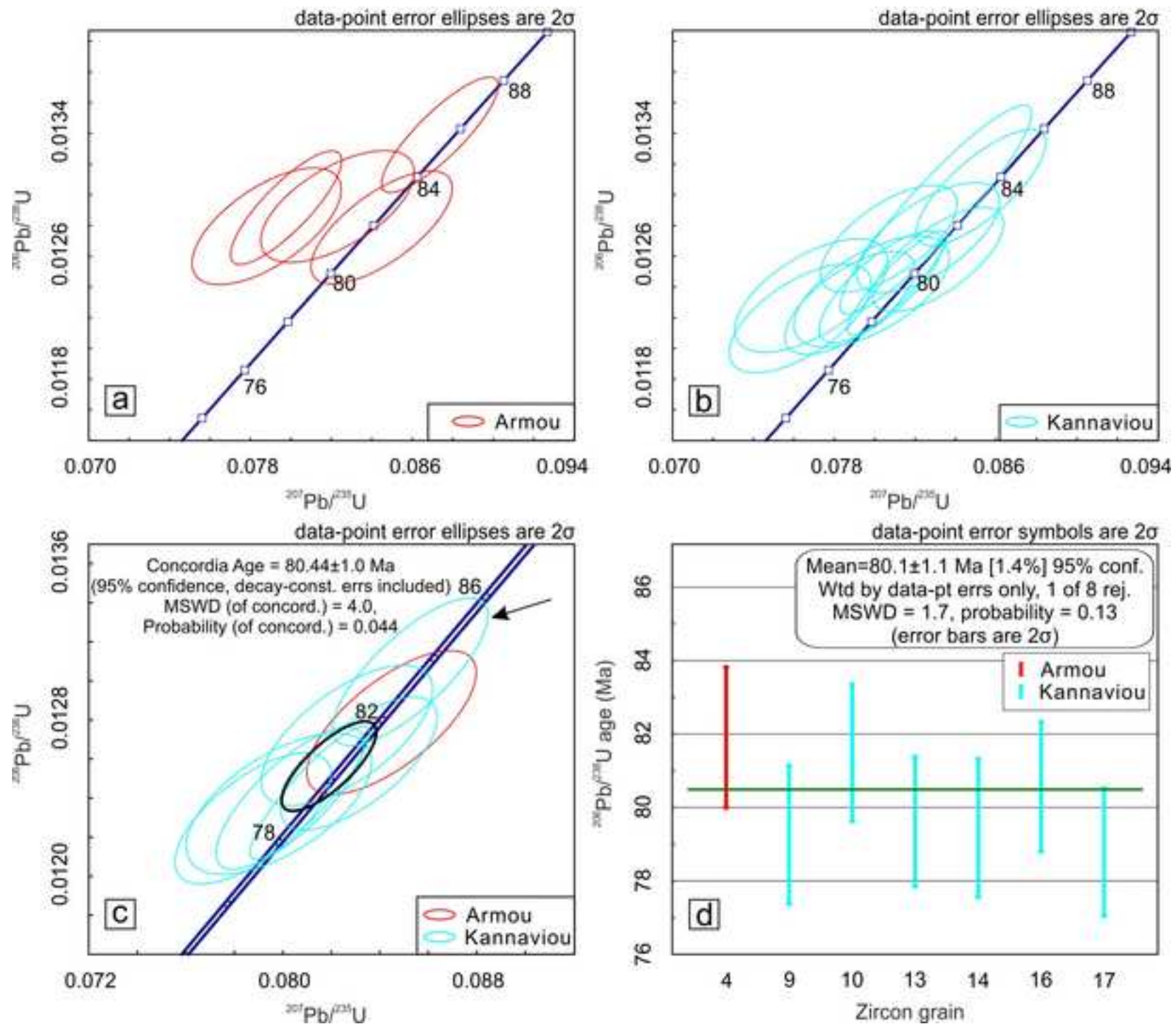


Fig. 14

[Click here to download high resolution image](#)

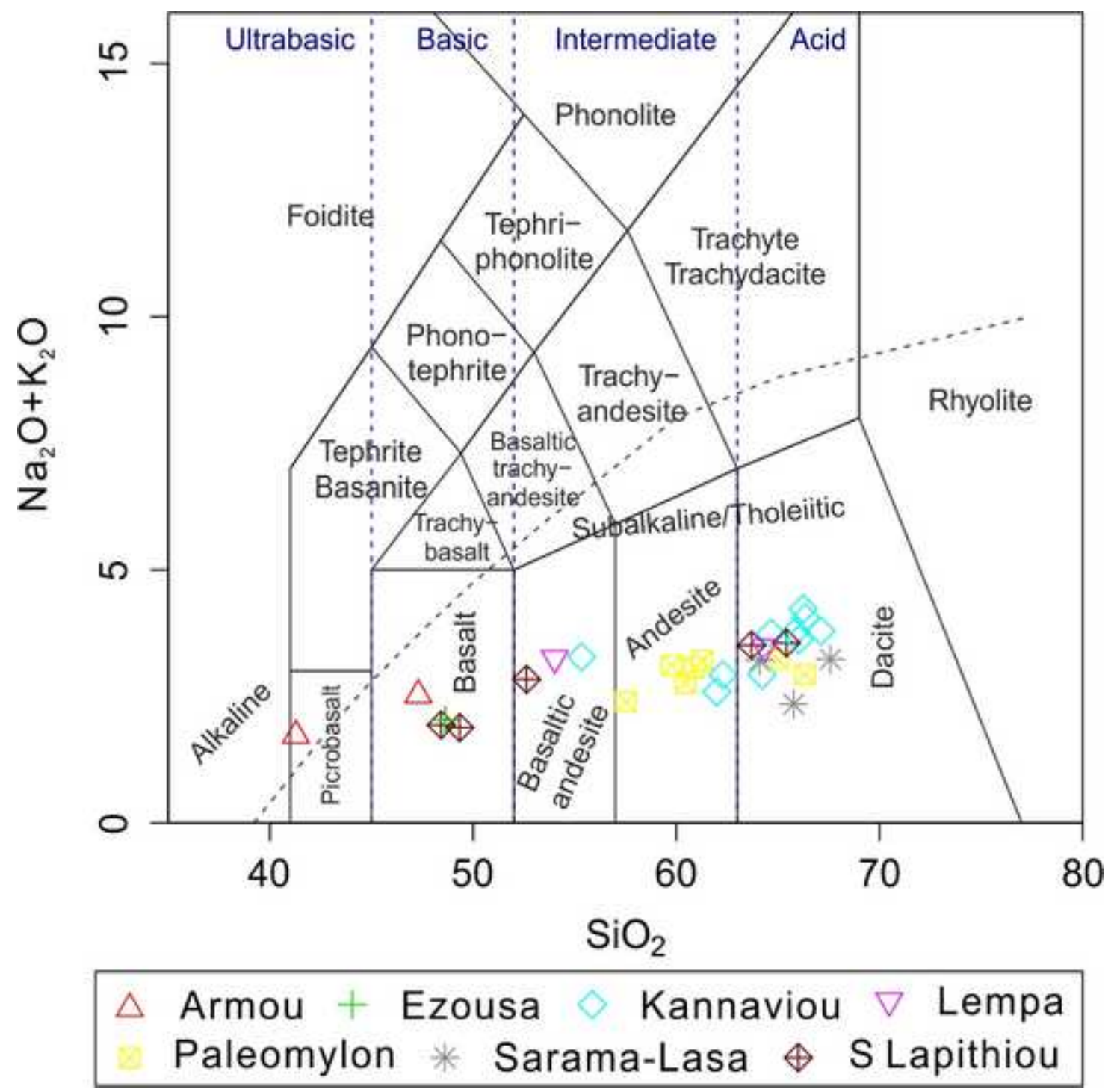


Fig. 15

[Click here to download high resolution image](#)

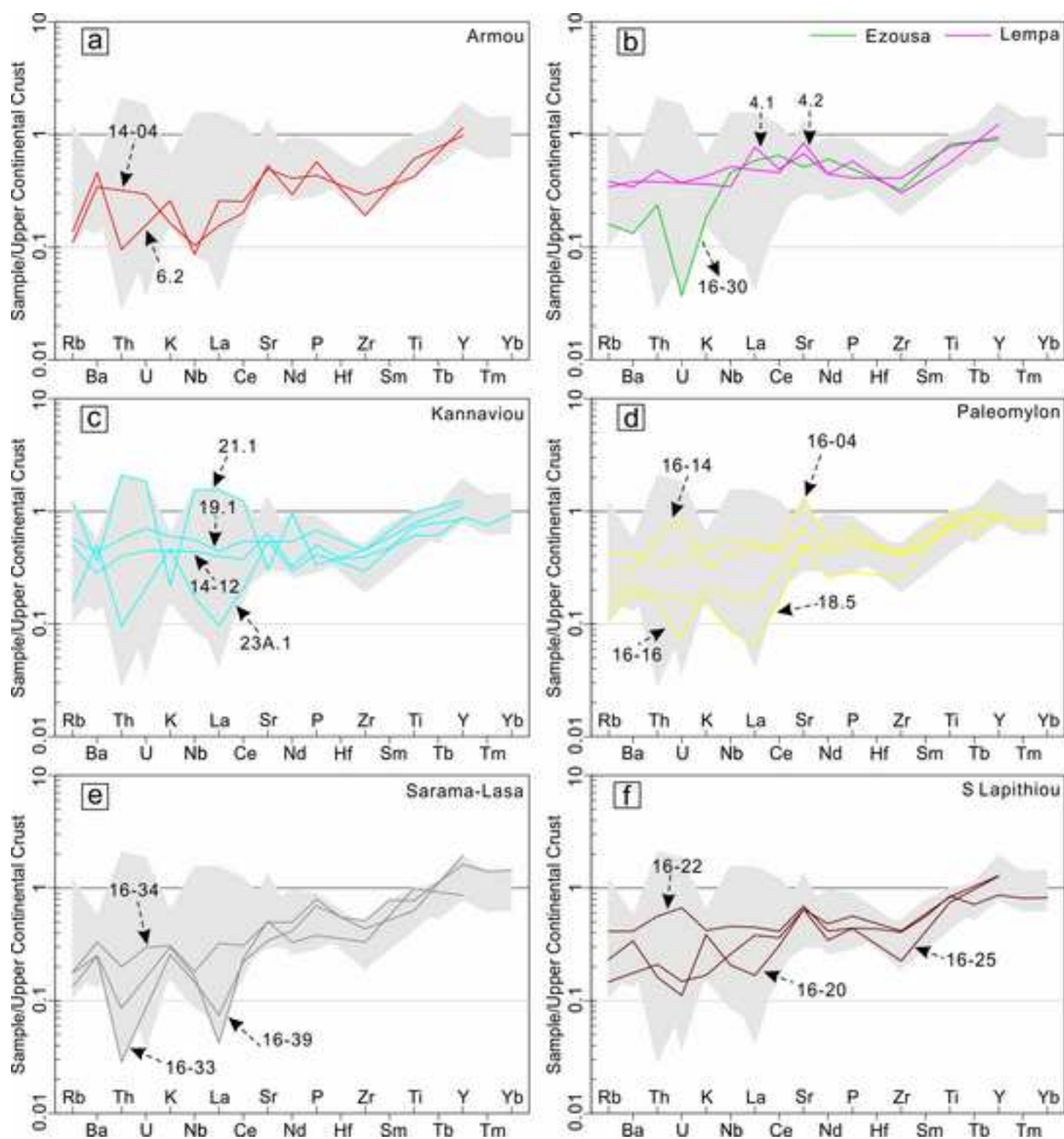


Fig. 16
[Click here to download high resolution image](#)

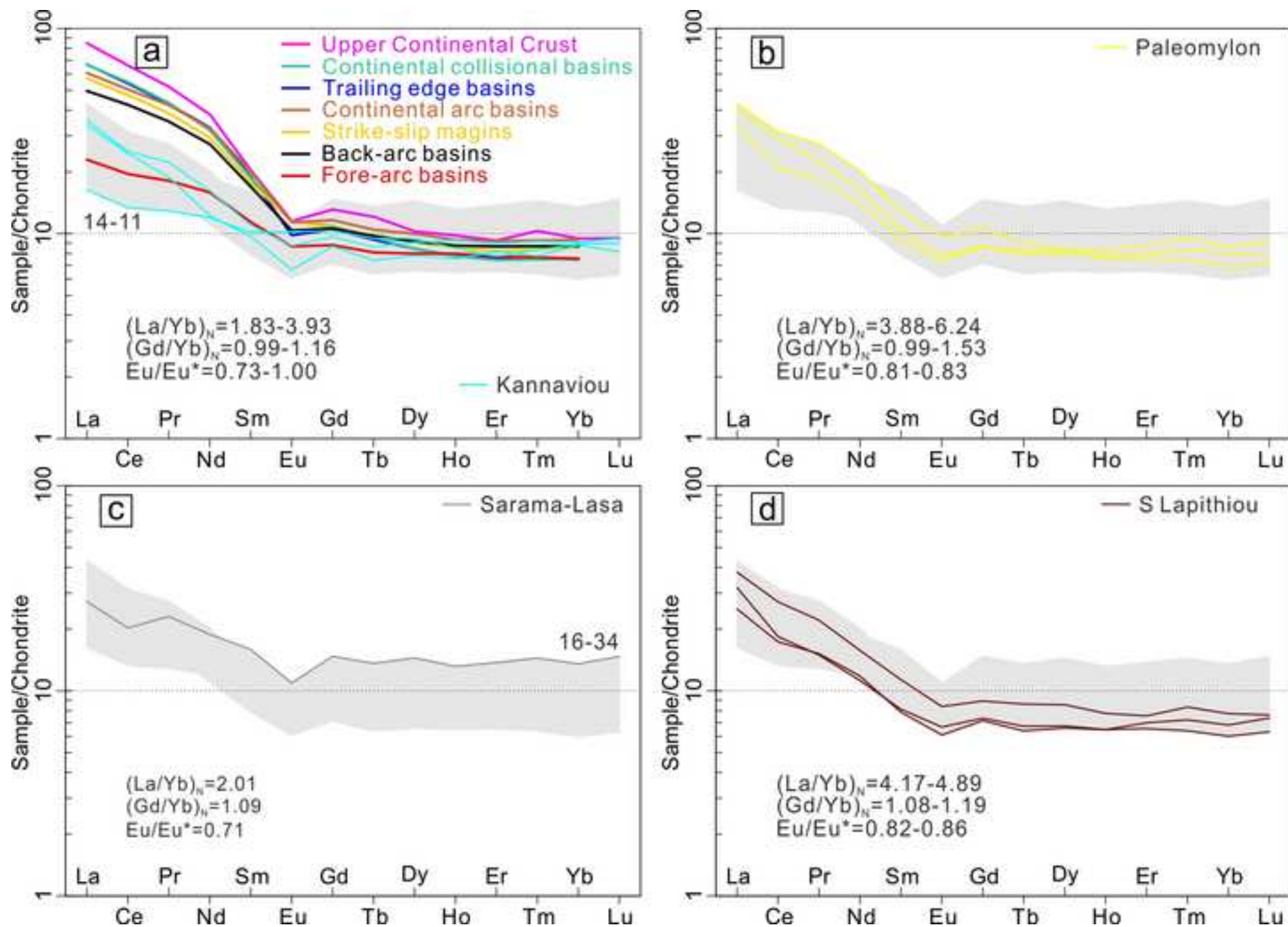


Fig. 17
[Click here to download high resolution image](#)

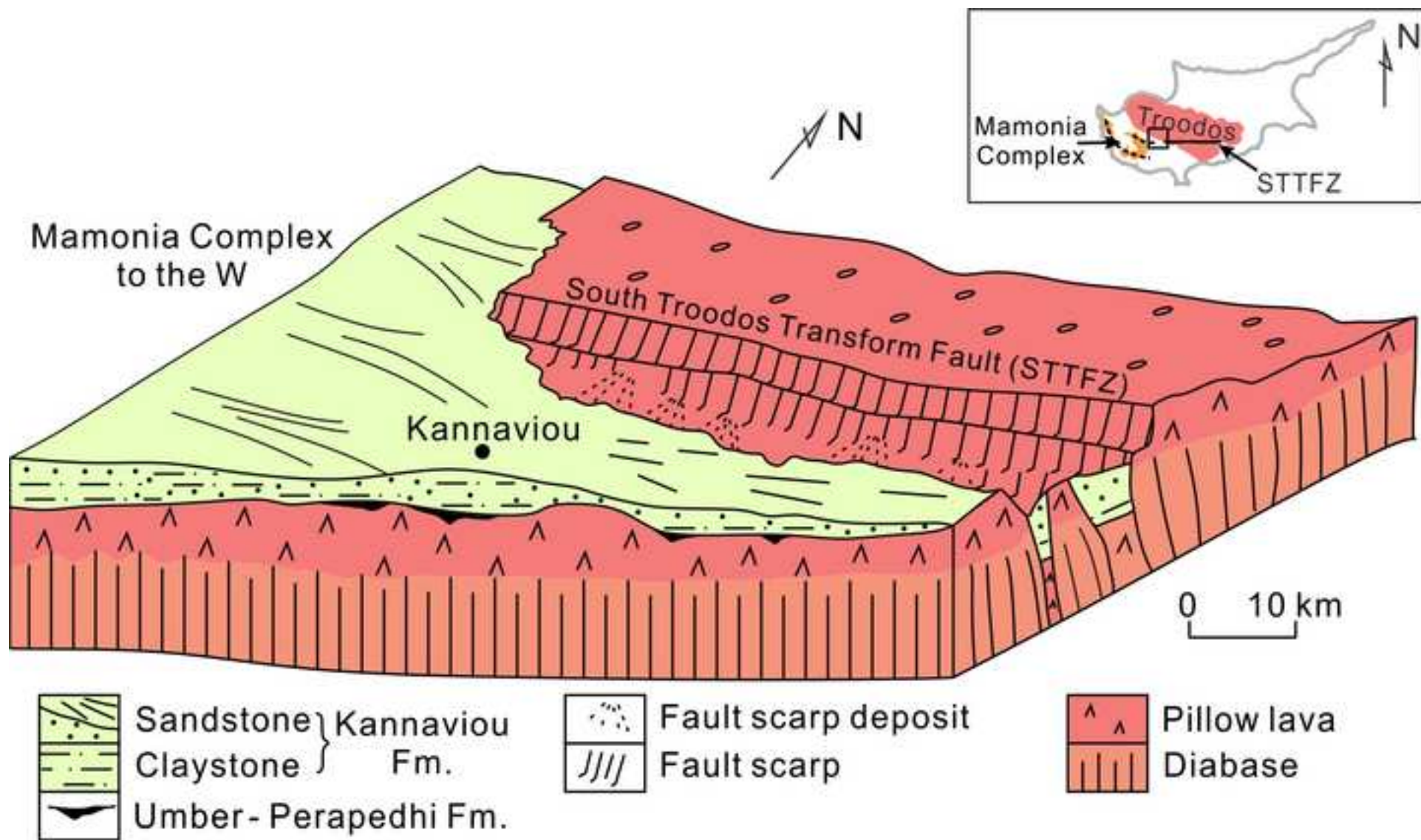


Fig. 18
[Click here to download high resolution image](#)

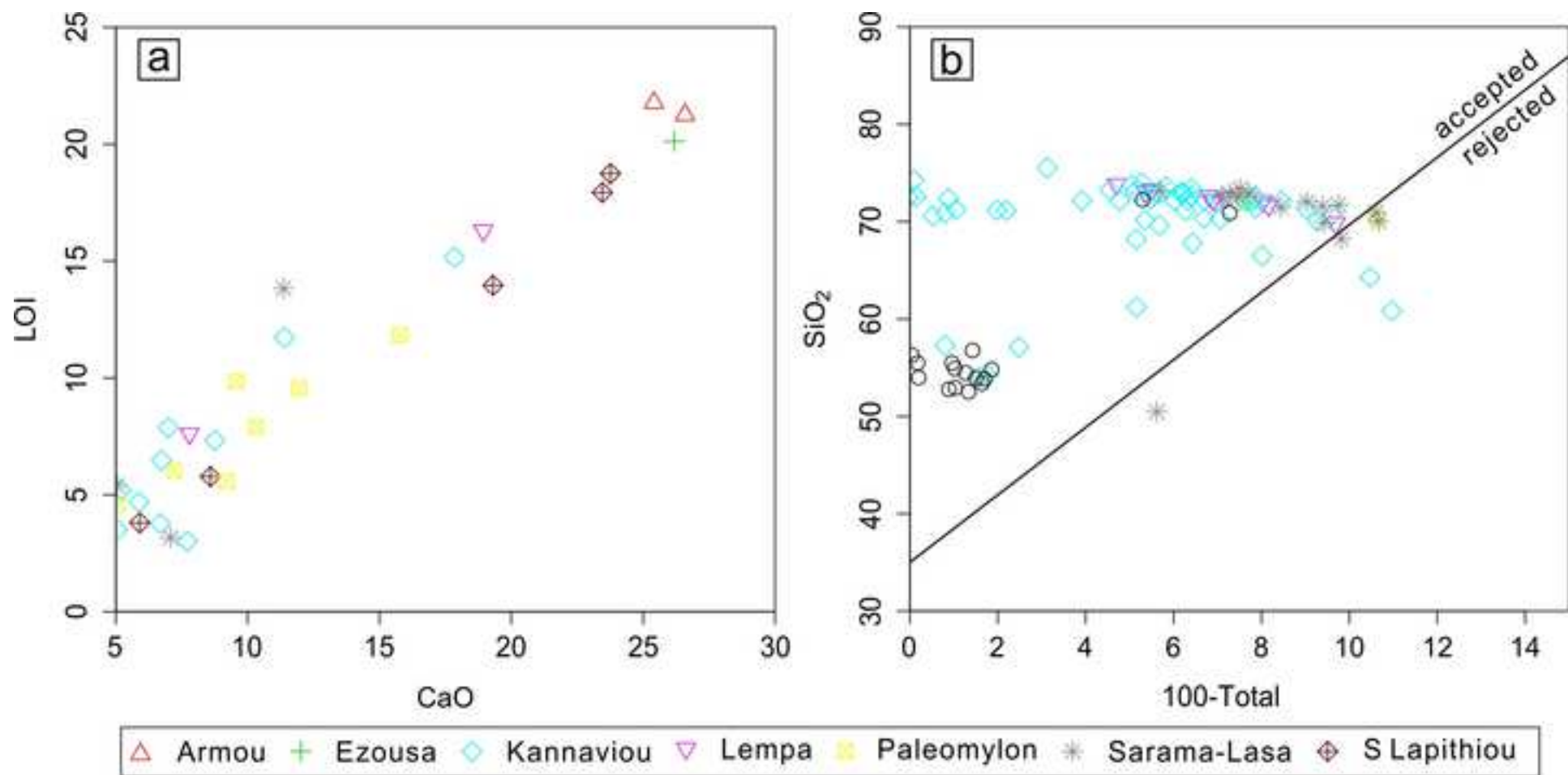


Fig. 19

[Click here to download high resolution image](#)

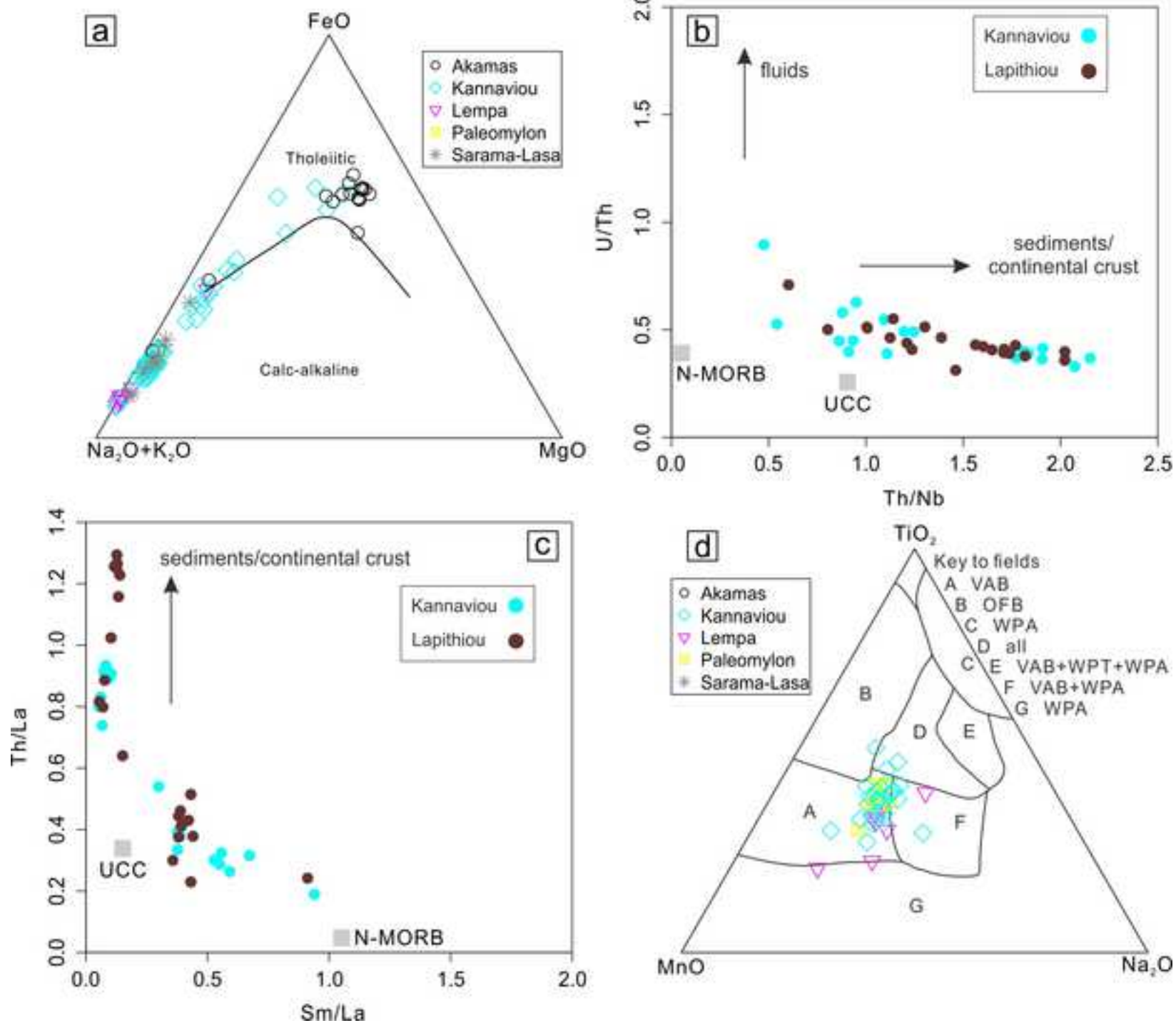


Fig. 20

[Click here to download high resolution image](#)

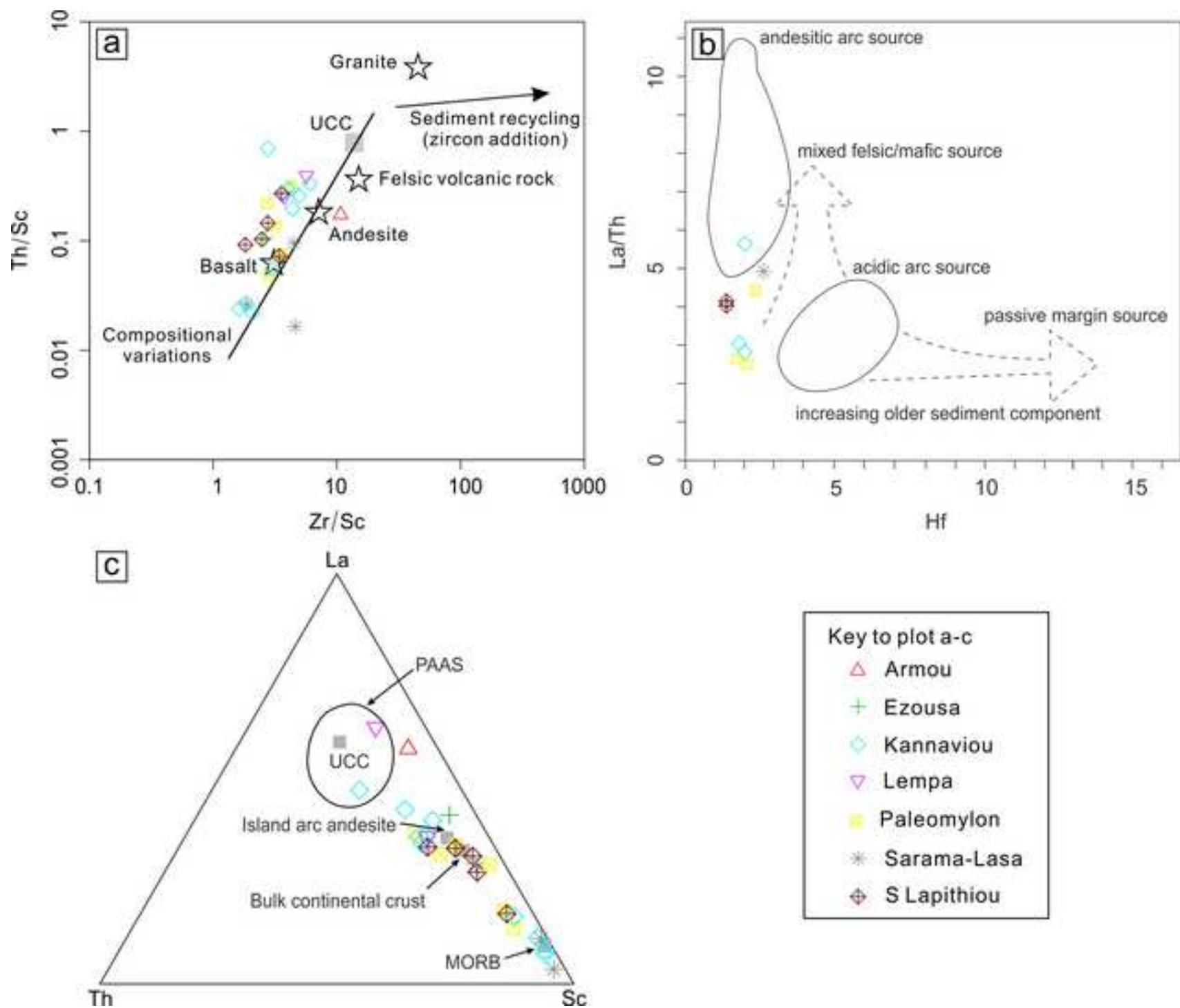


Fig. 21

[Click here to download high resolution image](#)

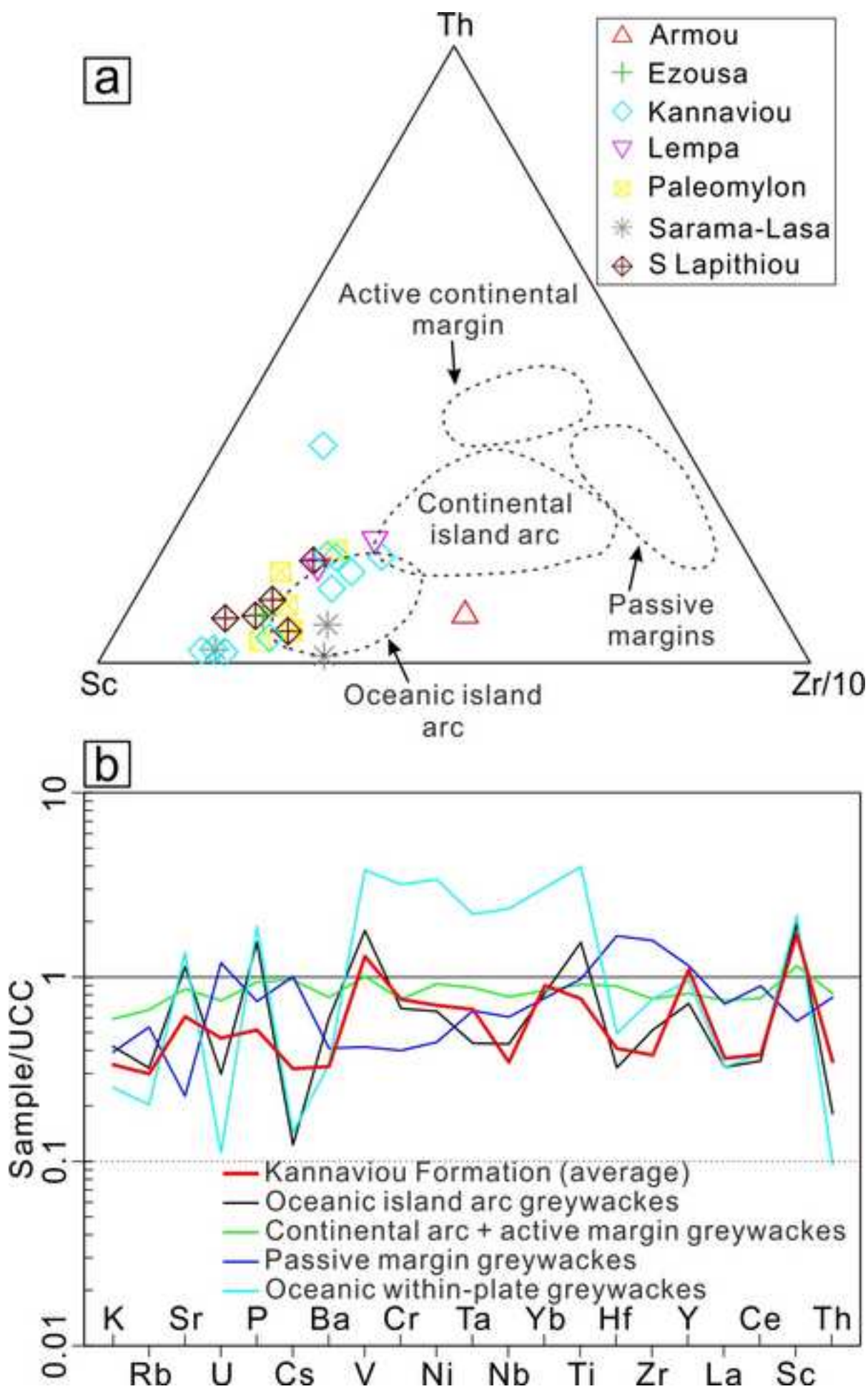


Fig. 22

[Click here to download high resolution image](#)

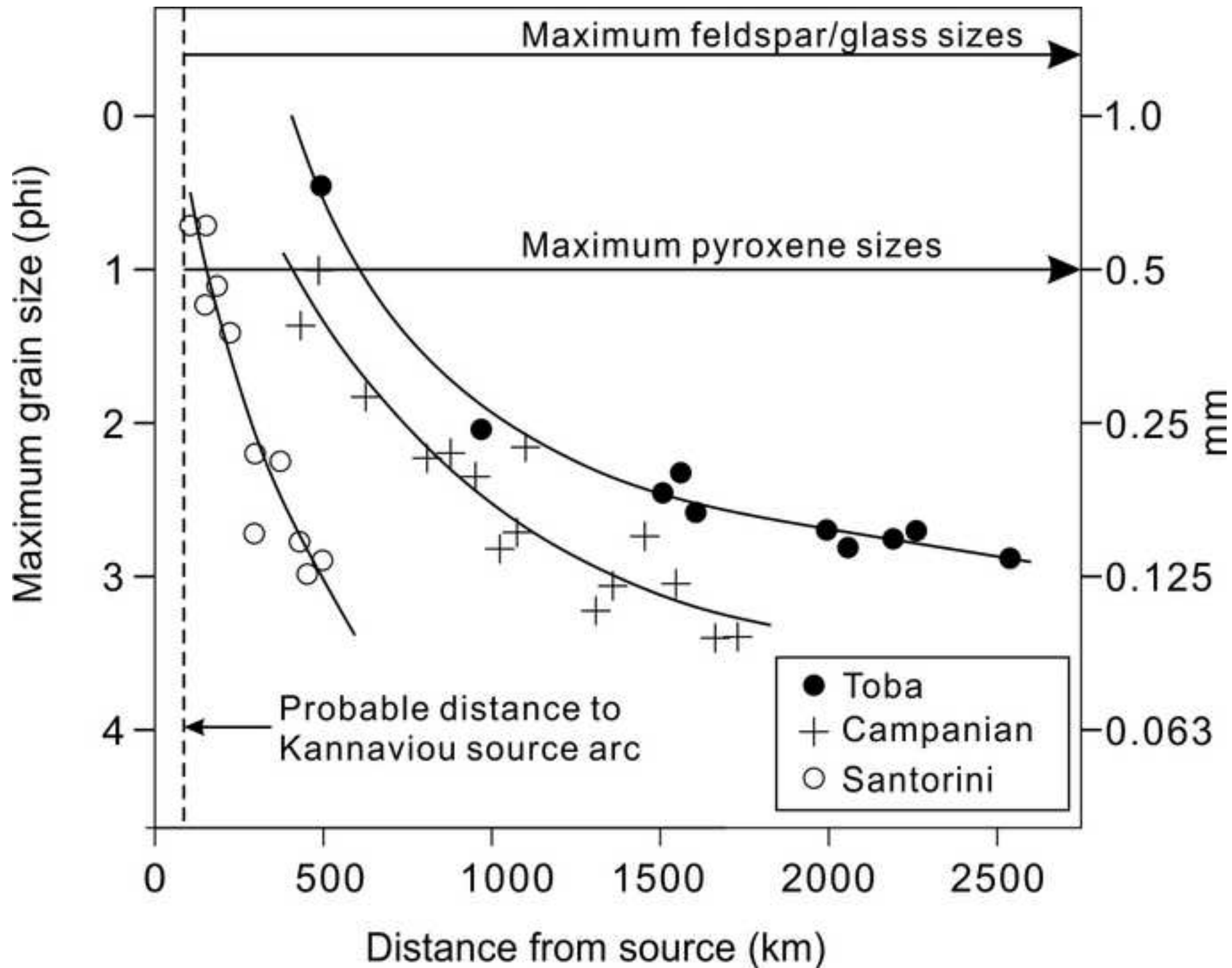


Fig. 23

[Click here to download high resolution image](#)

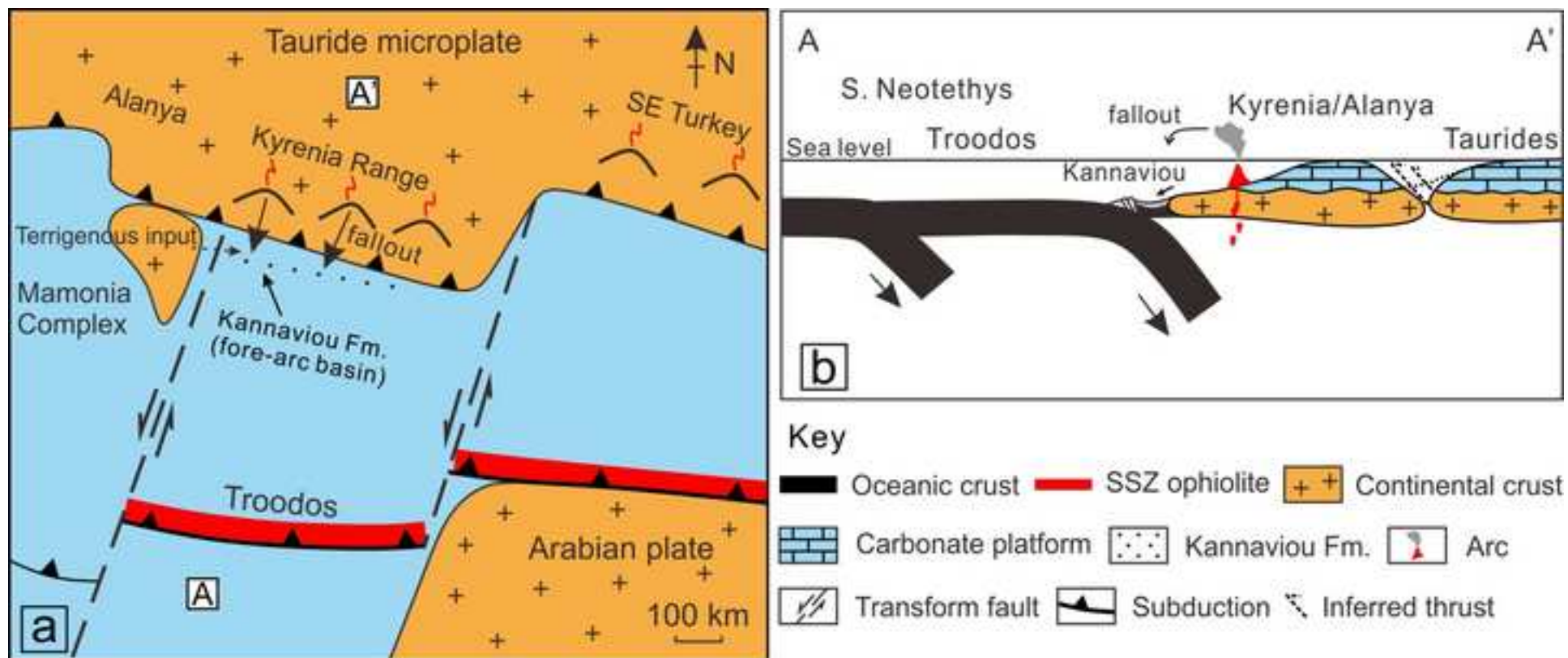


Table 1

[Click here to download Table: Table 1.xlsx](#)

Sample	Geographic location	Geographic coordinates	QFL	XRF ^a	ICP-MS	EMPA ^a	IMS-4f	U-Pb	Note ^b
14-04	Armou	34°47'40"N, 32°28'19"E		X				X	
14-11	Kannaviou	34°54'48"N, 32°32'59"E	X	X	X		X		
14-12	Kannaviou	34°54'53"N, 32°33'29"E	X	X	X			X	
14-13	Kannaviou	34°54'53"N, 32°34'16"E	X	X					
14-14	Kannaviou	34°55'20"N, 32°34'34"E	X	X	X		X	X	
16-04	Paleomylon	34°55'08"N, 32°35'01"E		X	X				
16-13	Paleomylon	34°55'06"N, 32°35'18"E		X	X				
16-14	Paleomylon	34°55'02"N, 32°35'29"E		X	X				
16-15	Paleomylon	34°54'44"N, 32°35'44"E		X					
16-16	Paleomylon	34°55'03"N, 32°36'03"E		X					
16-20	south of Lapithiou	34°53'55"N, 32°36'25"E		X			X		Newly collected
16-22	south of Lapithiou	34°53'44"N, 32°35'36"E		X	X		X		
16-23	south of Lapithiou	34°53'50"N, 32°35'07"E		X	X				
16-25	south of Lapithiou	34°53'54"N, 32°34'51"E		X					
16-29	south of Lapithiou	34°54'09"N, 32°35'19"E		X	X				
16-30	Ezousa River	34°55'36"N, 32°35'00"E		X					
16-31	Kannaviou-Kri. Marottou	34°55'50"N, 32°33'53"E		X					
16-33	Sarama	34°57'25"N, 32°32'28"E		X					
16-34	Sarama	34°56'52"N, 32°32'02"E		X	X				
16-39	Lasa	34°55'47"N, 32°31'51"E		X					
4.1	Lempa	34°48'52"N, 32°24'08"E		X ^a					Gilbert and Robertson (2013)
4.2	Lempa	34°48'52"N, 32°24'08"E		X ^a		X ^a			
6.2	Armou	34°47'43"N, 32°28'22"E		X ^a					
14.5	south of Episkopi	34°46'08"N, 32°32'28"E	X						
18.4	Paleomylon	34°55'02"N, 32°36'00"E		X ^a					
18.5	Paleomylon	34°55'02"N, 32°36'00"E	X	X ^a		X ^a			
19.1	Kannaviou	34°55'07"N, 32°34'33"E	X	X ^a		X ^a			
21.1	Kannaviou	34°54'53"N, 32°34'10"E		X ^a		X ^a			
21.2	Kannaviou	34°54'48"N, 32°34'20"E	X	X ^a		X ^a			
22.1	Kannaviou	34°54'48"N, 32°34'20"E	X						
23.1	Kannaviou	34°55'14"N, 32°33'09"E	X	X ^a					
23A.1	Kannaviou	34°55'03"N, 32°33'05"E		X ^a		X ^a			
1074	Akamas	34°59'31"N, 32°19'56"E				X			
2124	Lasa	NA	X						
2141	Sarama	NA	X						
2156	Sarama	NA	X						
2158	Sarama	NA	X						
2164	Sarama	NA				X			

QFL: petrographic thin section study for point counting;

XRF: major and trace element analysed by X-ray fluorescence spectrometry;

ICP-MS: trace and rare earth element analysed by inductively coupled plasma mass spectrometry;

EMPA: mineral chemistry analysed by electron microprobe;

IMS-4f: glass trace element analysed by ion microprobe;

U-Pb: zircon U-Pb geochronology analysed by secondary-ion mass spectrometry;

^a Data from Gilbert and Robertson (2013);^b Thin section, polished section source.

Table 2[Click here to download Table: Table 2.xlsx](#)

<i>Main parameter</i>		<i>Calculated parameter</i>	
Qm	Monocrystalline quartz	Q	Total quartz grains (=Qm+Qp)
Qp	Polycrystalline quartz	F	Total feldspar grains (=Fg)
Fg ^a	Feldspar grains	Lv	Volcanic lithics (=Vg+Lvm+Lvf)
Fl	Feldspar in lithics	Lsm	Sedimentary and metamorphic lithics (=Ls+Lm)
Vg ^b	Volcanic glass	L	Total unstable lithic fragments (=Lv+Lsm+Lo+Fl)
Lvm ^c	Intermediate to mafic volcanic lithics	Lt	Total lithic fragments (=L+Qp)
Lvf ^d	Felsic volcanic lithics		
Ls	Sedimentary lithics		
Lm	Metamorphic lithics		
Lo	Other lithics		
Px	Detrital pyroxenes		
Am	Detrital amphiboles		
Bt	Detrital biotite grains		
Ms	Detrital muscovite flakes		
Cal	Carbonate grains		
Bio	Bioclastic detritus		
M	Matrix		
C	Cement		

^a no differentiation of feldspar;

^b volcanic glass (relatively pure, with very minor phenocrysts);

^c dark coloured volcanic lithics, with common pyroxene and opaque crystals;

^d pale coloured volcanic lithics with common quartz and feldspar laths.

Table 3[Click here to download Table: Table 3.xlsx](#)

	Kannaviou Formation							Sediment from felsic sources ^a		Sediment from mafic sources ^a	
	Armou	Ezousa	Kanaviou	Lempa	Paleomylon	Sarama-Lasa	S Lapithiou	Coarse fractions	Fine fractions	Coarse fractions	Fine fractions
La/Co	-	-	0.24-0.84	-	0.69-1.13	0.59	0.67	1.8-13.8	1.4-22.4	0.14-0.38	-
Th/Co	-	-	0.05-0.31	-	0.16-0.44	0.12	0.21	0.67-19.4	0.3-7.5	0.04-1.4	-
Th/Cr	0.03	0.01	0.03-0.71	0.08	0.03-0.12	0.02-0.05	0.05	0.13-2.7	0.067-4.0	0.018-0.046	0.002-0.045
La/Sc	0.27-1.58	-	0.08-1.52	0.70-2.30	0.04-0.77	0.04-0.45	0.47	2.5-16.3	0.7-27.7	0.43-0.86	0.4-1.1
Th/Sc	0.17	-	0.69	0.26-0.39	0-0.32	0.02-0.10	0.14	0.84-20.5	0.64-18.1	0.05-0.22	0.05-0.4
Eu/Eu*	-	-	0.73-1.00	-	0.81-0.83	0.71	0.81-0.86	0.40-0.94	0.32-0.83	0.71-0.95	0.7-1.02

^a data from Cullers (1995, 2000)

Supplementary Appendix A

[Click here to download Supplementary material for on-line publication only: Supplementary Appendix A.docx](#)

Supplementary Appendix B

[Click here to download Supplementary material for on-line publication only: Supplementary Appendix B.docx](#)

Supplementary Figure 1

[Click here to download Supplementary material for on-line publication only: Supplementary Figure 1.jpg](#)

Supplementary Figure 2

[Click here to download Supplementary material for on-line publication only: Supplementary Figure 2.jpg](#)

Supplementary Figure 3

[Click here to download Supplementary material for on-line publication only: Supplementary Figure 3.jpg](#)

Supplementary Figure 4

[Click here to download Supplementary material for on-line publication only: Supplementary Figure 4.jpg](#)

Supplementary Table 1

[Click here to download Supplementary material for on-line publication only: Supplementary Table 1.xlsx](#)

Supplementary Table 2

[Click here to download Supplementary material for on-line publication only: Supplementary Table 2.xlsx](#)

Supplementary Table 3

[Click here to download Supplementary material for on-line publication only: Supplementary Table 3.xlsx](#)

Supplementary Table 4

[Click here to download Supplementary material for on-line publication only: Supplementary Table 4.xlsx](#)

Supplementary Table 5

[Click here to download Supplementary material for on-line publication only: Supplementary Table 5.xlsx](#)

Supplementary Table 6

[Click here to download Supplementary material for on-line publication only: Supplementary Table 6.xlsx](#)